

Evidence for mass-dependent peculiar velocities in compact object binaries: Towards better constraints on natal kicks

Yue Zhao^{1*}, Poshak Gandhi¹, Cordelia Dashwood Brown¹, Christian Knigge¹, Phil A. Charles¹, Thomas J. Maccarone², and Pornisara Nuchvanichakul^{1,3}

¹*School of Physics & Astronomy, University of Southampton, Highfield, Southampton SO17 1BJ, UK*

²*Department of Physics & Astronomy, Texas Tech University, Lubbock TX, 79410-1051, USA*

³*Department of Physics and Materials Science, Faculty of Science, Chiang Mai University, Chiang Mai, Thailand 50200*

Revised 2023 June 27; in original form 2023 April 5

ABSTRACT

We compile a catalogue of low-mass and high-mass X-ray binaries, some recently reported binaries that likely host a neutron star (NS) or a black hole (BH), and binary pulsars (a pulsar and a non-degenerated companion) that have measured systemic radial velocities (γ). Using *Gaia* and radio proper motions together with γ , we integrate their Galactic orbits and infer their post-supernova (post-SN) 3D peculiar velocities ($v_{\text{pec}}^{z=0}$ at Galactic plane crossing); these velocities bear imprint of natal kicks that compact objects received at birth. With the sample totalling 85 objects, we model the overall distribution of $v_{\text{pec}}^{z=0}$ and find a two-component Maxwellian distribution with a low- ($\sigma_v \approx 21 \text{ km s}^{-1}$) and a high-velocity ($\sigma_v \approx 107 \text{ km s}^{-1}$) component. A further comparison between distributions of binary subgroups suggests that binaries hosting high-mass donors/luminous companions mostly have $v_{\text{pec}}^{z=0} \lesssim 100 \text{ km s}^{-1}$, while binaries with low-mass companions exhibit a broader distribution that extends up to $\sim 400 \text{ km s}^{-1}$. We also find significant anti-correlations of $v_{\text{pec}}^{z=0}$ with binary total mass (M_{tot}) and orbital period (P_{orb}), at over 99% confidence. Specifically, our fit suggests $v_{\text{pec}}^{z=0} \propto M_{\text{tot}}^{-0.5}$ and $v_{\text{pec}}^{z=0} \propto P_{\text{orb}}^{-0.2}$. Discussions are presented on possible interpretation of the correlations in the context of kinematics and possible biases. The sample should enable a range of follow-up studies on compact object binary kinematics and evolution.

Key words: stars: neutron – stars: black holes – supernovae: general – parallaxes – proper motions

1 INTRODUCTION

The deaths of massive stars can deliver an extra acceleration to their remnant black holes (BHs; Brandt et al. 1995; Jonker & Nelemans 2004) and neutron stars (NSs; Trimble 1971; Lyne et al. 1982; Lyne & Lorimer 1994) at the instant of supernovae (SNe). This impulse, termed a natal kick or NK, connects SN mechanisms to the kinematics of compact objects, providing a way of constraining multiple aspects of SN models. For example, NKs can be a result of recoil due to baryonic ejecta at the instant of SNe (Blaauw 1961; Brandt & Podsiadlowski 1995; Nelemans et al. 1999), or, in later stages, due to anisotropy in gravitational attraction of compact object by the asymmetric ejecta (Janka 2013, 2017) — NKs could therefore be related to ejecta mass and/or morphology, and some observational support for this scenario exists (Holland-Ashford et al. 2017). The recoil momentum can also be contributed by asymmetric neutrino emission, typically in highly magnetised and hot nuclear matter of nascent NSs, where neutrino emissivity and opacity is dependent on its direction relative to local magnetic fields (Chugai 1984; Dorofeev et al. 1985; Arras & Lai 1999). More fundamentally, causes of asymmetries in ejecta or neutrino emission are related to intrinsic hydrodynamical processes (see Lai 2004, for a review).

Observations of NSs or BHs or binaries that host them have put

some constraints on NKs. Pulsars have long been observed to have high space velocities (mean velocity of $\approx 300 \text{ km s}^{-1}$) relative to their presumed OB progenitors (Gunn & Ostriker 1970; Lyne & Lorimer 1994; Hobbs et al. 2005; Kapil et al. 2023), suggestive of high NKs, although a relatively low-velocity (mean $\approx 120 \text{ km s}^{-1}$) population is also present (Brisken et al. 2003; Verbunt et al. 2017; Igoshev 2020). While isolated NSs might be observed as radio pulsars, constraining the kinematics of isolated BHs can only be done in rare microlensing events (Sahu et al. 2022; Lam et al. 2022; Andrews & Kalogera 2022) or via accretion from the interstellar medium (Fujita et al. 1998; Maccarone 2005). X-ray binaries (XRBs) that host a NS or BH are advantageous targets in this regard, because the luminous companion can be used to constrain orbital parameters and track systemic motion; inference on NKs can therefore be made using observed peculiar motions of BH and NS XRBs in Galactic potential (e.g., Mirabel et al. 2001; Gandhi et al. 2019; Atri et al. 2019; Fortin et al. 2022; O’Doherty et al. 2023) and results of binary evolutionary models (e.g., Fragos et al. 2009; Kimball et al. 2022).

In addition to the kinematic inferences of NKs, there have also been indirect constraints from other perspectives. The eccentric ($e \gtrsim 0.3$) orbits of Be X-ray binaries are indicative of large NKs (Verbunt & van den Heuvel 1995; Brandt & Podsiadlowski 1995; van den Heuvel et al. 2000), but there might also be a separate population of long-orbit and low-eccentricity high-mass X-ray binaries (HMXBs) that argue against a large NK (Pfahl et al. 2002b; Podsiadlowski et al.

* E-mail: zhao.yue@soton.ac.uk

2004; Knigge et al. 2011). The retention fraction of NSs in globular clusters is another indicator of NK magnitude: even a moderate number of NSs (in XRBs) is at odds with large NKs derived from pulsar observations as they are hard to be retained by typical escape velocities of globular clusters ($\lesssim 50 \text{ km s}^{-1}$; Pfahl et al. 2002a; Smits et al. 2006; Ivanova et al. 2008).

In this work, we compile a more comprehensive sample of binaries that host a NS or BH (so they have experienced only one NK), calculate their peculiar motion in Galactic potential, and investigate possible dependencies of their observed peculiar velocities on binary total mass and other orbital parameters. The sample includes binary pulsars (a binary that hosts a pulsar and a non-degenerate companion or sometimes a white dwarf), low- and high-mass XRBs, and non-interacting binaries hosting NSs or BHs. In Sec 2, we describe sample compilation, inference of distances, and calculation of peculiar velocities; in Sec 3 we describe statistical methods used in our analyses and present the results; in Sec 4, we discuss possible interpretation of and possible biases in the results; and in Sec 5, we summarise the results and draw conclusions.

2 METHODOLOGY

2.1 The raw sample

To construct our sample, we start by concatenating compilations of different types of BH or NS binaries. For XRBs, we use the BlackCAT catalogue¹ (Corral-Santana et al. 2016, and references therein) and the catalogues of low-mass and high-mass XRBs (LMXBs and HMXBs) compiled by Liu et al. (2007) and Liu et al. (2006), respectively (L06 and L07, hereafter), and a recent HMXB catalogue compiled by Fortin et al. (2023). Additionally, we include binaries that have been recently suggested to host BHs or NSs, including 2MASS J05215658+4359220 (Thompson et al. 2019, J052156), AS 386 (Khokhlov et al. 2018), HD 96670 (Gomez & Grindlay 2021), 2XMM J125556.57+565846.4 (Mazeh et al. 2022, J125556), Gaia BH1 (El-Badry et al. 2023b), Gaia BH2 (Tanikawa et al. 2022; El-Badry et al. 2023a), LAMOST J112306.9+400736 (Yi et al. 2022, J112306), 2MASS J15274848+3536572 (Lin et al. 2023, J15274848), 2MASS J06163552+2319094 (Yuan et al. 2022, J06163552), and LAMOST J235456.76+335625.7 (Zheng et al. 2022, J235456). Finally, we also include a sample of binary pulsars selected from the Australia Telescope National Facility (ATNF version 1.67) pulsar catalogue² (Manchester et al. 2005), using `type(binary)` to select pulsars with one or more companions.

2.2 Binaries excluded

We exclude XRBs in globular clusters from our sample because their present-day velocities do not reflect the kinematics and SN kicks at birth. Most XRBs in globular clusters are thought to form via dynamical encounters between compact objects and normal stars (e.g., Fabian et al. 1975; Hills 1976; Camilo & Rasio 2005), after which the systems have lost track of the SN impact. Even if there are XRBs in globular clusters that formed through primordial binary evolution (similar to field XRBs), their systemic motion could have been greatly modified by encounters after formation. We also do not consider double pulsars as their progenitors might have experienced two

supernovae, which makes them distinct from the single-degenerate binaries in our sample.

2.3 Binary type names

Binaries in our compilation are labelled based on their compact objects, NS or BH, and the mass of the non-degenerate companions, either low-mass (LM) or high-mass (HM) according to classification in the literature; for non-interacting binaries (NIs), we consider those with non-degenerate companion mass below $2 M_{\odot}$ as LM, while those above as HM. Concretely, there are BH or NS low-mass and high-mass XRBs (labelled: BH- or NS-LMXBs or HMXBs), low-mass or high-mass non-interacting (NI) binaries that host BH or NS (BH or NS-HMNI/LMNI). Pulsars are labelled separately from the XRBs by the mass of their non-degenerate companions (as LM or HM-PSR), although they are evolutionarily related to NS XRBs.

2.4 Binary masses and orbital periods

We also include available component masses and orbital periods from the literature. For binary component masses, we use the following notation: in any binary, M_1 is used to denote mass of the compact object (either a BH or a NS), while M_2 refers to the mass of the non-degenerate component: for XRBs it refers to the mass donor; and for NIs, this is the luminous component. $M_{\text{tot}} = M_1 + M_2$ is the total mass of a binary. For binaries that host a NS, we assume a canonical NS mass (M_1) of $1.4 M_{\odot}$ when there are no constraints in the literature. We denote orbital period by P_{orb} , as distinct from the value at time of SN ($P_{\text{orb,SN}}$) used in the discussion sections (Sec 4). A list of notations is presented in Appendix D.

2.5 Identification with *Gaia*

We cross-match literature positions of our sample with source positions in *Gaia* Data Release 3 (Gaia Collaboration et al. 2016, 2022). Since position uncertainties are not consistently estimated and some are unavailable, we use a relatively large search radius of $2''$ to find potential counterparts. Inevitably, some binaries in our list have multiple *Gaia* sources within the search radius; we therefore further compare their literature astrometric (available for some PSRs and XRBs) and photometric properties (of the optical counterparts) to those measured by *Gaia*, manually removing unlikely matches.

The HMXBs are cross-checked with Fortin et al. (2022), who complemented L06 with the latest *INTEGRAL* catalogue (Bird et al. 2016), compiling a list of 58 unambiguous *Gaia* identifications with Galactic HMXBs. For LMXBs, Gandhi et al. (2019) reported a list of 18 matches dynamically confirmed BH systems with *Gaia* DR2, including at most 16 BH-LMXBs; all their matches are confirmed by our search; a larger catalogue of *Gaia* (DR2) counterparts to LMXBs is summarised in Arnason et al. (2021), where a total of 32 LMXBs are identified. Jennings et al. (2018) cross-matched the binary pulsars from the ATNF with *Gaia* DR2, giving a total 22 binary pulsars that have confident *Gaia* counterparts; for this work, we exclude the extragalactic PSR J0045–7319 (Storm et al. 2004), and the triple system PSR J0337+1715 (Ransom et al. 2014). Finally, we also cross-check our compilation of NS-LMXBs and binary pulsars with O’Doherty et al. (2023).

The identified *Gaia* `source_id` values are further cross-checked with sources in the `gaiadr3.nss_two_body_orbit` table. This table contains sources whose astrometric solution is compatible with a two-body system, compared to the single-body solutions in the

¹ <https://www.astro.puc.cl/BlackCAT/index.php>

² <https://www.atnf.csiro.au/research/pulsar/psrcat/>

main table, some bright sources could have much more constrained parameters with a two-body model. Three of our sources are also in this table, including Gaia BH1, Gaia BH2, and J125556; however, only Gaia BH1 and BH2 have derived parallaxes and proper motions. We thus adopt two-body solution for these two sources, while using solutions in the main table for the other binaries. Parallaxes from the main *Gaia* table are corrected for zeropoint offset using the `GAIAADR3_ZEROPPOINT` package³ (Lindgren et al. 2021) except for Gaia BH1 and BH2 whose parallaxes are from non-single star solutions.

2.5.1 New binary pulsar matches with *Gaia* DR3

Our positional match confirms all confident counterparts in Jennings et al. (2018) and finds 7 new matches; four of these matches have a literature systemic radial velocity so are included for our calculation and analyses (Sec 2.7). We therefore further investigate the four pulsars by comparing literature (from ATNF) and *Gaia* astrometry, and by searching for identification in literature. Here we summarise the confident matches.

PSR J1306–4035 is a millisecond pulsar (MSP) that was discovered by the SURvey for Pulsars and Extragalactic Radio Bursts (SUPERB; Keane et al. 2018). Linares et al. (2018) discovered a variable optical source (SSS J130656.3–403522) within the radio error circle ($\approx 7''$); the source is modulated at the same period ($P \approx 1.1$ day) as its X-ray flux, confirming its association with the pulsar. We found that the *Gaia* source 6140785016794586752 is within the $0.36''$ error circle (combining positional error in Linares et al. (2018) and in *Gaia*), and the *Gaia* G-band magnitude (18.09) is consistent with the V-band magnitudes reported in Linares et al. (2018, 17.4–18.4); we therefore consider this match genuine.

PSR J1622–0315 is a MSP discovered in Fermi unassociated sources (Sanpa-Arsa 2016). The orbital light curve is modulated at half of its orbital period (≈ 0.16 days), varying between $R = 19.1$ and 19.4 . There is only one *Gaia* source, 4358428942492430336, in our search radius. This source is $0.07''$ away from the nominal position and has a *Gaia* G-band magnitude of 19.21, consistent with the observed light curve in Sanpa-Arsa (2016). This match is therefore confident.

PSR J1653–0158 is a fast-spinning ($P_{\text{spin}} = 1.97$ ms) and very compact ($P_{\text{orb}} = 75$ min) binary pulsar that was recently discovered to be associated with the *Fermi Large Area Telescope* (LAT) source 4FGL J1653.6–0158 (Nieder et al. 2020). The pulsar nature is confirmed by gamma-ray pulsations with Einstein@Home (Allen et al. 2013). Consistency in astrometry with *Gaia* has been confirmed by (Nieder et al. 2020). We therefore also include this pulsar in our calculation.

PSR J2039–5617 is another pulsar confirmed by detection of gamma-ray pulsations (Clark et al. 2021), where a *Gaia* DR2 counterpart was confirmed. In our search, this counterpart is ≈ 8 mas from the *Gaia* DR3 source 6469722508861870080, and has consistent and better constrained astrometry compared to DR2. This match is therefore also robust.

2.6 Radio interferometric and timing astrometry

There are a few of XRBs and binary pulsars with literature astrometry measured by radio observations (interferometric or timing), which might be more constrained compared to *Gaia*. We adopt radio measurement in our analyses if *Gaia* astrometry is not available or if radio

parallax or any of the proper motion component is more constrained than *Gaia* measurement.

Of the selected binaries, 14 have known radio parallaxes and/or proper motions, ten of which have more constrained radio astrometry. These binaries are summarised in Table 1 and are indicated with superscripts that point to the corresponding references.

2.7 The final sample

The analysis in this work (Sec 3.3) is built on 3D physical velocities, which in turn requires input of proper motion, systemic radial velocity (γ), and distance (or parallax). Therefore, from the list of binaries that have *Gaia* counterparts, we are specifically interested in those with already established γ , as well as

- well-constrained *Gaia* parallaxes (ϖ) such that $0 < \sigma_{\varpi}/\varpi < 0.2$, or
- already constrained distances in literature.

Including the two BH-LMXBs that only have radio parallaxes and proper motions, i.e., GRS 1915+105 and MAXI J1836–194, our final sample contains a total of 89 binaries. There are 4 binaries that have known γ values but has no well-constrained parallaxes or established distances, including 2S 0921–630, GX 1+4, BW Cir, and GX 339–4. BW Cir and GX 339–4 have lower limits on d_{lit} (Table C1, available online), while 2S 0921–630 and GX 1+4 only have approximate distances. The latter are also listed in Table C1 but are not used in modelling the distance prior (Sec 2.8). All of these 89 sources are summarised in Table 1.

2.8 The distances

We denote the distances estimated from trigonometric parallaxes by d_{ϖ} . For our estimation, we treat relatively nearby binaries ($\varpi > 2$) that have well-constrained ($\sigma_{\varpi}/\varpi < 0.2$) parallaxes separately from the other binaries. Since they have good-quality astrometric solution, we directly invert the parallax to get the distance, i.e., $d_{\varpi} = 1/\varpi$, and the uncertainty is simply propagated from the uncertainty in parallax, i.e., $\sigma_{d_{\varpi}} = \sigma_{\varpi}/\varpi^2$. For other binaries, we follow a Bayesian approach to infer distances from parallaxes.

2.8.1 Pulsars

Lorimer et al. (2006) derived a Galactic pulsar distribution in the vertical (z) and radial (r) directions (eq 10 and 11 in Lorimer et al. 2006). Based on the distributions, Verbiest et al. (2012) derived a distance prior for pulsars as:

$$p(d|z, r) \propto d^2 r^{1.9} \exp \left[-\frac{|z|}{E} - \frac{5(r - R_{\odot})}{R_{\odot}} \right]. \quad (1)$$

Here, r is the Galactocentric distance projected in the Galactic plane, and z is the vertical coordinate in cylindrical Galactocentric frame, which are both implicitly dependent on d . E is the vertical scale height, for which we choose $E = 500$ pc as suggested by Verbiest et al. (2012).

We use a Gaussian likelihood (see e.g., Bailer-Jones et al. 2021) that centres on the inverse of the distance and spreads according to the uncertainty on parallax, i.e.,:

$$p(\varpi|d, \sigma_{\varpi}) = \frac{1}{\sqrt{2\pi}\sigma_{\varpi}} \exp \left[-\frac{1}{2\sigma_{\varpi}^2} \left(\varpi - \frac{1}{d} \right)^2 \right], \quad (2)$$

³ https://gitlab.com/icc-ub/public/gaiadr3_zeropoint

Table 1. Selected *Gaia* counterparts.

Name	Class	Gaia DR3	α (ICRS) (h:m:s)	δ (ICRS) ($^{\circ}$: ' : ")	ϖ (mas)	$\mu_{\alpha} \cos \delta$ (mas yr $^{-1}$)	μ_{δ} (mas yr $^{-1}$)
2S 0921–630	NS-LMXB	5250451391698996992	09:22:34.669	−63:17:41.288	0.10 ± 0.02	−3.16 ± 0.03	4.25 ± 0.03
4U 1254–69	NS-LMXB	5844938121765636864	12:57:37.167	−69:17:19.018	0.18 ± 0.16	−5.34 ± 0.19	−1.32 ± 0.21
Cen X-4	NS-LMXB	6205715168442046592	14:58:21.936	−31:40:08.406	0.55 ± 0.13	0.84 ± 0.15	−55.68 ± 0.13
Sco X-1	NS-LMXB	4328198145165324800	16:19:55.061	−15:38:25.215	0.47 ± 0.02	−7.19 ± 0.03	−12.33 ± 0.02
4U 1636–536	NS-LMXB	5930753870442684544	16:40:55.587	−53:45:05.081	0.29 ± 0.12	−5.90 ± 0.16	−8.33 ± 0.12
Her X-1	NS-LMXB	1338822021487330304	16:57:49.809	+35:20:32.361	0.14 ± 0.01	−1.21 ± 0.01	−7.86 ± 0.02
MXB 1659–298	NS-LMXB	6029391608332996224	17:02:06.534	−29:56:44.286	0.22 ± 0.23	−1.62 ± 0.52	−1.51 ± 0.33
4U 1700+24	NS-LMXB	4571810378118789760	17:06:34.503	+23:58:18.550	1.87 ± 0.05	−8.73 ± 0.04	−5.57 ± 0.05
GX 1+4	NS-LMXB	4110236324513030656	17:32:02.149	−24:44:44.161	−0.02 ± 0.07	−3.52 ± 0.08	−1.99 ± 0.06
4U 1735–444	NS-LMXB	5955379701104735104	17:38:58.233	−44:27:00.820	0.12 ± 0.10	−3.47 ± 0.12	−7.54 ± 0.07
XTE J1814–338	NS-LMXB	4039437121598306176	18:13:39.102	−33:46:23.865	1.07 ± 0.48	2.80 ± 0.47	−3.99 ± 0.40
2A 1822–371	NS-LMXB	6728016172687965568	18:25:46.806	−37:06:18.570	0.18 ± 0.03	−9.15 ± 0.04	−2.53 ± 0.03
Ser X-1	NS-LMXB	4283919201304278912	18:39:57.544	+05:02:09.433	−0.00 ± 0.27	−1.14 ± 0.36	−3.63 ± 0.27
Aql X-1	NS-LMXB	4264296556603631872	19:11:16.055	+00:35:05.786	0.21 ± 0.28	−1.80 ± 0.58	−5.13 ± 0.58
Cyg X-2	NS-LMXB	1952859683185470208	21:44:41.152	+38:19:17.061	0.10 ± 0.02	−1.79 ± 0.02	−0.32 ± 0.02
IGR J00370+6122	NS-HMXB	427234969757165952	00:37:09.632	+61:21:36.479	0.29 ± 0.01	−1.80 ± 0.01	−0.53 ± 0.01
2S 0114+650	NS-HMXB	524924310153249920	01:18:02.694	+65:17:29.841	0.22 ± 0.01	−1.24 ± 0.01	0.76 ± 0.01
RX J0146.9+6121	NS-HMXB	511220031584305536	01:47:00.210	+61:21:23.662	0.37 ± 0.02	−1.03 ± 0.02	−0.08 ± 0.02
LS I +61 303	NS-HMXB	465645515129855872	02:40:31.664	+61:13:45.590	0.40 ± 0.01	−0.42 ± 0.01	−0.26 ± 0.01
X Persi	NS-HMXB	168450545792009600	03:55:23.076	+31:02:45.010	1.67 ± 0.04	−1.28 ± 0.05	−1.87 ± 0.03
XTE J0421+560	NS-HMXB	276644757710014976	04:19:42.135	+55:59:57.698	0.24 ± 0.01	−0.47 ± 0.02	−0.51 ± 0.01
EXO 051910+3737.7	NS-HMXB	184497471323752064	05:22:35.233	+67:40:33.575	0.76 ± 0.03	1.30 ± 0.04	−4.00 ± 0.03
1A 0535+262	NS-HMXB	3441207615229815040	05:38:54.574	+26:18:56.791	0.56 ± 0.02	−0.59 ± 0.03	−2.88 ± 0.02
HD 259440	NS-HMXB	3131822364779745536	06:32:59.257	+05:48:01.154	0.57 ± 0.02	−0.03 ± 0.02	−0.43 ± 0.02
IGR J08408–4503	NS-HMXB	5522306019626566528	08:40:47.780	−45:03:30.138	0.45 ± 0.02	−7.46 ± 0.02	6.10 ± 0.02
Vela X-1	NS-HMXB	5620657678322625920	09:02:06.854	−40:33:16.751	0.51 ± 0.02	−4.82 ± 0.01	9.28 ± 0.02
2FGL J1019.0–5856	NS-HMXB	5255509901121774976	10:18:55.574	−58:56:45.939	0.23 ± 0.01	−6.45 ± 0.01	2.26 ± 0.01
Cen X-3	NS-HMXB	5337498593446516480	11:21:15.085	−60:37:25.593	0.15 ± 0.01	−3.12 ± 0.02	2.33 ± 0.01
1E 1145.1–6141	NS-HMXB	5334851450481641088	11:47:28.546	−61:57:13.389	0.12 ± 0.01	−6.23 ± 0.01	2.36 ± 0.01
2S 1145–619	NS-HMXB	5334823859608495104	11:48:00.007	−62:12:24.877	0.49 ± 0.02	−6.23 ± 0.02	1.60 ± 0.02
GX 301–2	NS-HMXB	6054569565614460800	12:26:37.548	−62:46:13.294	0.28 ± 0.02	−5.23 ± 0.02	−2.07 ± 0.02
1H 1253–761	NS-HMXB	5837600152935767680	12:39:14.458	−75:22:14.269	4.79 ± 0.03	−27.34 ± 0.03	−8.93 ± 0.04
1H 1249–637	NS-HMXB	6055103928246312960	12:42:50.236	−63:03:31.112	2.30 ± 0.08	−12.86 ± 0.07	−3.68 ± 0.07
1H 1255–567	NS-HMXB	6060547335455660032	12:54:36.828	−57:10:07.361	8.29 ± 0.12	−28.39 ± 0.09	−10.45 ± 0.11
4U 1538–52	NS-HMXB	5886085557746480000	15:42:23.352	−52:23:09.643	0.18 ± 0.02	−6.71 ± 0.01	−4.11 ± 0.01
4U 1700–37	NS-HMXB	5976382915813535232	17:03:56.776	−37:50:38.833	0.67 ± 0.03	2.41 ± 0.03	5.02 ± 0.02
IGR J17544–2619	NS-HMXB	4063908810076415872	17:54:25.272	−26:19:52.588	0.42 ± 0.03	−0.51 ± 0.03	−0.67 ± 0.02
LS 5039	NS-HMXB	4104196427943626624	18:26:15.064	−14:50:54.378	0.53 ± 0.02	7.43 ± 0.01	−8.15 ± 0.01
1H 2202+501	NS-HMXB	1979911002134040960	22:01:38.206	+50:10:04.629	0.90 ± 0.01	2.36 ± 0.01	−0.29 ± 0.01
4U 2206+543	NS-HMXB	2005653524280214400	22:07:56.229	+54:31:06.356	0.32 ± 0.01	−4.17 ± 0.02	−3.32 ± 0.01
A 0620–00	BH-LMXB	3118721026600835328	06:22:44.542	−00:20:44.373	0.73 ± 0.12	−0.44 ± 0.11	−5.14 ± 0.10
XTE J1118+480	BH-LMXB	789430249033567744	11:18:10.764	+48:02:12.208	0.18 ± 0.27	−18.10 ± 0.16	−6.69 ± 0.22
GRS 1124–684	BH-LMXB	5234956524083372544	11:26:26.588	−68:40:32.900	0.19 ± 0.24	−2.93 ± 0.24	−1.39 ± 0.26
MAXI J1305–704	BH-LMXB	5843823766718594560	13:06:55.280	−70:27:05.101	−0.50 ± 0.57	−7.89 ± 0.62	−0.16 ± 0.72
BW Cir	BH-LMXB	5852296053620905472	13:58:09.710	−64:44:05.292	1.28 ± 0.53	−5.07 ± 0.63	−2.11 ± 0.58
4U 1543–475	BH-LMXB	5986117923045619072	15:47:08.265	−47:40:10.370	0.22 ± 0.06	−7.54 ± 0.05	−5.36 ± 0.05
XTE J1550–564	BH-LMXB	5884099221246440064	15:50:58.651	−56:28:35.314	2.29 ± 2.58	−6.49 ± 1.96	−3.49 ± 1.74
GRO 1655–40	BH-LMXB	5969790961312131456	16:54:00.136	−39:50:44.881	0.33 ± 0.05	−4.33 ± 0.06	−7.46 ± 0.05
GX 339–4	BH-LMXB	5938658156448950528	17:02:49.381	−48:47:23.166	0.21 ± 0.12	−3.95 ± 0.07 ^a	−4.71 ± 0.06 ^a
H 1705–250	BH-LMXB	4112450294268643456	17:08:14.500	−25:05:30.296	2.15 ± 1.67	−6.97 ± 2.83	−8.51 ± 1.38
Swift J1753.5–0127	BH-LMXB	4178766135477201408	17:53:28.291	−01:27:06.313	0.17 ± 0.09	0.99 ± 0.09	−3.54 ± 0.09
MAXI J1820+070	BH-LMXB	4477902563164690816	18:20:21.939	+07:11:07.184	0.40 ± 0.08	−3.09 ± 0.09	−6.29 ± 0.09
MAXI J1836–194	BH-LMXB	...	18:35:43.445 ^b	−19:19:10.484 ^b	...	−2.30 ± 0.60 ^c	−6.10 ± 1.00 ^c
GRS 1915+105	BH-LMXB	...	19:15:11.550 ^d	+10:56:44.800 ^d	...	−2.86 ± 0.07 ^e	−6.20 ± 0.09 ^e
V404 Cyg	BH-LMXB	2056188624872569088	20:24:03.818	+33:52:01.837	0.42 ± 0.02 ^f	−5.18 ± 0.08	−7.78 ± 0.09
HD 96670	BH-HMXB?	5337747731560719616	11:07:13.920	−59:52:23.153	0.32 ± 0.03	−6.75 ± 0.03	1.69 ± 0.03
V4641 Sgr	BH-HMXB	4053096388919082368	18:19:21.633	−25:24:25.843	0.21 ± 0.03	−0.78 ± 0.03	0.43 ± 0.02
SS 433	BH-HMXB?	4293406612283985024	19:11:49.562	+04:58:57.751	0.13 ± 0.02	−3.03 ± 0.02	−4.78 ± 0.02
Cyg X-1	BH-HMXB	2059383668236814720	19:58:21.671	+35:12:05.684	0.47 ± 0.01	−3.80 ± 0.01 ^g	−6.28 ± 0.02 ^g
MWC 656	BH-HMXB?	1982359580155628160	22:42:57.298	+44:43:18.209	0.51 ± 0.02	−3.48 ± 0.02	−3.16 ± 0.02

Table 1 – *continued* Selected *Gaia* counterparts.

Name	Class	<i>Gaia</i> ID	α (ICRS) (h:m:s)	δ (ICRS) ($^{\circ}$: ' : ")	ϖ (mas)	$\mu_{\alpha} \cos \delta$ (mas yr $^{-1}$)	μ_{δ} (mas yr $^{-1}$)
PSR J0348+0432	LM-PSR	3273288485744249344	03:48:43.640	+04:32:11.458	0.47 ± 0.47^h	4.04 ± 0.16^h	3.50 ± 0.60^h
PSR J1012+5307	LM-PSR	851610861391010944	10:12:33.439	+53:07:02.134	1.75 ± 0.29	2.64 ± 0.04^i	-25.54 ± 0.04^i
PSR J1023+0038	LM-PSR	3831382647922429952	10:23:47.689	+00:38:40.729	0.73 ± 0.02^j	4.76 ± 0.03^j	-17.34 ± 0.04^j
PSR J1024-0719	LM-PSR	3775277872387310208	10:24:38.661	-07:19:19.819	0.83 ± 0.13^k	-35.28 ± 0.01^k	-48.23 ± 0.03^k
PSR J1048+2339	LM-PSR	3990037124929068032	10:48:43.416	+23:39:53.392	0.50 ± 0.44	-15.45 ± 0.35	-11.62 ± 0.34
XSS J12270-4859	LM-PSR	6128369984328414336	12:27:58.717	-48:53:42.708	0.49 ± 0.13	-18.77 ± 0.11	7.30 ± 0.09
PSR B1259-63	HM-PSR	5862299960127967488	13:02:47.637	-63:50:08.632	0.46 ± 0.01	-7.09 ± 0.01	-0.34 ± 0.01
PSR J1306-4035	LM-PSR	6140785016794586752	13:06:56.272	-40:35:23.399	0.34 ± 0.15	-6.18 ± 0.14	4.16 ± 0.11
PSR J1311-3430	LM-PSR	6179115508262195200	13:11:45.721	-34:30:30.376	1.95 ± 0.97	-6.13 ± 1.60	-5.14 ± 0.68
PSR J1417-4402	LM-PSR	6096705840454620800	14:17:30.566	-44:02:57.580	0.24 ± 0.05	-4.76 ± 0.04	-5.10 ± 0.05
PSR J1431-4715	LM-PSR	6098156298150016768	14:31:44.613	-47:15:27.632	0.56 ± 0.13	-11.82 ± 0.14	-14.52 ± 0.15
PSR J1622-0315	LM-PSR	4358428942492430336	16:22:59.627	-03:15:37.266	0.64 ± 0.30	-13.18 ± 0.32	2.30 ± 0.23
PSR J1628-3205	LM-PSR	6025344817107454464	16:28:07.002	-32:05:49.021	0.69 ± 0.41	-6.19 ± 0.47	-21.43 ± 0.34
PSR J1653-0158	LM-PSR	4379227476242700928	16:53:38.053	-01:58:36.895	1.79 ± 0.78	-17.30 ± 0.95	-3.24 ± 0.72
PSR J1723-2837	LM-PSR	4059795674516044800	17:23:23.179	-28:37:57.595	1.11 ± 0.04	-11.73 ± 0.04	-24.05 ± 0.03
PSR J1816+4510	LM-PSR	2115337192179377792	18:16:35.934	+45:10:33.847	0.22 ± 0.10	5.30 ± 0.80^l	-3.00 ± 1.00^l
PSR J2039-5617	LM-PSR	6469722508861870080	20:39:34.968	-56:17:09.276	0.51 ± 0.17	3.86 ± 0.14	-15.18 ± 0.12
PSR J2129-0429	LM-PSR	2672030065446134656	21:29:45.060	-04:29:06.811	0.51 ± 0.07	12.10 ± 0.07	10.19 ± 0.06
PSR J2215+5135	LM-PSR	2001168543319218048	22:15:32.687	+51:35:36.437	0.32 ± 0.23	0.01 ± 0.24	2.24 ± 0.24
PSR J2339-0533	LM-PSR	2440660623886405504	23:39:38.745	-05:33:05.273	0.55 ± 0.18	3.92 ± 0.20	-10.28 ± 0.19
J05215658	BH-HMNI	207628584632757632	05:21:56.591	+43:59:21.899	0.41 ± 0.02	-0.50 ± 0.02	-3.46 ± 0.01
J06163552	NS-LMNI	3425175331243738240	06:16:35.525	+23:19:09.285	0.96 ± 0.02	-1.43 ± 0.02	-4.97 ± 0.01
J112306.9	NS-LMNI	770431444010267392	11:23:06.909	+40:07:36.366	3.19 ± 0.04	-20.60 ± 0.03	-24.28 ± 0.04
J125556.57	NS-LMNI	1577114915964797184	12:55:56.553	+56:58:46.498	1.73 ± 0.01	-9.12 ± 0.01	10.67 ± 0.01
Gaia BH2	BH-LMNI	5870569352746779008	13:50:16.732	-59:14:20.418	0.86 ± 0.02	-10.48 ± 0.10	-4.61 ± 0.06
J15274848	NS-LMNI	1375051479376039040	15:27:48.437	+35:36:57.376	8.48 ± 0.01	-32.00 ± 0.01	4.07 ± 0.01
Gaia BH1	BH-LMNI	4373465352415301632	17:28:41.090	-00:34:51.931	2.10 ± 0.02	-7.70 ± 0.02	-25.85 ± 0.03
AS 386	BH-HMNI	2061686870220386816	20:10:54.197	+38:18:09.284	0.17 ± 0.01	-2.66 ± 0.01	-4.88 ± 0.01
J235456.76	NS-LMNI	2874966759081257728	23:54:56.765	+33:56:25.697	7.86 ± 0.02	23.21 ± 0.02	-18.93 ± 0.01

ϖ is the parallax after zeropoint correction except for Gaia BH1 and BH2.

Classes: (NS)BH-(H)LMXB: (neutron star) black hole (high) low-mass X-ray binary; (NS)BH-(H)LMNI: non-interacting neutron star (black hole) binary with a (high) low-mass companions; (H)LM-PSR: binary pulsar with a (high) low-mass companion.

References: ^a: Atri et al. (2019), ^b: Russell et al. (2015), ^c: Russell et al. (2014), ^d: Dhawan et al. (2000), ^e: Reid et al. (2014b), ^f: Miller-Jones et al. (2009), ^g: Miller-Jones et al. (2021), ^h: Antoniadis et al. (2013), ⁱ: ATNF, ^j: Deller et al. (2012), ^k: Reardon et al. (2021), ^l: Stovall et al. (2014).

where the ϖ and σ_{ϖ} are parallax and the associated uncertainty, respectively. The posterior of distance is then given by Bayes' theorem:

$$p(d|\varpi, \sigma_{\varpi}, z, r) \propto p(d|z, r)p(\varpi|d, \sigma_{\varpi}). \quad (3)$$

2.8.2 XRBs and others

The remaining binaries are primarily XRBs and several NI binaries that likely host a BH or NS. To make a probabilistic estimate of their distances, we use the same likelihood as that for the pulsars (eq 2), and the exponential prior following Gandhi et al. (2019), which has the form of:

$$p(d) = \begin{cases} \frac{1}{2L^3} d^2 \exp\left(-\frac{d}{L}\right) & r > 0 \\ 0 & r \leq 0 \end{cases}. \quad (4)$$

This prior is characterised only by a scaling parameter L , which was found to be 2.17 ± 0.12 kpc by Gandhi et al. (2019).

In this work, we use a more extended sample to model this prior. Since this prior is used for XRBs and non-interacting binaries with compact objects, we cross-check the list of sources in L06, L07, and BlackCAT for distances not inferred from parallaxes (denoted by d_{lit}), including only values of d_{lit} that have reported uncertainties

or lower limits. The final d_{lit} sample includes a total of 125 such binaries, which are summarised in Table C1. Most of the constrained values of d_{lit} have symmetric uncertainties, while for the asymmetric uncertainties, we use the central value $((d_{\text{lit,low}} + d_{\text{lit,up}})/2)$ for our modelling. For the constrained values, we draw 10,000 random distances for each binary in the sample as per a Gaussian distribution, with the standard deviation set to the maximum between upper and lower uncertainties; for the lower limits on d_{lit} , we sample from a flat distribution between $d_{\text{lit,low}}$ and $d_{\text{lit,low}} + 5$ kpc — this upper limit was used by Gandhi et al. (2019) who also found that the result is not sensitive on choices of this limit. For each set of random distances, we compute the joint probability

$$\mathcal{L}_n = \prod_i p(d_{i,n}|L), \quad (5)$$

where p is given by eq (4), i indicates binaries in the sample, and n indexes the random realisations. We search on a grid of L for the value that maximises the joint probability — considered a best-fitting scaling parameter. This procedure results in a distribution of L with a median of $1.97^{+0.05}_{-0.05}$ kpc (errors correspond to 16th and 84th percentiles).

With the constructed likelihood and priors, we make Bayesian distance inference for binaries with good astrometry ($\sigma_{\varpi}/\varpi < 0.2$) and sample a total of 10^6 random distances as per their posterior

distributions using inverse transform sampling. In Table 3, we report medians and calculating a 68.27% equal-tailed interval of the sampled distances for each binary.

2.9 The peculiar velocities

Peculiar velocity (v_{pec}) is the magnitude of 3-dimensional velocity relative to local Galactic rotation. For our calculation, we want to propagate uncertainties not only in source-specific parameters (parallax, proper motion, and radial velocity) but also in Galactic constants (Table 2) to the final v_{pec} ; we therefore follow the formulation derived by Reid et al. (2009), assuming a Gaussian distribution for the source kinematic parameters, viz. proper motion and radial velocity, and for the Galactic constants. Distances are sampled from the posterior derived in Sec 2.8; for binaries that have poorly constrained or invalid (zero or negative) *Gaia* parallaxes (Sec 2.7), we sample from a Gaussian distribution that centres at the distances inferred from dispersion measures from Yao et al. (2017) with 20% uncertainty as standard deviation for pulsars, and a Gaussian distribution that centres at the d_{lit} with symmetrised (averaged upper and lower error) uncertainty for the others (Table C1). In the last step of the calculation, the local Galactic rotation needs to be subtracted (Reid et al. 2009) from the Galactocentric 3D velocity; for this, we adjust the MWPotential2014 potential in the GALPY package⁴ (version 1.8.3, Bovy 2015) to adopt the Galactic constants used in this work (Table 2) and use it to find the local rotation velocity.

As mentioned in Sec 2.7, there are 4 binaries that have neither well-constrained *Gaia* parallaxes nor d_{lit} , but two of them have lower limits on d_{lit} ($d_{\text{lit,low}}$), i.e., BW Cir and GX 339–4; for these two binaries, we sample from the same distribution as that in modelling the exponential prior (Sec 2.8), i.e., a uniform distribution between $d_{\text{lit,low}}$ and $d_{\text{lit,low}} + 5$ kpc, while for the other two, we sample from a Gaussian distribution that centres at the nominal d_{lit} with a 20% uncertainty. v_{pec} is calculated for these 4 binaries but should be treated with care. Indeed, physical velocities have a non-negligible dependence on distances; these 4 binaries are therefore not included in further statistical analyses.

With all the randomised parameters, we compute a sample of 10^6 v_{pec} values for each binary. Because the calculation uses present-day astrometric parameters, we refer to the calculated v_{pec} as present-day peculiar velocity, denoted by $v_{\text{pec,p}}$. We report median values and errors corresponding to 16th and 84th percentiles of $v_{\text{pec,p}}$ in Table 3.

2.10 Potential peculiar velocity at birth

The calculated $v_{\text{pec,p}}$ could deviate from the v_{pec} at birth depending on the binary’s position and kinematics under the influence of Galactic potential. We therefore also calculate the potential birth peculiar velocities (denoted by $v_{\text{pec}}^{z=0}$) following the methods used by Atri et al. (2019), who referred to these as “potential kick velocities”. In short, for each binary, we set up a total of 5,000 orbit instances by randomly drawing proper motions and γ values from a Gaussian and distances from the posteriors calculated in Sec 2.8. We then integrate these orbits of the binaries backward in time for 10 Gyr using GALPY and record the v_{pec} values every time the binary passes the Galactic plane (i.e., at $z = 0$). The plane crossing epochs are found by linearly interpolating the $z(t)$ component of the orbit near the Galactic plane, which are then fed to the time-dependent v_{pec} functions to obtain the

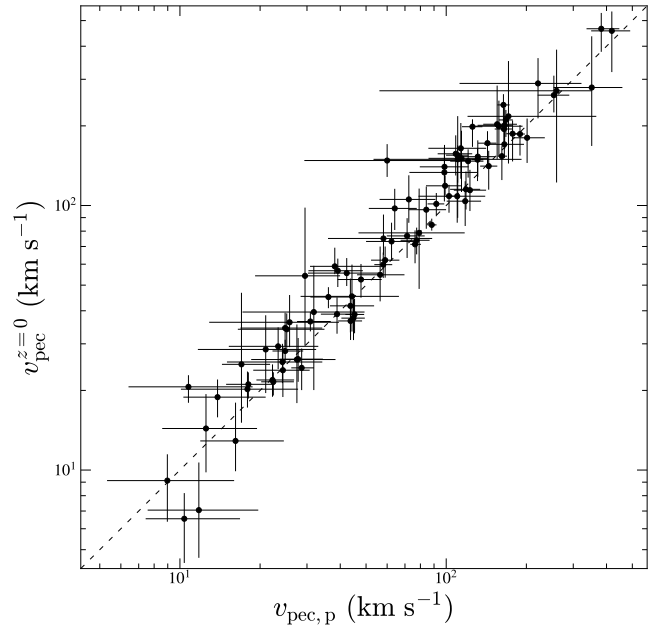


Figure 1. Median values of present-day peculiar velocity ($v_{\text{pec,p}}$) vs. those of potential peculiar velocity at birth ($v_{\text{pec}}^{z=0}$) for binaries that have measured systemic radial velocity. The error bars correspond to 16th and 84th percentiles of the distributions. The dashed line indicates $v_{\text{pec,p}} = v_{\text{pec}}^{z=0}$. Overall, $v_{\text{pec}}^{z=0}$ values agree with $v_{\text{pec,p}}$ at 68% level.

$v_{\text{pec}}^{z=0}$ distributions. The resulting $v_{\text{pec}}^{z=0}$ are the potential v_{pec} values at birth under the assumption that the binaries are born in the Galactic plane. Similar to $v_{\text{pec,p}}$, the $v_{\text{pec}}^{z=0}$ and the errors corresponding to 16th and 84th percentiles are summarised in Table 3.

Given the same uncertainties in all other parameters, $v_{\text{pec}}^{z=0}$ involves time as an extra variable that could complicate the final distributions over $v_{\text{pec,p}}$. However, calculation of $v_{\text{pec}}^{z=0}$ also reduces possible effects of time by bringing all binaries to the same epoch (the birth time) of their evolution. Moreover, $v_{\text{pec}}^{z=0}$ relates to the epoch near the birth, while using $v_{\text{pec,p}}$ as the proxy could underestimate the effect of binary evolution on the kinematics (e.g., mass loss due to stellar winds, unconservative mass transfer, etc.).

Our statistical analyses (Sec 3.2, 3.3, 3.4, 3.5) are performed on $v_{\text{pec}}^{z=0}$ and $v_{\text{pec,p}}$, but in this paper, we only report results obtained with $v_{\text{pec}}^{z=0}$. Because $v_{\text{pec,p}}$ are generally consistent with $v_{\text{pec}}^{z=0}$ at 68% confidence level (Figure 1), results using $v_{\text{pec,p}}$ are in agreement with those using $v_{\text{pec}}^{z=0}$.

3 ANALYSIS AND RESULTS

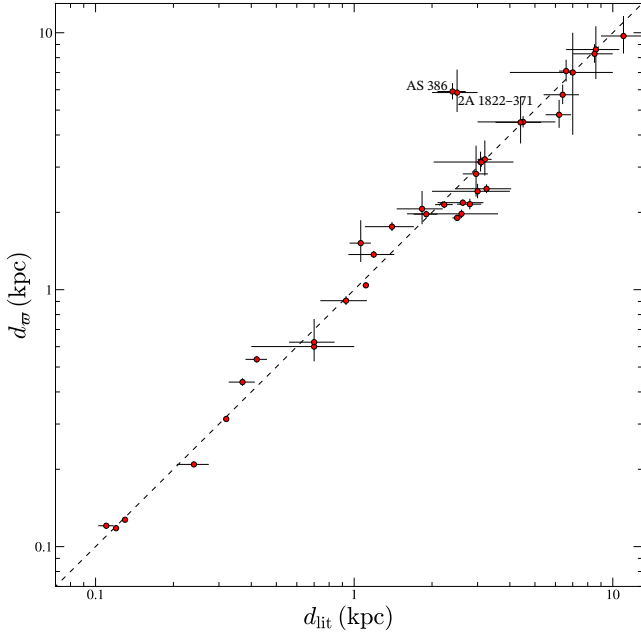
3.1 Comparing with literature distances

Distances are clearly crucial in interpreting our peculiar velocities, and so we compare the well-constrained parallax-inferred distances (d_{σ} ; Sec 2.7), with values in the literature (d_{lit} ; Table C1) if available. In Figure 2, we can see that d_{σ} agrees with d_{lit} for most binaries. However, there are two clear outliers, 2A 1822–371 and AS 386, that have somewhat smaller d_{lit} , despite both sources having an acceptable *Gaia* Renormalised Unit Weight Error (ruwe) value of

⁴ <http://github.com/jobovy/galpy>

Table 2. Galactic and solar constants used in this work.

Name	Value	Unit	Ref	Description
E	0.5	kpc	[1]	Galactic scale height of pulsar distribution; used in eq (1)
L	1.97 ± 0.05	kpc	[2]	Scaling parameter of the distance prior in eq (4)
R_{\odot}	8.34 ± 0.16	kpc	[3]	Galactocentric solar distance projected onto the plane
Θ_{\odot}	240 ± 8	km s^{-1}	[3]	Galactic rotation velocity at the location of the Sun
U_{\odot}	10.7 ± 1.8	km s^{-1}	[3]	Cartesian components of solar motion relative to the local standard of rest
V_{\odot}	15.6 ± 6.8	km s^{-1}	[3]	
W_{\odot}	8.9 ± 0.9	km s^{-1}	[3]	

 References: [1] [Verbiest et al. \(2012\)](#), [2] This work, [3] [Reid et al. \(2014a\)](#).

Figure 2. A comparison between literature distances (d_{lit}) and parallax-inferred distances (d_{π}), showing that they agree for most binaries. The error bars on d_{π} correspond to 68% confidence intervals. The two obvious outliers are labelled with their names.

0.9 and 1.2, respectively (for a satisfactory fit to a single-star model, ruwe is expected to be close to 1).⁵

The distance to 2A 1822–371 was estimated to be between 2 and 3 kpc based on the emitting region area at peak brightness of the light curve, while assuming a black-body for the inner emitting region gives an upper limit of ≈ 5 kpc ([Mason & Cordova 1982](#)), which is marginally consistent with our estimate at the 68% level.

[Khokhlov et al. \(2018, K18\)](#) estimated a distance of 2.4 ± 0.3 kpc for AS 386, which is less than half of its d_{π} ($5.9^{+0.5}_{-0.4}$ kpc). The K18 estimate is based on a fitted extinction law and an estimated reddening of ≈ 0.9 . However, with the updated 3D “Bayestar19” dust map ([Green et al. 2019](#)), we get a similar reddening at a larger distance of at least 4.7 kpc (calculated using the `DUSTMAP` package; see [Green 2018](#)). We thus adopt our estimate of distance even though the astrometric solution is mildly argued against by its ruwe value.

⁵ *Gaia* pipeline flags including ruwe and $\text{astrometric_excess_noise}$ provide an estimate of the quality of the astrometric fit, but these are degenerate with non-single star solutions (cf., [Belokurov et al. 2020](#); [Gandhi et al. 2022](#)), so we purposely do not preselect on these flags.

3.2 Distribution of peculiar velocities

With the calculated $v_{\text{pec}}^{z=0}$ samples, the first analysis we can do is to get an overview of their distribution among different subclasses. We therefore divide our compilation into four subgroups, including (1) binaries with BHs, (2) binaries with NSs, (3) binaries with LM companions, and (4) binaries with HM companions. With the calculated $v_{\text{pec}}^{z=0}$ distributions of individual binaries, we model the overall $v_{\text{pec}}^{z=0}$ distribution for these subgroups following a Bayesian approach. Given a binary class, we first construct 1,000 bootstrapped data sets for each subgroup by randomly sampling (with replacement) from the individual $v_{\text{pec}}^{z=0}$ distributions. The Bayesian model is constructed as follows: for the likelihood, we use a Maxwellian distribution:

$$f(v|\sigma_v) = \sqrt{\frac{2}{\pi}} \frac{v^2}{\sigma_v^3} \exp\left(-\frac{v^2}{2\sigma_v^2}\right), \quad (6)$$

where σ_v is the scale parameter, or a two-component Maxwellian distribution:

$$f(v|\sigma_{v,1}, \sigma_{v,2}, w) = w f(v|\sigma_{v,1}) + (1-w) f(v|\sigma_{v,2}), \quad (7)$$

where w is a weighting factor that determines contribution of the single Maxwellians that are characterised by $\sigma_{v,1}$ and $\sigma_{v,2}$, respectively. We use uninformative (flat) priors for all parameters: for a two-component Maxwellian likelihood, a flat prior between 0 and 100 km s^{-1} ($U(0, 100)$) is used for low-velocity component, while $U(0, 500)$ is used to represent the high-velocity component; for the single-component Maxwellian, we choose $U(0, 500)$ for the only scale parameter σ_v .

The established posterior given the bootstrapped data set is then sampled with a Markov Chain Monte Carlo (MCMC) algorithm using the `PyMC` (version 5.0.2) package ([Salvatier et al. 2016](#)) which applies the No-U-Turn Sampler (NUTS; [Hoffman & Gelman 2011](#)). We set up four chains and run each chain for 3,000 iterations including 1,000 for tuning; convergence is checked using the Gelman-Rubin diagnostic (\hat{R} ; [Gelman & Rubin 1992](#), converged chains should have $\hat{R} \approx 1$). We check \hat{R} for each bootstrapped data set, and consider simulations that have relative deviation of \hat{R} from unity greater than 0.01 (i.e., $|\hat{R} - 1|/\hat{R} \geq 0.01$) as diverging chains.

For model comparison, we use the `ARVIZ` package ([Kumar et al. 2019](#)) to compute the leave-one-out cross-validation (LOO; [Vehtari et al. 2017](#)) for the bootstrapped data sets, which assigns a weight value (w_{loo}) to each set of our fits (single vs. two-component Maxwellian) to represent the probability of each model being true. As a complementary diagnostic, we also compute the fraction of diverging chains for each parameter, which is denoted as f_{diverge} . Chains not converging could be a result of insufficient iterations, or simply because the assumed likelihood is not appropriate for the underlying population. In this regard, f_{diverge} can be used as a diagnostic for the suitability of the specified model. Table 4 summarises median and

Table 3. Binary properties: (1) Name. (2) Class. (3) Systemic radial velocity. (4) Distance (used in calculation). (5) Present-day peculiar velocity. (6) Potential peculiar velocity at birth. (7) Compact object mass. (8) Mass of non-degenerate companion. (9) Orbital period.

Name	Class	γ (km s ⁻¹)	d (kpc)	$v_{\text{pec,p}}$ (km s ⁻¹)	$v_{\text{pec}}^{z=0}$ (km s ⁻¹)	M_1 (M _⊙)	M_2 (M _⊙)	P_{orb} (d)
(1)	(2)	(3)	(4)	(5)	(6)	(7)	(8)	(9)
2S 0921–630	NS-LMXB	44.4 ± 2.4 [1]	8.5*	38.2 ^{+18.6} _{-7.4}	58.9 ^{+10.4} _{-3.9}	1.4 ^{+0.1} _{-0.1} [2]	0.3 ^{+0.0} _{-0.0} [2]	9.00 [3]
4U 1254–69	NS-LMXB	183.0 ± 3.0 [4]	13.0 ^{+3.0} _{-3.0} †	155.3 ^{+29.0} _{-17.6}	202.9 ^{+81.1} _{-52.9}	1.5 ^{+0.3} _{-0.1} [4]	0.5 ^{+0.1} _{-0.1} [4]	0.16 [5]
Cen X-4	NS-LMXB	194.5 ± 0.2 [6]	1.4 ^{+0.3} _{-0.3}	418.7 ^{+72.1} _{-68.5}	457.2 ^{+84.1} _{-137.8}	1.9 ^{+0.4} _{-0.1} [6]	0.3 ^{+0.2} _{-0.1} [6]	0.63 [6]
Sco X-1	NS-LMXB	-113.8 ± 0.6 [7]	2.2 ^{+0.1} _{-0.1}	167.5 ^{+10.3} _{-9.8}	210.6 ^{+19.0} _{-29.0}	1.4*	0.4* [8]	0.79 [9]
4U 1636–536	NS-LMXB	-34.0 ± 5.0 [10]	6.0 ^{+0.5} _{-1.3} †	164.7 ^{+12.6} _{-12.6}	194.6 ^{+15.0} _{-25.7}	1.4*	0.5* [10]	0.16 [10]
Her X-1	NS-LMXB	-65.0 ± 2.0 [11]	7.1 ^{+0.8} _{-0.6}	125.5 ^{+11.3} _{-10.9}	198.5 ^{+13.2} _{-32.0}	1.5 ^{+0.3} _{-0.3} [11]	2.3 ^{+0.3} _{-0.3} [11]	1.70 [11]
MXB 1659–298	NS-LMXB	-49.0 ± 16.0 [12]	9.0 ^{+2.0} _{-2.0} †	259.7 ^{+92.1} _{-203.6}	271.4 ^{+116.9} _{-149.3}	2.1 ^{+0.9} _{-0.9} [12]	0.6 ^{+0.2} _{-0.2} [12]	0.30 [13]
4U 1700+24	NS-LMXB	-47.4 ± 0.1 [14]	0.5 ^{+0.0} _{-0.0}	39.2 ^{+9.5} _{-8.8}	56.7 ^{+6.3} _{-7.5}	1.4*	1.6 ^{+0.1} _{-0.2} [14]	4391.00 [14]
GX 1+4	NS-LMXB	-176.7 ± 0.2 [15]	4.3*	189.3 ^{+8.1} _{-8.3}	186.3 ^{+15.2} _{-31.8}	1.4*	< 1.2 [15]	1160.80 [15]
4U 1735–444	NS-LMXB	-140.0 ± 3.0 [10]	8.5 ^{+1.3} _{-1.3} †	60.0 ^{+62.1} _{-30.7}	147.9 ^{+22.7} _{-19.7}	1.4*	0.5* [10]	0.19 [10]
XTE J1814–338	NS-LMXB	-30.0 ± 20.0 [16]	8.0 ^{+1.6} _{-1.6} †	171.3 ^{+194.8} _{-51.1}	217.3 ^{+134.3} _{-73.2}	2.0 ^{+0.7} _{-0.5} [16]	0.2 ^{+0.1} _{-0.1} [16]	0.18 [16]
2A 1822–371	NS-LMXB	-44.0 ± 5.0 [17]	5.9 ^{+1.3} _{-0.9}	253.7 ^{+36.2} _{-33.2}	261.3 ^{+48.3} _{-36.4}	2.0 ^{+0.4} _{-0.4} [18]	0.5 ^{+0.1} _{-0.1} [18]	0.23 [19]
Ser X-1	NS-LMXB	92.0 ± 4.0 [4]	7.7 ^{+0.9} _{-0.9} †	110.0 ^{+30.2} _{-31.3}	108.4 ^{+25.7} _{-22.3}	1.4*	0.1* [4]	0.09 [4]
Aql X-1	NS-LMXB	104.0 ± 3.0 [20]	5.2 ^{+0.8} _{-0.8} †	42.3 ^{+13.2} _{-12.0}	55.5 ^{+7.8} _{-5.9}	1.4*	< 0.8 [20]	0.79 [20]
Cyg X-2	NS-LMXB	-207.8 ± 0.3 [21]	9.7 ^{+1.9} _{-1.9} †	164.0 ^{+9.0} _{-8.5}	240.0 ^{+23.5} _{-48.1}	1.7 ^{+0.2} _{-0.2} [21]	0.6 ^{+0.1} _{-0.1} [21]	9.84 [21]
IGR J00370+6122	NS-HMXB	-77.3 ± 1.4 [22]	3.4 ^{+0.1} _{-0.1}	23.4 ^{+4.1} _{-8.1}	29.4 ^{+5.3} _{-5.3}	1.4*	10.0 ^{+5.0} _{-5.0} [22]	15.66 [23]
2S 0114+650	NS-HMXB	-58.2 ± 0.5 [24]	4.5 ^{+0.2} _{-0.2}	22.4 ^{+4.4} _{-2.2}	21.6 ^{+1.9} _{-2.4}	1.4*	16.0 ^{+5.0} _{-5.0} [25]	11.59 [26]
RX J0146.9+6121	NS-HMXB	-37.0 ± 4.3 [27]	2.8 ^{+0.2} _{-0.2}	11.8 ^{+7.9} _{-4.2}	7.1 ^{+3.6} _{-2.4}	1.4*	11.0 ^{+2.0} _{-2.0} [28]	330.00* [27]
LS I +61 303	NS-HMXB	-41.4 ± 0.6 [29]	2.5 ^{+0.1} _{-0.1}	9.0 ^{+7.0} _{-3.6}	9.1 ^{+2.3} _{-2.7}	1.4*	12.5 ^{+2.9} _{-2.5} [30]	24.50 [31]
X Persi	NS-HMXB	1.0 ± 0.9 [32]	0.6 ^{+0.0} _{-0.0}	17.9 ^{+9.8} _{-7.8}	20.2 ^{+3.4} _{-3.0}	1.4*	14.0 ^{+3.0} _{-3.0} [32]	250.30 [33]
XTE J0421+560	NS-HMXB	-51.0 ± 2.0 [34]	4.1 ^{+0.3} _{-0.3}	18.1 ^{+4.6} _{-3.2}	21.1 ^{+2.3} _{-2.5}	1.4*	...	19.41 [34]
EXO 051910+3737.7	NS-HMXB	-20.5 ± 4.4 [35]	1.3 ^{+0.1} _{-0.1}	24.4 ^{+6.4} _{-5.5}	23.8 ^{+5.4} _{-5.0}	1.4*
1A 0535+262	NS-HMXB	-30.0 ± 4.0 [36]	1.8 ^{+0.1} _{-0.1}	44.9 ^{+4.6} _{-4.5}	37.5 ^{+6.7} _{-6.5}	1.6 ^{+0.6} _{-0.6} [36]	7.5 ^{+2.5} _{-2.5} [36]	111.00 [37]
HD 259440	NS-HMXB	36.9 ± 0.8 [38]	1.8 ^{+0.1} _{-0.1}	10.4 ^{+6.4} _{-2.9}	6.5 ^{+1.6} _{-2.1}	1.4*	16.1 ^{+2.9} _{-2.9} [39]	308.00* [38]
IGR J08408–4503	NS-HMXB	15.3 ± 0.5 [40]	2.2 ^{+0.1} _{-0.1}	38.9 ^{+6.8} _{-5.1}	38.8 ^{+6.1} _{-6.1}	1.4*	33.0* [40]	9.54 [40]
Vela X-1	NS-HMXB	-3.4 ± 1.0 [41]	2.0 ^{+0.1} _{-0.1}	59.0 ^{+7.7} _{-6.8}	62.1 ^{+7.9} _{-8.8}	2.1 ^{+0.2} _{-0.2} [42]	26.0 ^{+1.0} _{-1.0} [42]	8.96 [41]
2FGL J1019.0–5856	NS-HMXB	30.4 ± 1.3 [43]	4.3 ^{+0.2} _{-0.2}	30.9 ^{+6.0} _{-3.4}	36.4 ^{+3.2} _{-3.0}	1.4*	23.2* [44]	16.54 [45]
Cen X-3	NS-HMXB	39.0 ± 3.0 [46]	6.9 ^{+0.7} _{-0.6}	102.4 ^{+4.2} _{-3.9}	108.5 ^{+11.2} _{-14.6}	1.6 ^{+0.1} _{-0.1} [42]	24.0 ^{+1.0} _{-1.0} [42]	2.09* [47]
1E 1145.1–6141	NS-HMXB	-13.0 ± 3.0 [48]	8.3 ^{+0.8} _{-0.6}	56.5 ^{+13.2} _{-10.2}	54.7 ^{+15.3} _{-11.3}	1.7 ^{+0.3} _{-0.3} [48]	14.0 ^{+4.0} _{-4.0} [48]	14.37 [49]
2S 1145–619	NS-HMXB	-17.0 ± 7.4 [50]	2.1 ^{+0.1} _{-0.1}	16.2 ^{+8.4} _{-2.9}	12.9 ^{+5.1} _{-2.1}	1.4*	13.0 ^{+2.0} _{-2.0} [51]	187.50* [47]
GX 301–2	NS-HMXB	4.1 ± 2.4 [52]	3.6 ^{+0.2} _{-0.2}	58.0 ^{+4.7} _{-4.3}	59.8 ^{+6.0} _{-6.5}	1.9 ^{+0.6} _{-0.6} [52]	43.0 ^{+10.0} _{-10.0} [52]	41.50 [52]
1H 1253–761	NS-HMXB	-20.0 ± 7.4 [50]	0.2 ^{+0.0} _{-0.0}	27.5 ^{+10.9} _{-9.0}	26.2 ^{+9.3} _{-8.3}	1.4*	7.5* [53]	...
1H 1249–637	NS-HMXB	22.0 ± 7.0 [50]	0.4 ^{+0.0} _{-0.0}	21.0 ^{+11.5} _{-9.3}	28.6 ^{+9.9} _{-9.0}	1.4*
1H 1255–567	NS-HMXB	13.0 ± 3.7 [50]	0.1 ^{+0.0} _{-0.0}	12.5 ^{+7.0} _{-3.9}	14.4 ^{+5.0} _{-4.6}	1.4*
4U 1538–52	NS-HMXB	-148.1 ± 0.9 [54]	5.7 ^{+0.5} _{-0.5}	77.5 ^{+9.2} _{-10.0}	73.9 ^{+8.6} _{-8.5}	1.0 ^{+0.2} _{-0.2} [42]	16.0 ^{+2.0} _{-2.0} [42]	3.71 [55]
4U 1700–37	NS-HMXB	-60.0 ± 12.0 [56]	1.5 ^{+0.1} _{-0.1}	71.3 ^{+11.7} _{-10.5}	76.7 ^{+12.8} _{-13.4}	2.0 ^{+0.2} _{-0.2} [42]	46.0 ^{+5.0} _{-5.0} [42]	3.41 [57]
IGR J17544–2619	NS-HMXB	-46.8 ± 4.0 [58]	2.4 ^{+0.2} _{-0.1}	43.7 ^{+4.6} _{-4.4}	36.6 ^{+6.0} _{-5.6}	1.4*	23.0 ^{+2.0} _{-2.0} [59]	12.17 [58]
LS 5039	NS-HMXB	17.2 ± 0.7 [30]	1.9 ^{+0.1} _{-0.1}	88.2 ^{+3.7} _{-3.2}	84.5 ^{+4.7} _{-4.1}	3.7 ^{+1.3} _{-1.0} [30]	22.9 ^{+3.4} _{-2.9} [30]	3.91 [30]
1H 2202+501	NS-HMXB	-16.8 ± 2.5 [60]	1.1 ^{+0.0} _{-0.0}	28.7 ^{+3.2} _{-2.5}	24.3 ^{+4.5} _{-3.3}	1.4*
4U 2206+543	NS-HMXB	-61.5 ± 1.6 [61]	3.1 ^{+0.1} _{-0.1}	27.8 ^{+6.0} _{-4.1}	26.3 ^{+5.3} _{-4.7}	1.4*	23.5 ^{+14.5} _{-8.0} [61]	9.55 [61]
A 0620–00	BH-LMXB	8.5 ± 1.8 [62]	1.5 ^{+0.3} _{-0.2}	43.7 ^{+9.9} _{-7.1}	41.8 ^{+11.2} _{-8.6}	6.6 ^{+0.3} _{-0.3} [63]	0.5 ^{+0.1} _{-0.1} [63]	0.32 [64]
XTE J1118+480	BH-LMXB	2.7 ± 1.1 [65]	1.7 ^{+0.1} _{-0.1} †	142.9 ^{+11.4} _{-11.2}	172.0 ^{+18.9} _{-28.4}	7.5 ^{+0.7} _{-0.6} [66]	0.2 ^{+0.1} _{-0.1} [66]	0.17 [64]
GRS 1124–684	BH-LMXB	14.2 ± 6.3 [67]	5.0 ^{+0.7} _{-0.7} †	118.6 ^{+15.5} _{-15.2}	115.1 ^{+19.3} _{-18.5}	11.0 ^{+2.1} _{-1.4} [68]	0.9 ^{+0.2} _{-0.1} [68]	0.43 [69]
MAXI J1305–704	BH-LMXB	-9.0 ± 5.0 [70]	7.7 ^{+1.6} _{-1.6} †	58.1 ^{+30.4} _{-22.1}	75.1 ^{+17.4} _{-10.0}	8.9 ^{+1.6} _{-1.0} [70]	0.4 ^{+0.2} _{-0.2} [70]	0.40 [70]
BW Cir	BH-LMXB	102.0 ± 4.0 [71]	≥ 25.0	352.0 ^{+106.9} _{-98.8}	279.3 ^{+156.9} _{-111.3}	> 7.6 [72]	> 0.9 [72]	2.54 [72]
4U 1543–475	BH-LMXB	-87.0 ± 3.0 [73]	7.5 ^{+0.5} _{-0.5} †	99.0 ^{+14.5} _{-15.1}	118.7 ^{+11.1} _{-9.1}	9.4 ^{+1.0} _{-1.0} [74]	2.6 ^{+0.6} _{-0.6} [74]	1.12 [74]
XTE J1550–564	BH-LMXB	-68.0 ± 19.0 [75]	4.5 ^{+0.5} _{-0.5} †	79.1 ^{+38.2} _{-32.3}	78.8 ^{+37.1} _{-30.4}	11.7 ^{+3.9} _{-3.9} [76]	0.3 ^{+0.1} _{-0.1} [76]	1.54 [76]
GRO 1655–40	BH-LMXB	-167.1 ± 0.6 [77]	3.2 ^{+0.6} _{-0.4}	161.8 ^{+7.4} _{-5.7}	153.6 ^{+13.9} _{-28.9}	6.0 ^{+0.4} _{-0.4} [78]	2.5 ^{+0.3} _{-0.3} [78]	2.62 [79]
GX 339–4	BH-LMXB	26.0 ± 2.0 [80]	≥ 5.0	165.8 ^{+10.7} _{-34.7}	201.0 ^{+53.0} _{-37.2}	5.9 ^{+3.6} _{-3.6} [80]	1.1 ^{+1.7} _{-0.8} [80]	1.76 [80]
H 1705–250	BH-LMXB	-54.0 ± 15.0 [81]	8.6 ^{+2.1} _{-2.1} †	221.2 ^{+100.8} _{-109.0}	289.4 ^{+71.3} _{-75.9}	6.4 ^{+1.5} _{-1.5} [81]	0.3 ^{+0.1} _{-0.1} [81]	0.52 [82]
Swift J1753.5–0127	BH-LMXB	6.0 ± 6.0 [83]	6.0 ^{+2.0} _{-2.0} †	110.4 ^{+81.4} _{-7.1}	149.5 ^{+68.2} _{-29.6}	> 7.4 [84]	0.5* [84]	0.14 [85]
MAXI J1820+070	BH-LMXB	-21.6 ± 2.3 [86]	2.8 ^{+0.8} _{-0.5}	72.4 ^{+18.7} _{-16.2}	105.4 ^{+29.6} _{-19.4}	8.4 ^{+0.8} _{-0.7} [87]	0.6 ^{+0.1} _{-0.1} [87]	0.69 [86]
MAXI J1836–194	BH-LMXB?	61.0 ± 15.0 [88]	7.0 ^{+3.0} _{-3.0}	98.4 ^{+32.2} _{-25.7}	133.4 ^{+32.1} _{-29.8}
GRS 1915+103	BH-LMXB	12.3 ± 1.0 [89]	8.6 ^{+2.0} _{-2.0}	31.8 ^{+17.5} _{-19.5}	39.6 ^{+19.6} _{-19.5}	12.4 ^{+2.0} _{-1.8} [89]	0.5 ^{+0.4} _{-0.3} [89]	33.83 [90]
V404 Cyg	BH-LMXB	-0.4 ± 2.2 [91]	2.4 ^{+0.1} _{-0.1}	45.3 ^{+3.6} _{-3.5}	38.7 ^{+5.7} _{-5.9}	9.0 ^{+0.2} _{-0.2} [92]	0.6 ^{+0.1} _{-0.1} [92]	6.47 [93]
HD 96670	BH-LMXB?	-27.5 ± 0.0 [94]	3.1 ^{+0.3} _{-0.3}	24.3 ^{+10.0} _{-9.2}	25.6 ^{+4.4} _{-4.3}	6.2 ^{+0.9} _{-0.7} [94]	22.7 ^{+5.2} _{-3.6} [94]	5.28 [94]
V4641 Sgr	BH-LMXB	107.4 ± 2.9 [76]	4.8 ^{+0.7} _{-0.5}	91.8 ^{+6.6} _{-6.7}	101.4 ^{+10.1} _{-10.3}	6.4 ^{+0.6} _{-0.6} [95]	2.9 ^{+0.4} _{-0.4} [95]	2.82 [96]

Table 3 – continued

Name	Class	γ (km s ⁻¹)	d (kpc)	$v_{\text{pec,p}}$ (km s ⁻¹)	$v_{\text{pec}}^{\sigma=0}$ (km s ⁻¹)	M_1 (M _⊙)	M_2 (M _⊙)	P_{orb} (d)
SS 433	BH-HMXB?	69.0 ± 4.7 [97]	7.4 ^{+1.4} _{-0.3}	44.3 ^{+22.2} _{-15.9}	45.3 ^{+14.4} _{-12.0}	4.3 ^{+0.4} _{-0.4} [97]	11.3 ^{+0.6} _{-0.9} [97]	13.08* [98]
Cyg X-1	BH-HMXB	-5.1 ± 0.5 [99]	2.1 ^{+0.1} _{-0.1}	22.3 ^{+4.6} _{-2.9}	21.9 ^{+3.2} _{-3.0}	21.2 ^{+2.2} _{-2.2} [100]	40.6 ^{+7.1} _{-7.1} [100]	5.60 [101]
MWC 656	BH-HMXB?	-2.8 ± 9.4 [102]	2.0 ^{+0.1} _{-0.1}	25.8 ^{+13.7} _{-12.9}	36.2 ^{+9.7} _{-7.0}	4.1 ^{+1.4} _{-1.4} [102]	7.8 ^{+2.0} _{-2.0} [103]	60.37 [103]
PSR J0348+0432	LM-PSR	-1.0 ± 20.0 [104]	2.1 ^{+0.4} _{-0.4}	62.3 ^{+13.4} _{-12.3}	73.1 ^{+13.0} _{-11.4}	2.0 ^{+0.0} _{-0.0} [104]	0.2 ^{+0.0} _{-0.0} [104]	0.10 [104]
PSR J1012+5307	LM-PSR	44.0 ± 8.0 [105]	0.6 ^{+0.1} _{-0.1}	84.2 ^{+15.7} _{-11.9}	96.4 ^{+21.5} _{-14.7}	1.6 ^{+0.2} _{-0.2} [105]	0.2 ^{+0.0} _{-0.0} [105]	0.60 [106]
PSR J1023+0038	LM-PSR	1.0 ± 3.0 [107]	1.4 ^{+0.0} _{-0.0}	131.1 ^{+6.7} _{-6.3}	149.0 ^{+15.1} _{-25.3}	1.6 ^{+0.2} _{-0.2} [108]	0.2 ^{+0.0} _{-0.0} [108]	0.20 [109]
PSR J1024-0719	LM-PSR	185.0 ± 4.0 [110]	1.2 ^{+0.2} _{-0.2}	382.2 ^{+64.7} _{-45.8}	465.7 ^{+68.7} _{-84.7}	1.4*	0.4* [111]	...
PSR J1048+2339	LM-PSR	-24.0 ± 8.0 [108]	2.0 ^{+0.4} _{-0.4}	157.7 ^{+35.8} _{-35.4}	199.4 ^{+49.7} _{-46.0}	> 2.0 [108]	> 0.4 [108]	0.25 [112]
XSS J12270-4859	LM-PSR	67.0 ± 2.0 [113]	1.6 ^{+0.3} _{-0.3}	131.4 ^{+21.1} _{-20.8}	153.0 ^{+23.4} _{-24.5}	1.4*	> 0.3 [108]	0.29 [113]
PSR B1259-63	HM-PSR	0.0 ± 0.0 [114]	2.2 ^{+0.1} _{-0.1}	24.8 ^{+9.4} _{-8.0}	34.4 ^{+4.9} _{-5.0}	1.4*	23.0* [114]	1236.72 [114]
PSR J1306-4035	LM-PSR	32.0 ± 1.8 [115]	4.7 ^{+0.9} _{-0.9}	120.9 ^{+17.1} _{-17.3}	147.1 ^{+16.0} _{-19.6}	1.8 ^{+0.1} _{-0.0} [115]	0.5 ^{+0.0} _{-0.0} [115]	1.10 [116]
PSR J1311-3430	LM-PSR	62.5 ± 4.5 [117]	2.4 ^{+0.5} _{-0.5}	108.6 ^{+16.6} _{-15.7}	156.8 ^{+27.4} _{-27.0}	2.1 ^{+0.1} _{-0.1} [117]	0.0 ^{+0.0} _{-0.0} [117]	0.07 [118]
PSR J1417-4402	LM-PSR	-15.3 ± 0.9 [43]	4.5 ^{+1.1} _{-0.8}	98.5 ^{+22.8} _{-19.0}	140.0 ^{+29.4} _{-23.6}	2.0 ^{+0.1} _{-0.1} [43]	0.3 ^{+0.0} _{-0.0} [43]	5.37 [43]
PSR J1431-4715	LM-PSR	-91.0 ± 2.0 [108]	1.6 ^{+0.3} _{-0.3}	122.8 ^{+18.4} _{-16.0}	114.3 ^{+22.1} _{-19.0}	1.4*	> 0.1 [119]	0.45 [119]
PSR J1622-0315	LM-PSR	-135.0 ± 6.0 [108]	1.1 ^{+0.2} _{-0.2}	144.4 ^{+11.1} _{-10.3}	140.9 ^{+20.1} _{-26.1}	> 1.4 [108]	> 0.1 [108]	0.16 [120]
PSR J1628-3205	LM-PSR	-4.0 ± 7.0 [108]	1.2 ^{+0.2} _{-0.2}	114.1 ^{+28.4} _{-28.3}	150.8 ^{+40.9} _{-38.3}	1.4*	> 0.2 [121]	0.21 [108]
PSR J1653-0158	LM-PSR	-174.6 ± 5.1 [122]	0.8 ^{+0.2} _{-0.2}	177.5 ^{+10.3} _{-9.4}	186.8 ^{+22.8} _{-40.0}	2.2 ^{+0.2} _{-0.1} [123]	0.0 ^{+0.0} _{-0.0} [123]	0.05 [123]
PSR J1723-2837	LM-PSR	33.0 ± 2.0 [108]	0.9 ^{+0.0} _{-0.0}	110.4 ^{+10.8} _{-10.6}	155.0 ^{+13.8} _{-33.0}	1.2 ^{+0.3} _{-0.2} [124]	0.4 ^{+0.1} _{-0.1} [108]	0.62 [125]
PSR J1816+4510	LM-PSR	-99.0 ± 8.0 [126]	4.4 ^{+0.9} _{-0.9}	165.3 ^{+30.6} _{-26.3}	170.3 ^{+24.6} _{-19.1}	> 1.8 [126]	> 0.2 [126]	0.36 [127]
PSR J2039-5617	LM-PSR	6.0 ± 3.0 [108]	1.8 ^{+0.4} _{-0.4}	113.5 ^{+27.8} _{-27.8}	164.5 ^{+40.5} _{-38.3}	1.3 ^{+0.3} _{-0.2} [128]	0.2 ^{+0.0} _{-0.0} [128]	0.23 [128]
PSR J2129-0429	LM-PSR	-64.0 ± 2.0 [129]	2.1 ^{+0.4} _{-0.3}	201.3 ^{+33.0} _{-24.2}	180.3 ^{+33.0} _{-35.5}	1.7 ^{+0.2} _{-0.2} [129]	0.4 ^{+0.0} _{-0.0} [129]	0.64 [129]
PSR J2215+5135	LM-PSR	49.0 ± 8.0 [130]	2.8 ^{+0.6} _{-0.6}	117.8 ^{+17.4} _{-17.4}	103.8 ^{+19.7} _{-20.2}	2.3 ^{+0.2} _{-0.1} [108]	0.3 ^{+0.0} _{-0.0} [130]	0.17 [108]
PSR J2339-0533	LM-PSR	-49.0 ± 8.0 [131]	1.1 ^{+0.2} _{-0.2}	64.1 ^{+13.5} _{-12.9}	97.5 ^{+18.1} _{-16.7}	1.6 ^{+0.3} _{-0.2} [132]	0.3 ^{+0.1} _{-0.1} [108]	0.19 [132]
J05215658	BH-HMNI	-0.4 ± 0.1 [133]	2.5 ^{+0.1} _{-0.1}	24.8 ^{+4.2} _{-2.6}	28.2 ^{+2.9} _{-2.8}	3.3 ^{+1.1} _{-0.4} [133]	3.2 ^{+0.4} _{-0.5} [133]	83.20 [133]
J06163552	NS-LMNI	29.2 ± 0.7 [134]	1.0 ^{+0.0} _{-0.0}	17.0 ^{+4.8} _{-6.6}	25.1 ^{+21.7} _{-10.0}	1.3 ^{+0.1} _{-0.1} [134]	1.7 ^{+0.1} _{-0.1} [134]	0.87 [134]
J112306.9	NS-LMNI	-8.0 ± 2.0 [135]	0.3 ^{+0.0} _{-0.0}	29.5 ^{+10.5} _{-10.3}	54.2 ^{+44.0} _{-24.7}	1.2 ^{+0.0} _{-0.0} [135]	0.6 ^{+0.0} _{-0.0} [135]	0.27 [135]
J125556.57	NS-LMNI	-3.4 ± 0.3 [136]	0.5 ^{+0.0} _{-0.0}	36.1 ^{+7.1} _{-5.2}	45.1 ^{+4.0} _{-4.2}	1.4 ^{+0.7} _{-0.3} [136]	1.2 ^{+0.1} _{-0.1} [136]	2.76 [136]
Gaia BH2	BH-LMNI	-4.2 ± 0.2 [137]	1.2 ^{+0.0} _{-0.0}	25.2 ^{+9.7} _{-8.7}	34.1 ^{+5.0} _{-5.1}	8.9 ^{+0.3} _{-0.3} [137]	1.1 ^{+0.2} _{-0.1} [137]	1276.70 [137]
J15274848	NS-LMNI	-26.1 ± 0.7 [138]	0.1 ^{+0.0} _{-0.0}	13.8 ^{+7.1} _{-3.5}	18.9 ^{+3.1} _{-3.0}	1.0 ^{+0.1} _{-0.1} [138]	0.6 ^{+0.1} _{-0.1} [138]	0.26 [139]
Gaia BH1	BH-LMNI	45.5 ± 0.8 [140]	0.5 ^{+0.0} _{-0.0}	76.4 ^{+4.0} _{-3.1}	71.3 ^{+9.2} _{-10.8}	9.8 ^{+0.2} _{-0.2} [140]	0.9 ^{+0.1} _{-0.1} [140]	185.59 [140]
AS 386	BH-HMNI	-31.8 ± 2.6 [141]	5.9 ^{+0.5} _{-0.4}	10.8 ^{+8.0} _{-7.7}	20.6 ^{+2.2} _{-2.7}	> 7.0 [141]	7.0 ^{+1.0} _{-1.0} [141]	131.27 [141]
J235456.76	NS-LMNI	41.0 ± 2.4 [142]	0.1 ^{+0.0} _{-0.0}	47.9 ^{+9.4} _{-8.7}	52.5 ^{+7.6} _{-7.7}	> 1.3 [142]	0.7 ^{+0.1} _{-0.1} [142]	0.48 [142]

References: [1] Jonker et al. (2005), [2] Steeghs & Jonker (2007), [3] Ashcraft et al. (2012), [4] Cornelisse et al. (2013), [5] Díaz Trigo et al. (2009), [6] Shahbaz et al. (2014), [7] Steeghs & Casares (2002), [8] Cherepashchuk et al. (2021), [9] LaSala & Thorstensen (1985), [10] Casares et al. (2006), [11] Reynolds et al. (1997), [12] Ponti et al. (2018), [13] Iaria et al. (2018), [14] Hinkle et al. (2019), [15] Hinkle et al. (2006), [16] Wang et al. (2017), [17] Casares et al. (2003), [18] Muñoz-Darias et al. (2005), [19] Jonker & van der Klis (2001), [20] Mata Sánchez et al. (2017), [21] Premachandra et al. (2016), [22] González-Galán et al. (2014), [23] den Hartog et al. (2004), [24] Grundstrom et al. (2007a), [25] Reig et al. (1996), [26] Crampton et al. (1985), [27] Sarty et al. (2009), [28] Reig et al. (1997), [29] Aragona et al. (2009), [30] Casares et al. (2005), [31] Gregory (2002), [32] Grundstrom et al. (2007b), [33] Delgado-Martí et al. (2001), [34] Barsukova et al. (2005), [35] Gontcharov (2006), [36] Hutchings (1984), [37] Priedhorsky & Terrell (1983), [38] Moritani et al. (2018), [39] Aragona et al. (2010), [40] Gamen et al. (2015), [41] Stickland et al. (1997), [42] Falanga et al. (2015), [43] Strader et al. (2015), [44] Waisberg & Romani (2015), [45] An et al. (2015), [46] van der Meer et al. (2007), [47] Nagase (1989), [48] Hutchings et al. (1987), [49] Ray & Chakrabarty (2002), [50] Kharchenko et al. (2007), [51] Stevens et al. (1997), [52] Kaper et al. (2006), [53] Waters et al. (1989), [54] Abubekkerov et al. (2004), [55] Davison et al. (1977), [56] Gies & Bolton (1986), [57] Islam & Paul (2016), [58] Nikolaeva et al. (2013), [59] Bikmaev et al. (2017), [60] Chojnowski et al. (2017), [61] Hambaryan et al. (2022), [62] González Hernández & Casares (2010), [63] Cantrell et al. (2010), [64] González Hernández et al. (2014), [65] González Hernández et al. (2008b), [66] Khargharia et al. (2013), [67] Wu et al. (2015), [68] Wu et al. (2016), [69] González Hernández et al. (2017), [70] Mata Sánchez et al. (2021), [71] Casares et al. (2004), [72] Casares et al. (2009), [73] Orosz et al. (1998), [74] Orosz (2003), [75] Orosz et al. (2002), [76] Orosz et al. (2011), [77] González Hernández et al. (2008a), [78] Shahbaz (2003), [79] van der Hoof et al. (1998), [80] Heida et al. (2017), [81] Harlaftis et al. (1997), [82] Remillard et al. (1996), [83] Neustroev et al. (2014), [84] Shaw et al. (2016), [85] Zurita et al. (2008), [86] Torres et al. (2019), [87] Torres et al. (2020), [88] Russell et al. (2014), [89] Reid et al. (2014b), [90] Steeghs et al. (2013), [91] Casares & Charles (1994), [92] Khargharia et al. (2010), [93] Casares et al. (2019), [94] Gomez & Grindlay (2021), [95] MacDonald et al. (2014), [96] Orosz et al. (2001), [97] Picchi et al. (2020), [98] Crampton & Hutchings (1981), [99] Gies et al. (2008), [100] Miller-Jones et al. (2021), [101] LaSala et al. (1998), [102] Casares et al. (2012), [103] Williams et al. (2010), [104] Antoniadis et al. (2013), [105] Callanan et al. (1998), [106] Nicastro et al. (1995), [107] Thorstensen & Armstrong (2005), [108] Strader et al. (2019), [109] Archibald et al. (2013), [110] Bassa et al. (2016), [111] Kaplan et al. (2016), [112] Deneva et al. (2016), [113] de Martino et al. (2014), [114] Miller-Jones et al. (2018), [115] Swihart et al. (2019), [116] Linares et al. (2018), [117] Romani et al. (2012), [118] Romani et al. (2012), [119] Bates et al. (2015), [120] Sanpa-Arsa (2016), [121] Ray et al. (2012), [122] Romani et al. (2014), [123] Nieder et al. (2020), [124] van Staden & Antoniadis (2016), [125] Crawford et al. (2013), [126] Kaplan et al. (2013), [127] Stovall et al. (2014), [128] Clark et al. (2021), [129] Bellm et al. (2016), [130] Linares (2018), [131] Romani & Shaw (2011), [132] Pletsch & Clark (2015), [133] Thompson et al. (2019), [134] Yuan et al. (2022), [135] Yi et al. (2022), [136] Mazeh et al. (2022), [137] El-Badry et al. (2023a), [138] Lin et al. (2023), [139] Jayasinghe et al. (2019), [140] El-Badry et al. (2023b), [141] Khokhlov et al. (2018), [142] Zheng et al. (2022)

†: literature distance (d_{lit} ; Table C1) used because the parallax is not well-constrained or not available (Sec 2.7); for PSRs, these are distances inferred from the Yao et al. (2017) dispersion measures.

*: values that have no literature constraints.

credible intervals of the posterior for the hyper-parameters, and in Figure 3, we show the distribution of median $v_{\text{pec}}^{z=0}$ overplotted with the models.

Our results show that a two-component Maxwellian distribution gives a sensible fit to all binaries as a whole, with \hat{R} consistent within 10^{-4} of 1 for all simulations (i.e., $f_{\text{diverge}} = 0$). All bootstrapped data sets strongly favour a two-component model ($w_{100} = 1$) over a single Maxwellian ($w_{100} = 0$). The posterior gives a low- and a high- $v_{\text{pec}}^{z=0}$ component that are characterised by $\sigma_{v,1} = 21 \pm 3 \text{ km s}^{-1}$ and $\sigma_{v,2} = 107_{-9}^{+10} \text{ km s}^{-1}$, respectively (uncertainties correspond to 68% credible level, and the same for other quoted parameters in this section). This two-component Maxwellian also applies to the NS subgroup, with a low- and high-velocity component at $\sigma_{v,1} = 21_{-3}^{+4} \text{ km s}^{-1}$ and $\sigma_{v,2} = 113_{-11}^{+12} \text{ km s}^{-1}$, and w_{100} also favours two-components ($w_{100} = 1$) over a single Maxwellian ($w_{100} = 0$). The two-component model also gives a higher w_{100} weight when applied to the BH subgroup; however, it leads to divergence in over 44% of the simulations; we thus conclude that the existence of a second component in BH subgroup is insignificant given the current sample.

Applying a two-component Maxwellian model to fit the LM and HM subgroups also leads to non-negligible divergence in over 26% and 34% of the simulations, respectively; whereas, a single Maxwellian fits the data without divergence, giving very distinct σ_v at $101_{-7}^{+8} \text{ km s}^{-1}$ and $27 \pm 2 \text{ km s}^{-1}$ for LM and HM binaries, respectively. By visual inspection, the HM subgroup seems to be restricted below 100 km s^{-1} , while the LM group shows a broader distribution up to a velocity of $\approx 400 \text{ km s}^{-1}$ (Figure 3). Despite the divergence fractions, the LOO diagnostic still favours a two-component ($w_{100} = 1$) over a single Maxwellian ($w_{100} \approx 10^{-15}$) for both LM and HM subgroups; this could be due to biases in w_{100} estimate for smaller sample sizes (Vehtari et al. 2017), so more robust conclusion can be made with more future identification of systems in each class.

3.3 Comparing distributions of peculiar velocities

There is some difference between the LM and HM subgroups and possibly also between the BH and NS subgroups, as suggested by our MCMC fits (Sec 3.2). These differences could relate to the possibility that different NK mechanisms apply to binaries with different compact objects; more importantly, it has been long suggested that observed recoil velocity is dependent on masses (component mass or total mass) following conservation of NK momentum, which might also lead to distinct distributions.

To investigate possible indication, we start by testing potential differences in distributions of $v_{\text{pec}}^{z=0}$ between subgroups. Since $v_{\text{pec}}^{z=0}$ has a rather strong dependence on distance ($v_{\text{pec}}^{z=0} \propto d$), we use the 85 binaries that have relatively well-defined distances (either from literature or inferred from *Gaia* parallaxes). For each binary, we randomly draw (with replacement) 10,000 velocities from the $v_{\text{pec}}^{z=0}$ sample of Sec 2.9 and perform two-tailed Kolmogorov-Smirnov (K-S) tests comparing BH vs. NS and LM vs. HM binaries at a pre-defined significance level (α) of 0.01, using the `ks_2sample` function in the `scipy` package⁶ (Virtanen et al. 2020).

As a measure of the significance of the difference, we calculate the fraction of simulations rejecting the null hypothesis (denoted by f_{rej}) that the two samples are drawn from the same underlying distribution. In Table 5, we summarise medians and uncertainties for the resulting test statistics and p -values, and in Figure 4, we present cumulative distributions comparing different subgroups.

⁶ <https://scipy.org/>

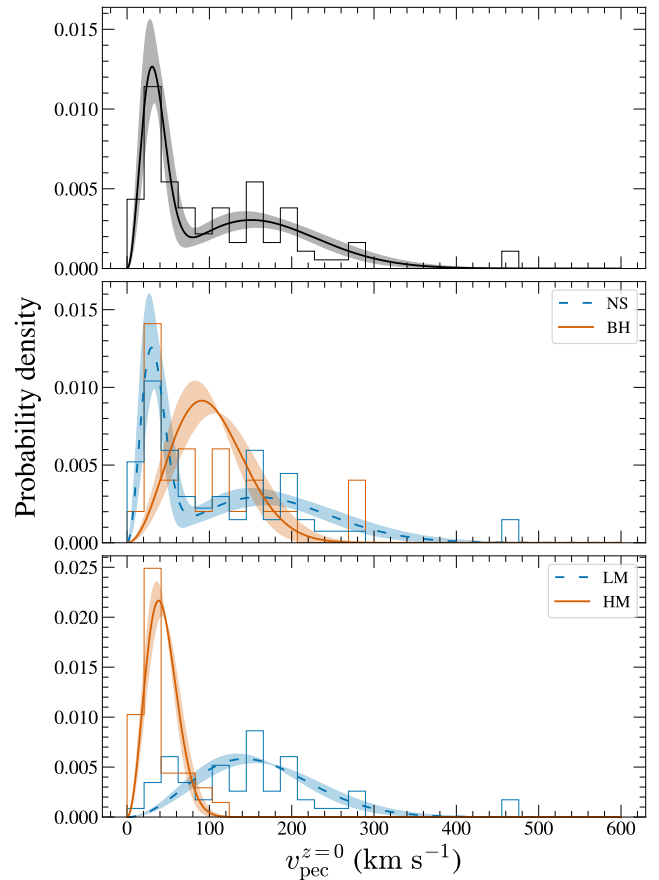


Figure 3. Distribution of $v_{\text{pec}}^{z=0}$ values of all binaries in Table 3 (top), binaries that host a BH or NS (middle), and binaries that host a HM or LM non-degenerate companion (bottom). The solid lines in each panel represent the single or two-component Maxwellian model characterised by the median parameters, while the shaded band represents the 68% credible region propagated from the parameter posteriors.

Comparing $v_{\text{pec}}^{z=0}$ distributions between subgroups suggests no difference between NS and BH binaries at a significance level of 0.01 ($f_{\text{rej}} = 0$); we further compare BH and NS binaries for the LM and HM subgroups and still find no difference in their $v_{\text{pec}}^{z=0}$ distributions. However, we find a marked difference between the LM and HM subgroups ($f_{\text{rej}} = 100\%$), suggesting that HM binaries are from a population with lower $v_{\text{pec}}^{z=0}$ compared to the LM group. This is in line with our Maxwellian fits to the LM and HM subgroups, where the majority of the HM binaries have median $v_{\text{pec}}^{z=0} \lesssim 100 \text{ km s}^{-1}$ (Figure 3), with the highest being Cen X-3 ($v_{\text{pec}}^{z=0} = 108 \pm 10 \text{ km s}^{-1}$), while the LM binaries have $v_{\text{pec}}^{z=0}$ up to $\sim 400 \text{ km s}^{-1}$. This difference is mostly contributed by the NS binaries in our sample as the difference persists for NS-LM vs. NS-HM ($f_{\text{rej}} = 100\%$) but is much less significant for BH-LM vs. BH-HM ($f_{\text{rej}} = 37\%$; Table 5).

3.4 Mass and peculiar velocity

The distinct distributions of LM vs. HM binaries suggest an anti-correlation of $v_{\text{pec}}^{z=0}$ on M_2 , while no strong dependence of $v_{\text{pec}}^{z=0}$ on M_1 , as the K-S test of NS vs. BH subgroups suggests no significant difference. With greater inertia, more massive binaries are harder to be accelerated, $v_{\text{pec}}^{z=0}$ (recoil obtained from NK) is expected to be

Table 4. Parameters of Maxwellian distribution from MCMC sampling.

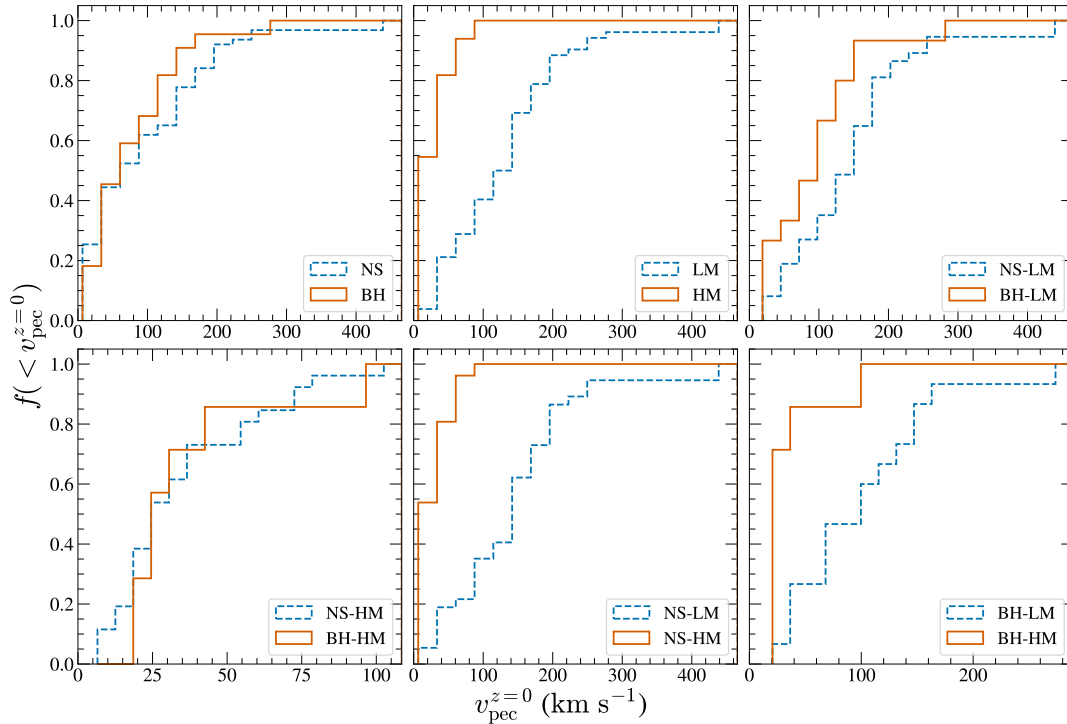
Class	Model	$\sigma_{v,1}$ (km s ⁻¹)	$\sigma_{v,2}$ (km s ⁻¹)	w	f_{diverge}^a (%)
BH	Single Maxwellian	64.2 ^{+8.5} _{-7.5}	(0,0)
	Two Maxwellians	26.1 ^{+28.0} _{-7.0}	87.4 ^{+29.1} _{-25.6}	0.5 ^{+0.2} _{-0.2}	(46, 45, 36)
NS	Single Maxwellian	85.5 ^{+6.5} _{-6.1}	(0)
	Two Maxwellians	20.9 ^{+3.8} _{-3.3}	112.7 ^{+12.5} _{-10.9}	0.4 ^{+0.1} _{-0.1}	(0, 0, 0)
LM	Single Maxwellian	100.8 ^{+7.9} _{-7.3}	(0)
	Two Maxwellians	73.5 ^{+9.5} _{-24.7}	177.3 ^{+80.1} _{-57.5}	0.8 ^{+0.1} _{-0.4}	(30, 29, 28)
HM	Single Maxwellian	27.1 ^{+2.3} _{-2.1}	(0)
	Two Maxwellians	15.9 ^{+6.4} _{-2.4}	40.7 ^{+9.8} _{-12.0}	0.6 ^{+0.1} _{-0.2}	(49, 49, 47)
All	Single Maxwellian	80.5 ^{+5.3} _{-5.0}	(0)
	Two Maxwellian	21.3 ^{+3.3} _{-2.8}	106.7 ^{+10.4} _{-9.2}	0.4 ^{+0.1} _{-0.1}	(0, 0, 0)

^a f_{diverge} values in parentheses correspond to the parameters in column 3–5.

Table 5. Two-sample K-S test results comparing $v_{\text{pec}}^{z=0}$ between different classes.

Subgroups	Sample sizes	Test statistic	p -value	f_{rej}^a (%)
NS vs. BH	63, 22	0.20 ± 0.04	0.48 ± 0.22	0
LM vs. HM	52, 33	0.67 ± 0.02	≤ 2.22 × 10 ⁻⁸	100
NS-LM vs. BH-LM	37, 15	0.37 ± 0.06	0.10 ± 0.09	4.6
NS-HM vs. BH-HM	26, 7	0.27 ± 0.06	0.73 ± 0.20	0
NS-LM vs. NS-HM	37, 26	0.74 ± 0.03	≤ 8.78 × 10 ⁻⁸	100
BH-LM vs. BH-HM	15, 7	0.66 ± 0.08	≤ 0.04	37.4

^a: Percentage of simulations that reject the null hypothesis at the given significance level (1%).


Figure 4. Cumulative distributions of median $v_{\text{pec}}^{z=0}$ for different binary subgroups.

negatively correlated with mass. Indeed, efforts have been made to find possible anti-correlation between peculiar velocity and binary component masses (e.g., Fryer & Kalogera 2001; Fryer et al. 2012; Mirabel 2017; Gandhi et al. 2019; Atri et al. 2019); however, past studies mostly focused only BH XRBs, and the peculiar velocities are only compared with BH masses (M_1). While M_1 is close to M_{tot} in BH-LMXBs, M_2 should be also be taken into account especially for binaries with massive companions (e.g., Cyg X-1). It is therefore more natural to investigate this potential correlation with M_{tot} .

We therefore pick binaries that have either constrained values or sensible estimates on M_1 and M_2 for our analysis. More specifically, a binary is included if it has a constrained value on M_1 and M_2 , or if either M_1 or M_2 has a lower limit while the other mass is constrained. Some binaries have no measurement of M_1 but the compact object has been confirmed to be a NS (e.g., by detection of pulsations); if such a binary has a constrained or just a lower limit on M_2 , we also include it in the analysis and assume a canonical NS mass of $1.4 M_{\odot}$ for M_1 with a 20% uncertainty. We then follow two methods to test for possible correlation: (1) fitting a log-linear model to, and (2) calculating the Pearson's (ρ_p) and Spearman's ρ_s correlation coefficient for bootstrapped velocities and Monte Carlo samples of M_{tot} .

We bootstrapped 1000 velocities from the calculated $v_{\text{pec}}^{z=0}$ distribution (Sec 2.9) for each of these binaries. To account for uncertainties in M_{tot} , we sample from a log-normal distribution that centres at the logarithm of the literature value with a standard deviation set to the maximum between upper and lower error; we also include binaries that only have lower limits on M_{tot} ; for these lower limits, we sample from a log-uniform distribution spanning from the lower limit ($M_{\text{tot, lolim}}$) to $2M_{\text{tot, lolim}}$.

We then follow a Bayesian approach to fit log-linear models to the 1,000 bootstrapped data set. We assume a likelihood (\mathcal{L}) that joins binary-specific Gaussian likelihoods $N(\mu_i, \sigma_i)$, i.e.:

$$\mathcal{L} = \prod_i N(\mu_i, \sigma_i)$$

$$\mu_i = \theta_{0, M_{\text{tot}}} + \theta_{1, M_{\text{tot}}} \left(\log M_{\text{tot}, i} - \overline{\log M_{\text{tot}}} \right), \quad (8)$$

$$\sigma_i^2 = \sigma_{v, i}^2 + \left(f_{\text{err}} \log v_{\text{pec}, i}^{z=0} \right)^2$$

Here, $\theta_{0, M}$ and $\theta_{1, M}$ are the fit parameters; $\log M_{\text{tot}}$ in the model is offset by the mean ($\overline{\log M_{\text{tot}}}$) over each bootstrapped data set to remove covariance between the two coefficients; $\sigma_{v, i}$ characterises the intrinsic uncertainty in our calculated distribution, which we set to the maximum between offsets of 16th and 84th percentiles from the median (i.e., the maximum between upper and lower errors reported in Table 3); we further inflate the uncertainty by assuming that it is underestimated by some fractional value f_{err} . We use flat priors for all hyperparameters: $\theta_{0, M_{\text{tot}}} \sim U(-5, 5)$, $\theta_{1, M_{\text{tot}}} \sim U(-5, 5)$, and $f_{\text{err}} \sim U(0, 1)$. The sampling is then performed with `PyMC` using the same configuration for the sampler as in Sec 3.2. All chains have good convergence with $|\hat{R} - 1|/\hat{R} < 0.001$, and samples from all MCMC runs are concatenated and presented in Figure 5. The fit results (Table 6) strongly suggest a negative slope ($\theta_{1, M_{\text{tot}}}$), with a 99.7% credible interval ranging from -0.84 to -0.16 ; the fit also suggests a moderate error fraction $f_{\text{err}} = 0.20$, indicating some additional uncertainty to the measured velocities.

With the simulated data, we use `scipy` to calculate ρ_p and ρ_s and the associated p -values. As a point of comparison, we also calculate the coefficients with velocities sampled from distributions that are ‘‘smeared’’ by f_{err} percent additional error (in Table 6). When no additional error is included, all simulations yield a negative

Table 6. Log-linear fit results, with 68% confidence uncertainties.

$v_{\text{pec}}^{z=0}$ vs.	θ_0	θ_1	f_{err}
M_{tot}	1.71 ± 0.05	-0.48 ± 0.11	0.20 ± 0.03
P_{orb}	1.80 ± 0.04	-0.19 ± 0.03	0.16 ± 0.02

coefficient, hinting at a significant anti-correlation (Table 7); a more sensible measure of robustness is the p -value; here, we compare the p -values to an a priori significance level of 1% and calculate f_{rej} (fraction of simulations that reject the null hypothesis; Sec 3.3).

When no additional error is incorporated, all simulations favour an anti-correlation according to the results using ρ_p and ρ_s , respectively. f_{rej} drops to a lower percentage of 85% (or 84% for ρ_s) when a fraction of f_{err} additional errors is added to $v_{\text{pec}}^{z=0}$ which still suggests a significant negative correlation.

3.5 Orbital period and peculiar velocity

The binaries in our compilation all survived their NKs; their observed orbital periods (P_{orb}) can give insights on how tightly bound they were and thus on distribution of NK magnitudes. We thus also include known P_{orb} in the compilation (Table 3).

It is also interesting to check if P_{orb} and $v_{\text{pec}}^{z=0}$ show any evidence of dependences, so we follow a Bayesian approach similar to that in Sec 3.4 to fit the data. The intercept and slope are denoted as $\theta_{0, P_{\text{orb}}}$ and $\theta_{1, P_{\text{orb}}}$.

This model is applied to simulated data generated by a similar bootstrapping process as in Sec 3.4, i.e., for each binary that has a well measured P_{orb} , we sample 1000 velocities from the calculated distribution; the only difference here is that we do not simulate P_{orb} but use the literature P_{orb} values for all simulated velocities as the compiled P_{orb} 's are all tightly-constrained (median fractional error of 5×10^{-6}). The fit result suggests a negative slope of -0.19 with a 99.7% credible interval between -0.29 and -0.09 . We plot the distribution of model parameters in Figure 5 and plot the scatters of $v_{\text{pec}}^{z=0}$ and P_{orb} in Figure 7.

Following the same approach, we also calculate the ρ_s and ρ_p for $v_{\text{pec}}^{z=0}$ vs. P_{orb} . The correlation is significant as all simulations yield p -values below 1%, and even with additional uncertainty in $v_{\text{pec}}^{z=0}$, the f_{rej} is still at a robust level (Table 7). We can therefore conclude that the anti-correlation between $v_{\text{pec}}^{z=0}$ and P_{orb} is statistically significant.

4 DISCUSSION

Our statistical analyses together suggest a significant anti-correlation between $v_{\text{pec}}^{z=0}$ and M_{tot} , and between $v_{\text{pec}}^{z=0}$ and P_{orb} . In this section, we present some physical interpretation of these results and discuss possible observational and physical biases that could have contributed to our results.

4.1 Peculiar velocity vs. binary total mass

NKs imparted on compact objects at SNe can be broadly attributed to two effects: recoil due to a sudden ejection of mass (also known as the ‘‘Blaauw kick’’, Blaauw 1961) and/or any additional impulses of momentum on the compact object. The difference between the two is that the former conserves system (ejecta-binary) linear momentum, so binaries in which the companion star of the compact object is more massive would acquire a smaller $v_{\text{pec}}^{z=0}$ if the ejecta momenta

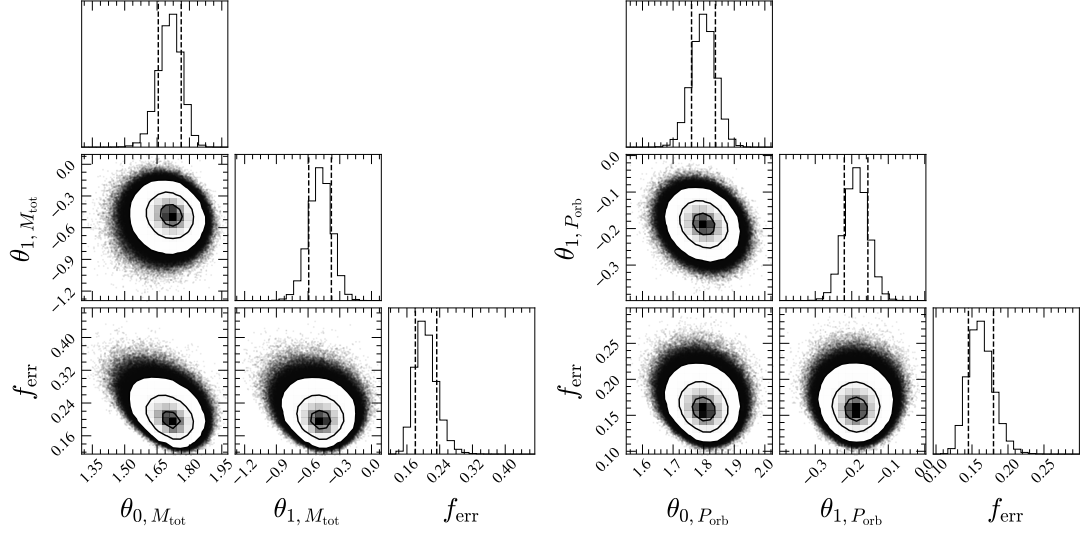


Figure 5. Corner plot made using the `corner` package (Foreman-Mackey et al. 2016) showing posterior distributions of fit parameters of $v_{\text{pec}}^{z=0}$ vs. M_{tot} (left) and $v_{\text{pec}}^{z=0}$ vs. P_{orb} (right). The contours in the projected distributions correspond to 1, 2, and 3 σ levels. The vertical dashed lines in the marginal panels indicate 68% credible intervals.

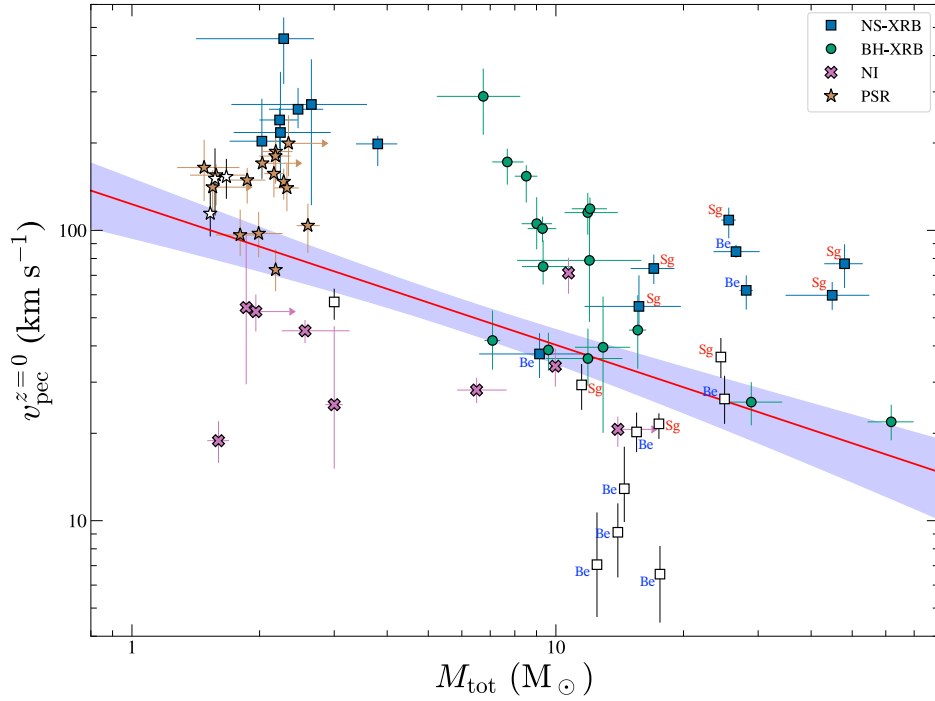


Figure 6. $v_{\text{pec}}^{z=0}$ vs. M_{tot} for binaries with constrained or lower limits on M_{tot} (filled markers) and those that have only approximate masses (empty markers with no error bars on M_{tot}). The error bars of $v_{\text{pec}}^{z=0}$ correspond to 16th and 84th percentiles. The red solid line indicates the best-fit model (Sec 3.4), with the blue shading indicating the 68% confidence region. The NS-HMXBs are further distinguished between those that have a supergiant companion (“Sg”) and a Be companion (“Be”).

are comparable among different binaries. This can, however, be complicated by the fact that the orbital speeds of the supernova progenitor can, in some cases, be faster in shorter-period binaries, which may be associated with lower mass companion stars. An impulse of an additional momentum beyond ejecta-induced recoil, on the other hand, is equivalent to having an external force on the compact object, so this conservation is no longer met. With an additional kick, even a

massive binary can end up with high $v_{\text{pec}}^{z=0}$ if the kick velocity is at a supportive magnitude and direction that keep the binary bound.

The kinematic formulation of $v_{\text{pec}}^{z=0}$ was derived by Kalogera (1996) (K96 hereafter) which incorporates the effect of both mass ejecta and additional kick velocity. According to K96, a bound binary that

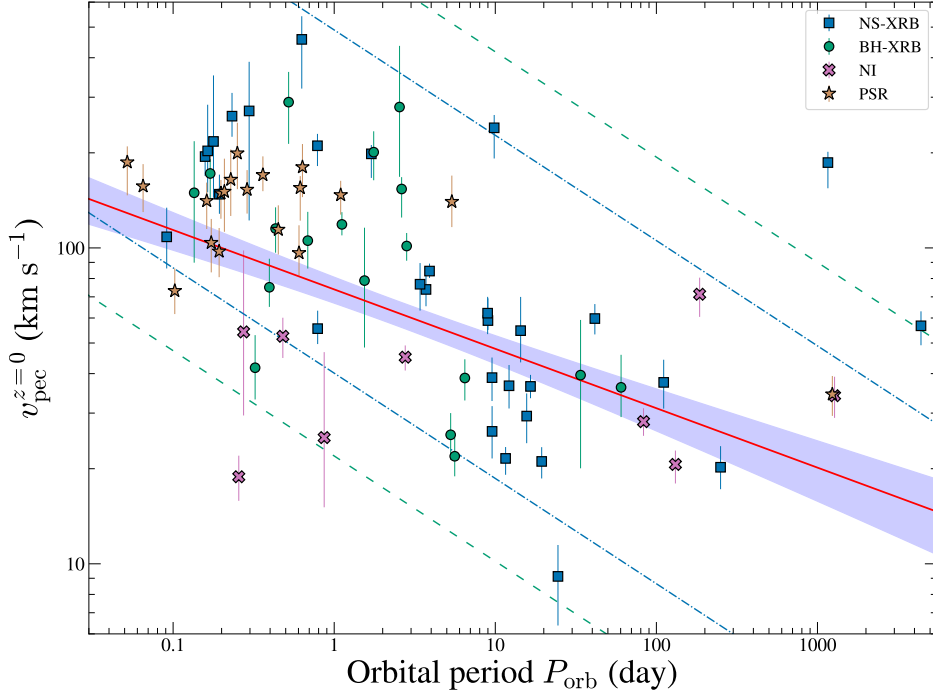


Figure 7. Scatter plot of $v_{\text{pec}}^{z=0}$ and P_{orb} for binaries with measured P_{orb} . The error bars on $v_{\text{pec}}^{z=0}$ correspond to 16th and 84th percentiles from Table 3. The model with the median bootstrapped fit parameters is shown with the solid red line; the blue shading indicates the 68% confidence region. The blue dashed-dotted line and green dashed line represent the K96 limits (as example trend lines) for a typical NS and BH-LMXB, respectively, assuming M_1 and ΔM in Table 8 and $M_2 = 0.5 M_{\odot}$.

Table 7. Pearson and Spearman's coefficients and the corresponding p -values. Uncertainties correspond to the 68% confidence level.

$v_{\text{pec}}^{z=0}$ vs.	ρ_p	p -value (ρ_p)	f_{rej} (%)	ρ_s	p -value (ρ_s)	f_{rej} (%)
With no additional error in $v_{\text{pec}}^{z=0}$						
M_{tot}	-0.52 ± 0.03	$4.69^{+15.05}_{-3.61} \times 10^{-6}$	100	-0.55 ± 0.03	$1.18^{+4.91}_{-0.96} \times 10^{-6}$	100
P_{orb}	-0.53 ± 0.02	$6.68^{+15.31}_{-4.69} \times 10^{-7}$	100	-0.57 ± 0.02	$5.15^{+17.48}_{-4.11} \times 10^{-8}$	100
With f_{err} percent additional error in $v_{\text{pec}}^{z=0}$						
M_{tot}	-0.39 ± 0.08	$9.96^{+80.36}_{-9.20} \times 10^{-4}$	85	-0.39 ± 0.08	$9.09^{+90.90}_{-8.49} \times 10^{-4}$	84
P_{orb}	-0.46 ± 0.06	$2.96^{+32.04}_{-2.80} \times 10^{-4}$	99	-0.50 ± 0.07	$5.81^{+108.85}_{-5.63} \times 10^{-6}$	99

survived the SN gets a $v_{\text{pec}}^{z=0}$ constrained between an upper and lower limit given by⁷:

$$v_{\text{pec,min}}^{z=0}/V_r = \frac{M_1 + \Delta M}{M_{\text{tot}} + \Delta M} - \frac{\sqrt{2}M_1}{M_{\text{tot}}^{1/2} (M_{\text{tot}} + \Delta M)^{1/2}}$$

$$v_{\text{pec,max}}^{z=0}/V_r = \frac{M_1 + \Delta M}{M_{\text{tot}} + \Delta M} + \frac{\sqrt{2}M_1}{M_{\text{tot}}^{1/2} (M_{\text{tot}} + \Delta M)^{1/2}}, \quad (9)$$

where ΔM is the ejecta mass; V_r is the relative orbital velocity at SN. If one assumes a circular orbit,

$$V_r = 212.9 \left(\frac{M_{\text{tot}} + \Delta M}{M_{\odot}} \right)^{1/3} \left(\frac{P_{\text{orb,SN}}}{\text{day}} \right)^{-1/3} \text{ km s}^{-1}, \quad (10)$$

where $P_{\text{orb,SN}}$ is the orbital period at the instant of SN. Physically, the upper limit is reached when the NK is in the opposite direction

to the orbital velocity of the BH/NS progenitor at the instant of SN while keeping the binary bound; the lower limit, on the other hand, corresponds to the minimum possible NK on the compact object to keep the binary from being disrupted by mass ejection. Eq 9 and 10 immediately point to an anti-correlation with M_{tot} ; this simply indicates that more massive systems are harder to be accelerated by NKs.

One can also get the difference between the maximum and minimum $v_{\text{pec}}^{z=0}$:

$$v_{\text{pec,max}}^{z=0} - v_{\text{pec,min}}^{z=0} = \frac{2\sqrt{2}M_1}{M_{\text{tot}}^{1/2} (M_{\text{tot}} + \Delta M)^{1/2}} V_r$$

$$\propto M_1 M_{\text{tot}}^{-1/2} (M_{\text{tot}} + \Delta M)^{-1/6} P_{\text{orb,SN}}^{-1/3} \quad (11)$$

This difference is related to the width of $v_{\text{pec}}^{z=0}$ distributions.

A simple comparison can then be performed between different binary subgroups hosting NSs, given that M_1 for these binaries are very similar. From eq 11, it immediately follows that NS-LMXBs exhibit a broader distribution compared to HMXBs because they have: (1) more compact orbits at SN, (2) smaller progenitor (helium core)

⁷ Note that the equations are slightly different from the K96 version because we re-write it with the notations in this paper (Sec D).

mass at SN thus less mass was ejected (smaller ΔM), and (3) apparently smaller M_{tot} values. The progenitors of LMXBs are thought to begin with a wide orbit which then dramatically shrinks through a common envelope (CE) process (Paczynski 1976). The shrunken orbits greatly increase the survivability against the coming SN and lead to higher $v_{\text{pec}}^{z=0}$. While some HMXBs could have a comparable pre-SN orbit (e.g., Cen X-3; see e.g., van den Heuvel & Heise 1972), the $M_{\text{tot}}^{-1/2} (M_{\text{tot}} + \Delta M)^{-1/6}$ factor contributes significantly considering a factor of few or even an order of magnitude difference in M_{tot} .

Our compiled NS-LMXBs are within the “allowed” range defined by the K96 limits (Figure 8); however, we noted that all of them are above $\approx 50 \text{ km s}^{-1}$, so the lower-left of Figure 6 is clearly underpopulated. It was pointed out by Kalogera (1998) that some LMXBs could have originated from progenitors in wide orbits which then shrink if the kick velocity is at a favourable magnitude and direction; this “direct-SN” scenario circumvents the need of a CE stage, and thus SN would occur at wide orbits, leading to low- $v_{\text{pec}}^{z=0}$ (typically between 20 – 50 km s^{-1}) binaries. Their absence could be a result of observational biases (see Sec 4.4).

It is also worth noting that the NIs that host NSs have systematically lower $v_{\text{pec}}^{z=0}$ than NS-LMXBs, but the significance of this difference can only be addressed with a greater sample and more confident identifications of NS-NIs. Indeed, the nature of the compact object is yet ambiguous in some systems, as their M_1 can also overlap with the range for massive white dwarfs. Nevertheless, it is also possible that NS-NIs might have also been formed through the “direct-SN” scenario similar to that for LMXBs, but the orbits were not perturbed sufficiently by the kick and shrunk enough for mass transfer to start. With the observed upper limit $\approx 60 \text{ km s}^{-1}$ for $v_{\text{pec}}^{z=0}$ and a $\Delta M = 1 M_{\odot}$, the progenitor has a $P_{\text{orb,SN}} \approx 560$ day following eq 9. Efficiency of such scenario is beyond the scope of this paper and can be addressed by future population synthesis studies.

One can also compare the range of $v_{\text{pec}}^{z=0}$ for subclasses of HMXBs. After the first mass-exchange stage (i.e., from the compact object progenitor to the companion), HMXBs with supergiant donors (SgXRBs) are thought to be in closer orbits (period could be as short as a few days; see e.g., De Loore et al. 1974), while those with Be stars (BeXRBs) could be much wider (periods of up to hundreds of days; e.g., Habets 1985). Although SgXRBs have slightly greater M_{tot} than BeXRBs, they are not drastically different. Therefore, $P_{\text{orb,SN}}$ plays a more crucial role. As a result, $v_{\text{pec}}^{z=0}$ for BeXRBs should be systematically downscaled by V_r compared to SgXRBs. This distinction has been suggested by past studies (van den Heuvel et al. 2000; Fortin et al. 2022), and will be tested with future statistical analyses (Nuchvanichakul et al., in prep).

In all, the decreasing trend with increasing M_{tot} could be roughly attributed to increasing inertia of binaries, regardless of additional kick velocity; this trend can also be guided by the K96 limits assuming some orbital parameters at SN for subgroups of binaries. To visualise this, in Figure 8, we plot K96 limits for different types of binaries assuming some typical parameters at SN (Table 8), where we further distinguish between SgXRBs and BeXRBs following the catalogue made by Fortin et al. (2023). Given the assumed $P_{\text{orb,SN}}$ and ΔM , most binaries are consistent with the K96 limits.

Several caveats should be considered in interpreting the results. Even though K96 is agnostic to detailed kick mechanism, it does rely on the assumption of a Gaussian distribution for the kick velocity components; however, it is possible that the distribution might differ for different kick mechanisms. Moreover, it should also be noted that we use the universal log-linear fit across different binary types

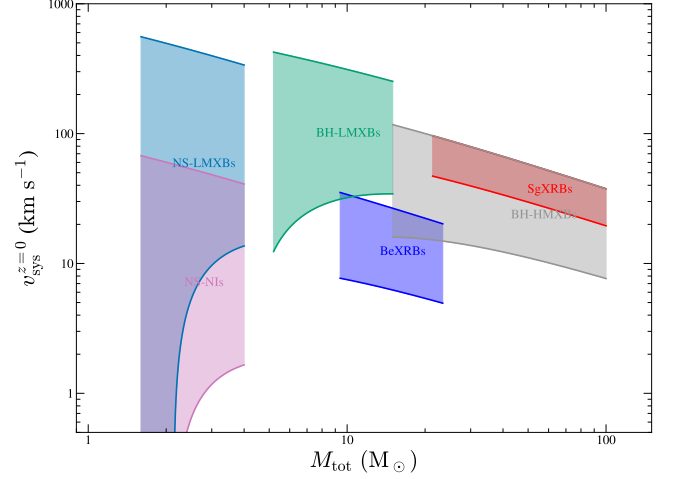


Figure 8. K96 limits (eq 9) plotted for different binary types hosting NSs or BHs, using orbital parameters from Table 8. A general decreasing trend with M_{tot} is present despite each group having a range of possible $v_{\text{pec}}^{z=0}$ values.

Table 8. Typical parameters for different binary types used to plot K96 limits in Figure 8.

Type	$M_1 (M_{\odot})$	$\Delta M (M_{\odot})$	$P_{\text{orb,SN}} (\text{day})$
NS-LMXB	1.4	1.0	1
BH-LMXB	5.0	6.0	10
BH-HMXB	5.0	6.0	100
SgXRB	1.4	5.0	10
BeXRB	1.4	2.0	300
NS-NI	1.4	1.0	560

as a complementary method to test for negative correlation, so caution should be exercised in drawing very detailed conclusions about the underlying physical processes; with discoveries of more binaries in each type, type-specific analyses (e.g., with Bayesian hierarchical modelling) would certainly be helpful to explore different kick mechanisms.

4.2 GX 1+4: a wide symbiotic X-ray binary with a high peculiar velocity

GX 1+4 is a rare case of symbiotic X-ray binary where a NS is in a wide orbit ($P_{\text{orb}} = 1160$ day) with a late-type giant (SyXRBs; Hinkle et al. 2006). In our compilation, it has a large $v_{\text{pec}}^{z=0} (\gtrsim 100 \text{ km s}^{-1})$ so stands out in the upper right region of Figure 7. A high $v_{\text{pec}}^{z=0}$ could be a result of a strong NK, but this then contradicts its wide orbit that is prone to disruption by strong kicks. GX 1+4 does not have a well-measured *Gaia* parallax, so we adopt the distance estimate of 4.5 kpc in Hinkle et al. (2006). Indeed, its negative parallax indicates that the true parallax is very small, so the distance should be greater than 4.5 kpc (Bailer-Jones et al. 2021), which will further increase its $v_{\text{pec}}^{z=0}$ value. As a comparison, another SyXRB, 4U 1700+24, has a wider orbit ($P_{\text{orb}} = 4391$ day; Hinkle et al. 2019) but is less of an outlier considering that its $v_{\text{pec}}^{z=0}$ is close to the velocity dispersion of the disc population ($\approx 40 \text{ km s}^{-1}$; Carlberg et al. 1985).

There are multiple scenarios where wide SyXRBs can survive SNe. One possibility is that NSs in some SyXRB progenitors were formed through electron capture SNe (Miyaji et al. 1980; Nomoto

1984) or accretion-induced collapse (AIC; Freire & Tauris 2014). Theoretical work suggests that these events generally impart low NKs on the NSs (Dessart et al. 2006; Kitaura et al. 2006; Gessner & Janka 2018), despite the fact that population synthesis suggested that only a small fraction formed in this way (Lü et al. 2012). Alternatively, the massive component (i.e., the NS progenitor) might have lost a considerable fraction of its envelope through a CE stage (Taam & Sandquist 2000), which in turn limits the amount of mass ejected in the following SNe and thus the Blaauw kick. However, this is hard to reconcile with the observed high $v_{\text{pec}}^{z=0}$ values based on either a weak kick or a small mass loss. Following the formulation of Nelemans et al. (1999), after a core-collapse SN, the ejecta mass has to be less than half of the total of helium core and companion mass to not disrupt the progenitor binary; if GX 1+4 starts in a compact binary at the SN with $P_{\text{orb,SN}} = 10$ day, and if one assumes a helium core mass of $3 M_{\odot}$ and a companion mass of $1 M_{\odot}$ at SN, mass loss can only contribute a maximum of only $\approx 63 \text{ km s}^{-1}$ to the $v_{\text{pec}}^{z=0}$; then post-SN evolution will have to involve mechanisms that expand the orbit to match its present-day P_{orb} . Fortuitous cases where the NS is accelerated by appropriately directed weak kicks might reconcile with the large $v_{\text{pec}}^{z=0}$ but should be very rare.

Alternatively, GX 1+4's proximity to the Galactic centre might suggest that it is a binary born in the bulge. In this case, it would have been dynamically perturbed by the dense stellar population there, so its $v_{\text{pec}}^{z=0}$ is not reflective of a NK. However, it is worth noting that SyXRBs with wide orbits are particularly susceptible to disruption due to dynamical encounters in dense environments (see e.g., Belloni et al. 2020). There have been no confirmed symbiotic stars in comparably dense globular clusters, although there is one controversial candidate (Henleywillis et al. 2018; Belloni et al. 2020).

4.3 Present-day orbital period vs. peculiar velocity

Interpreting the anti-correlation with P_{orb} following K96 can be more complex. One could naively ascribe the decreasing trend in $v_{\text{pec}}^{z=0}$ to the upper K96 limits that scale negatively with $P_{\text{orb,SN}}$ (see Figure 7); however, transposing from $P_{\text{orb,SN}}$ to the present-day P_{orb} requires knowledge of (1) the kick magnitude and direction on the compact object, and (2) post-SN orbital evolution. Brandt & Podsiadlowski (1995, B95, hereafter) have conducted a systematic investigation of pre- and post-SN orbital parameters and found that most binaries have a post-SN orbital period ($P_{\text{orb, post-SN}}$) close to $P_{\text{orb,SN}}$ within a factor of a few (fig 4a in B95). Additionally, B95 points out that among binaries that survived SNe, the ones with high v_{pec} values are preferentially those perturbed by NKs in approximately the *opposite* direction to the instantaneous orbital velocity of the compact objects; this can essentially decelerate the compact object and shrink the orbits, resulting in a decreasing trend with $P_{\text{orb, post-SN}}$ (e.g., fig 5b in B95).

After SNe, there are various mechanisms that can further change the orbital period. While $P_{\text{orb, post-SN}}$ should be reasonably close to their present-day values for the HM binaries considering their young ages, the orbit of LM binaries (especially LMXBs) is dependent on the synergy of mass transfer and/or processes that dissipate angular momentum. The former sets in when the mass donor fills its Roche lobe due to nuclear evolution (sub-giant donors, e.g., Cyg X-2) or orbit shrinkage induced by angular momentum loss (main-sequence donors); the orbit tends to expand on thermal timescale under stable and conservative mass transfer. However, to maintain the donor's contact with its Roche lobe, mechanisms are needed to extract angu-

lar momentum from the system to counteract orbit expansion. The current consensus is that angular momentum can be dissipated via gravitational wave radiation (Faulkner 1971; Verbunt 1993) and/or magnetic braking (Rappaport et al. 1983); the former only dominates in ultra-compact X-ray binaries, while magnetic braking is considered effective in the majority of LMXBs. Over these processes, orbits can expand or shrink at the bifurcation period (≈ 1 day; Tutukov et al. 1985; Pylyser & Savonije 1988). Depending on the initial (at the onset of mass transfer) state of the donor and magnetic braking prescription, the overall mass transfer phase can modify the orbital period by up to ≈ 2 orders of magnitude (see e.g., Ergma & Sarna 1996; Podsiadlowski et al. 2002; Van et al. 2019).

Despite this multitude of uncertainty, Figure 7 still shows a significant anti-correlation. So while different evolutionary trajectories probably account for much of the scatter visible in the figure, these do not erase underlying properties linking binaries across the dynamic range of our sample. Figure 7 thus provides a useful constraint for population synthesis models to satisfy. The strongest governing link is likely the system binding energy, with wider binaries being loosely bound and thus being more likely to be disrupted when $v_{\text{pec}}^{z=0}$ is higher. Testing this hypothesis, however, will require proper characterisation of XRB selection, combined with *Gaia*'s selection function (cf. Cantat-Gaudin et al. 2023) which is beyond the scope of the present work.

4.4 Possible biases

The $v_{\text{pec}}^{z=0}$ - M_{tot} and $v_{\text{pec}}^{z=0}$ - P_{orb} correlations could have been contributed by selection biases on our sample. It should be firstly noted that our compilation contains only NSs and BHs in *present-day* bound systems, which is not necessarily a representation of the binary demography at the instant of SNe. In part, either mass ejection or additional kicks would typically bias against wide binaries, which were more prone to being disrupted; NSs in very close pre-SN orbits, on the other hand, could be re-directed to collide with the companion and form Thorne-Żytkow objects (Thorne & Zytkov 1975, 1977).

Wide binaries are also prone to observational biases considering the difficulty of measuring long P_{orb} . There is an obvious paucity of binaries above $P_{\text{orb}} \approx 100$ day in Figure 7: six binaries are present including two wide SyXRBs (Sec 4.2), the non-interacting binary Gaia BH2 (El-Badry et al. 2023a), the massive binary pulsar PSR B1259-63, and two HMXBs (1A 0535+262 and X Persi). Compact objects in NIs can only be confirmed by robust constraints on mass function, which in turn asks for multi-epoch observations spanning at least one full orbital period; for very long P_{orb} 's, this could be time-expensive. Dedicated radial velocity campaign can therefore only be performed for a handful of well-justified cases, despite the fact that there might be a uncharted population of wide NIs (e.g., El-Badry et al. 2023b,a). Wide binaries can also be sought by searches for astrometric wobble with, e.g. *Gaia* (Gould & Salim 2002; Barstow et al. 2014).

There might also be more wide BeXRBs to be discovered (Vinciguerra et al. 2020). BeXRBs are mostly transient systems that exhibit periodic X-ray outbursts (Type I outbursts) that can be orders of magnitude brighter than their quiescence. Because these outbursts happen at roughly P_{orb} , they can be used to measure their P_{orb} . However, this relies on the consecutiveness of outburst detection, which is less feasible if P_{orb} is very long. Moreover, long P_{orb} might also restrict X-ray detectability, typically for wind-fed HMXBs. Identification of a NS in HMXBs can be assisted by detections of (accretion-induced) X-ray pulsations. However, at a given wind mass loss rate of the mass donor, X-ray luminosities of such binaries scale inversely

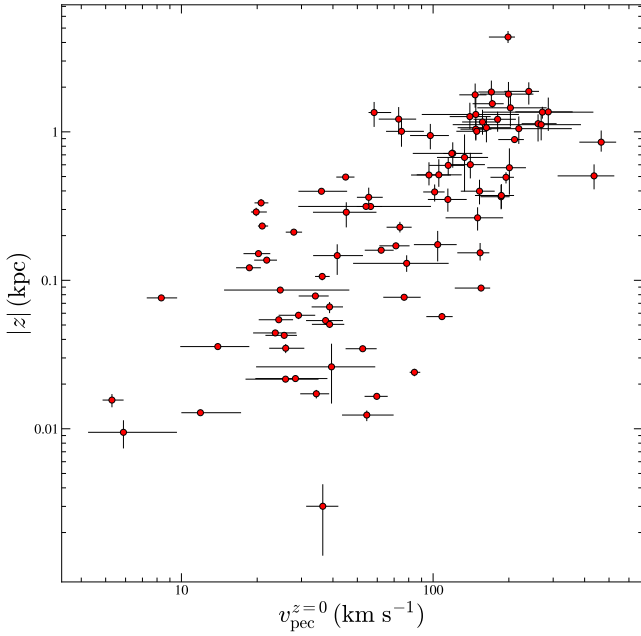


Figure 9. Galactic height $|z|$ vs. $v_{\text{pec}}^{z=0}$ showing a clear positive correlation for binaries in Table 3. Error bars correspond to 16th and 84th percentiles.

with orbital separation (Bondi & Hoyle 1944), so wide systems would be more difficult to detect. Contrary to wind-fed HMXBs, thinner stellar wind in wide binaries could in favour discovery of more OB-pulsar binaries like PSR B1259–63. The NS nature in such binaries can be confirmed by detection of radio pulsations (Johnston et al. 1992; Lyne et al. 2015), which can otherwise be greatly smeared out by stronger stellar wind in more compact systems.

We have excluded binaries in globular clusters from our sample; however, it is possible that some of the LMXBs in our sample were formed in globular clusters but were later dynamically ejected. This can account for typically (ultra-)compact X-ray binaries that are more likely to survive dynamical interactions in dense environment. Combining an escape velocity of 50 km s^{-1} (velocity relative to the cluster) and cluster velocity dispersion of $100\text{--}120 \text{ km s}^{-1}$ (Vasiliev 2019) results in $v_{\text{pec,p}}$ over 100 km s^{-1} ; therefore, the high-velocity part of our sample might have been contaminated, although simulations only suggest a small number of such binaries (Kremer et al. 2018). Future metallicity measurements will provide information to further identify/discover these ejected systems.

Another observational bias involves the Galactic height ($|z|$) of binaries off the plane. We select the binaries based on robust identification of compact objects. This would require optical/near-IR visibility of the luminous component and would therefore bias against potential low- $v_{\text{pec}}^{z=0}$ systems as they are less likely to reach large $|z|$ as the high- $v_{\text{pec}}^{z=0}$ ones (Figure 9) and therefore are more obscured by Galactic extinction (Gandhi et al. 2020; Jonker et al. 2021). This bias could be typically strong against LM binaries that have faint components, e.g., LM-NIs, and is even worse for the low- $v_{\text{pec}}^{z=0}$ LMXBs that formed through direct-SN (Kalogera 1998; Sec 4.1), which could have populated the lower-left region of the $v_{\text{pec}}^{z=0}$ - P_{orb} plot. It will be interesting to constrain the extent to which these low-velocity binaries are affected by observational biases while exploring possible physical mechanisms that contribute to the lack of such binaries.

5 CONCLUSION

We compile a sample of 89 binaries that host NSs and BHs and have measured astrometry and systemic radial velocities. We calculate their present-day peculiar velocities ($v_{\text{pec,p}}$) and their extrapolated peculiar velocity at the Galactic disc ($v_{\text{pec}}^{z=0}$) which are treated as the potential velocity at birth incorporating uncertainties in astrometric parameters and Galactic constants. These calculated velocity samples can be compared to simulated distributions in future population synthesis studies.

We performed some statistical modelling the overall distribution and comparison between distributions of different subgroups. Our findings suggest no statistically significant difference between BH and NS binaries; however, we find that HM binaries are restricted to $v_{\text{pec}}^{z=0}$ below $\approx 100 \text{ km s}^{-1}$ while LM binaries exhibit a much wider distribution that goes up to $\approx 400 \text{ km s}^{-1}$. The difference is mostly contributed by NS binaries, while comparing BH-LM and HM binaries only suggest a moderate significance.

Fitting a log-linear model of $v_{\text{pec}}^{z=0}$ vs. M_{tot} results in a negative slopes at over 99.7% confidence, while a similar log-linear fit to $v_{\text{pec}}^{z=0}$ vs. P_{orb} also gives a significant negative slope (at 99.7% confidence). Both fits suggest a non-negligible fraction of additional uncertainty, with which both anti-correlations are slightly weakened but are still at robust levels. The anti-correlation between $v_{\text{pec}}^{z=0}$ with M_{tot} follows the kinematic formulation derived by Kalogera (1996). Interpretation of the correlation with P_{orb} is complicated by uncertainty in underlying kick velocity distribution and binary evolution models, which would require more detailed population synthesis studies.

ACKNOWLEDGEMENTS

We thank the anonymous reviewer for their helpful feedback. This work has made use of data from the European Space Agency (ESA) mission *Gaia* (<https://www.cosmos.esa.int/gaia>), processed by the *Gaia* Data Processing and Analysis Consortium (DPAC, <https://www.cosmos.esa.int/web/gaia/dpac/consortium>). Funding for the DPAC has been provided by national institutions, in particular the institutions participating in the *Gaia* Multilateral Agreement. This research has also made use of the SIMBAD database, operated at CDS, Strasbourg, France. PG, YZ, and CDB acknowledge UKRI and STFC for support.

DATA AVAILABILITY

The *Gaia* astrometry data are available by querying the *Gaia* archive. The calculated $v_{\text{pec,p}}$ and $v_{\text{pec}}^{z=0}$ samples are available upon request.

REFERENCES

- Abubekurov M. K., Antokhina É. A., Cherepashchuk A. M., 2004, *Astronomy Reports*, 48, 89
- Allen B., et al., 2013, *ApJ*, 773, 91
- An H., et al., 2015, *ApJ*, 806, 166
- Andrews J. J., Kalogera V., 2022, *ApJ*, 930, 159
- Angelini L., White N. E., 2003, *ApJ*, 586, L71
- Antoniadis J., et al., 2013, *Science*, 340, 448
- Aragona C., McSwain M. V., Grundstrom E. D., Marsh A. N., Roettenbacher R. M., Hessler K. M., Boyajian T. S., Ray P. S., 2009, *ApJ*, 698, 514
- Aragona C., McSwain M. V., De Becker M., 2010, *ApJ*, 724, 306
- Archibald A. M., Kaspi V. M., Hessels J. W. T., Stappers B., Janssen G., Lyne A., 2013, *arXiv e-prints*, p. arXiv:1311.5161

- Arnason R. M., Papei H., Barmby P., Bahramian A., Gorski M. D., 2021, *MNRAS*, **502**, 5455
- Arras P., Lai D., 1999, *ApJ*, **519**, 745
- Ashcraft T. A., Hynes R. I., Robinson E. L., 2012, *MNRAS*, **424**, 620
- Atri P., et al., 2019, *MNRAS*, **489**, 3116
- Atri P., et al., 2020, *MNRAS*, **493**, L81
- Bailer-Jones C. A. L., Rybizki J., Fouesneau M., Demleitner M., Andrae R., 2021, *AJ*, **161**, 147
- Bandyopadhyay R. M., Shahbaz T., Charles P. A., Naylor T., 1999, *MNRAS*, **306**, 417
- Barstow M. A., et al., 2014, *arXiv e-prints*, p. [arXiv:1407.6163](https://arxiv.org/abs/1407.6163)
- Barsukova E. A., Borisov N. V., Burenkov A. N., Klochkova V. G., Goranskij V. P., Metlova N. V., 2005, *The Astronomer's Telegram*, **416**, 1
- Bassa C. G., et al., 2016, *MNRAS*, **460**, 2207
- Bates S. D., et al., 2015, *MNRAS*, **446**, 4019
- Bellm E. C., et al., 2016, *ApJ*, **816**, 74
- Belloni D., Mikołajewska J., Ikiiewicz K., Schreiber M. R., Giersz M., Rivera Sandoval L. E., Rodrigues C. V., 2020, *MNRAS*, **496**, 3436
- Belokurov V., et al., 2020, *MNRAS*, **496**, 1922
- Bikmaev I. F., et al., 2017, *Astronomy Letters*, **43**, 664
- Bird A. J., et al., 2016, *ApJS*, **223**, 15
- Blaauw A., 1961, *Bull. Astron. Inst. Netherlands*, **15**, 265
- Bondi H., Hoyle F., 1944, *MNRAS*, **104**, 273
- Bonnet-Bidaud J. M., Mouchet M., 1998, *A&A*, **332**, L9
- Bovy J., 2015, *ApJS*, **216**, 29
- Bradshaw C. F., Fomalont E. B., Geldzahler B. J., 1999, *ApJ*, **512**, L121
- Brandt N., Podsiadlowski P., 1995, *MNRAS*, **274**, 461
- Brandt W. N., Podsiadlowski P., Sigurdsson S., 1995, *MNRAS*, **277**, L35
- Brisken W. F., Fruchter A. S., Goss W. M., Herrnstein R. M., Thorsett S. E., 2003, *AJ*, **126**, 3090
- Cadolle Bel M., et al., 2007, *ApJ*, **659**, 549
- Cadolle Bel M., et al., 2009, *A&A*, **501**, 1
- Callanan P. J., Garnavich P. M., Koester D., 1998, *MNRAS*, **298**, 207
- Camilo F., Rasio F. A., 2005, in Rasio F. A., Stairs I. H., eds, *Astronomical Society of the Pacific Conference Series Vol. 328, Binary Radio Pulsars*. p. 147 ([arXiv:astro-ph/0501226](https://arxiv.org/abs/astro-ph/0501226)), doi:10.48550/arXiv.astro-ph/0501226
- Cantat-Gaudin T., et al., 2023, *A&A*, **669**, A55
- Cantrell A. G., et al., 2010, *ApJ*, **710**, 1127
- Carlberg R. G., Dawson P. C., Hsu T., Vandenberg D. A., 1985, *ApJ*, **294**, 674
- Casares J., Charles P. A., 1994, *MNRAS*, **271**, L5
- Casares J., Steeghs D., Hynes R. I., Charles P. A., O'Brien K., 2003, *ApJ*, **590**, 1041
- Casares J., Zurita C., Shahbaz T., Charles P. A., Fender R. P., 2004, *ApJ*, **613**, L133
- Casares J., Ribó M., Ribas I., Paredes J. M., Martí J., Herrero A., 2005, *MNRAS*, **364**, 899
- Casares J., Cornélisse R., Steeghs D., Charles P. A., Hynes R. I., O'Brien K., Strohmayer T. E., 2006, *MNRAS*, **373**, 1235
- Casares J., et al., 2009, *ApJS*, **181**, 238
- Casares J., Ribó M., Ribas I., Paredes J. M., Vilardell F., Noguera I., 2012, *MNRAS*, **421**, 1103
- Casares J., Muñoz-Darias T., Mata Sánchez D., Charles P. A., Torres M. A. P., Armas Padilla M., Fender R. P., García-Rojas J., 2019, *MNRAS*, **488**, 1356
- Chakrabarty D., 1998, *ApJ*, **492**, 342
- Chakrabarty D., Wang Z., Juett A. M., Lee J. C., Roche P., 2002, *ApJ*, **573**, 789
- Charles P., Matthews J. H., Buckley D. A. H., Gandhi P., Kotze E., Paice J., 2019, *MNRAS*, **489**, L47
- Chaty S., Bessolaz N., 2006, *A&A*, **455**, 639
- Chaty S., Mignani R. P., Israel G. L., 2006, *MNRAS*, **365**, 1387
- Chauhan J., et al., 2021, *MNRAS*, **501**, L60
- Chen Y. P., Zhang S., Torres D. F., Wang J. M., Li T. P., 2010, *A&A*, **510**, A81
- Chenevez J., et al., 2016, *ApJ*, **818**, 135
- Cherepashchuk A. M., Khruzina T. S., Bogomazov A. I., 2021, *MNRAS*, **508**, 1389
- Chevalier C., Ilovaisky S. A., 1990, *A&A*, **228**, 115
- Chevalier C., Ilovaisky S. A., 1998, *A&A*, **330**, 201
- Chojnowski S. D., et al., 2017, *AJ*, **153**, 174
- Chugai N. N., 1984, *Soviet Astronomy Letters*, **10**, 87
- Clark D. J., et al., 2010, *MNRAS*, **406**, L75
- Clark C. J., et al., 2021, *MNRAS*, **502**, 915
- Coleiro A., Chaty S., 2013, *ApJ*, **764**, 185
- Corbet R. H. D., Mason K. O., 1984, *A&A*, **131**, 385
- Cornélisse R., et al., 2002, *A&A*, **392**, 885
- Cornélisse R., Kotze M. M., Casares J., Charles P. A., Hakala P. J., 2013, *MNRAS*, **436**, 910
- Corral-Santana J. M., Casares J., Shahbaz T., Zurita C., Martínez-Pais I. G., Rodríguez-Gil P., 2011, *MNRAS*, **413**, L15
- Corral-Santana J. M., Casares J., Muñoz-Darias T., Bauer F. E., Martínez-Pais I. G., Russell D. M., 2016, *A&A*, **587**, A61
- Cowley A. P., Crampton D., Hutchings J. B., 1982, *ApJ*, **256**, 605
- Crampton D., Hutchings J. B., 1981, *ApJ*, **251**, 604
- Crampton D., Hutchings J. B., Cowley A. P., 1985, *ApJ*, **299**, 839
- Crawford F., et al., 2013, *ApJ*, **776**, 20
- Davison P. J. N., Watson M. G., Pye J. P., 1977, *MNRAS*, **181**, 73
- De Falco V., Kuiper L., Bozzo E., Galloway D. K., Poutanen J., Ferrigno C., Stella L., Falanga M., 2017, *A&A*, **599**, A88
- De Loore C., de Grève J. P., van den Heuvel E. P. J., de Cuyper J. P., 1974, *Mem. Soc. Astron. Italiana*, **45**, 893
- Delgado-Martí H., Levine A. M., Pfahl E., Rappaport S. A., 2001, *ApJ*, **546**, 455
- Deller A. T., et al., 2012, *ApJ*, **756**, L25
- Deneva J. S., et al., 2016, *ApJ*, **823**, 105
- Densham R. H., Charles P. A., 1982, *MNRAS*, **201**, 171
- Dessart L., Burrows A., Livne E., Ott C. D., 2006, *ApJ*, **645**, 534
- Dhawan V., Mirabel I. F., Rodríguez L. F., 2000, *ApJ*, **543**, 373
- Díaz Trigo M., Parmar A. N., Boirin L., Motch C., Talavera A., Balman S., 2009, *A&A*, **493**, 145
- Dorofeev O. F., Rodionov V. N., Ternov I. M., 1985, *Soviet Astronomy Letters*, **11**, 123
- El-Badry K., et al., 2023a, *arXiv e-prints*, p. [arXiv:2302.07880](https://arxiv.org/abs/2302.07880)
- El-Badry K., et al., 2023b, *MNRAS*, **518**, 1057
- Ergma E., Sarna M. J., 1996, *MNRAS*, **280**, 1000
- Fabian A. C., Pringle J. E., Rees M. J., 1975, *MNRAS*, **172**, 15
- Falanga M., Bozzo E., Lutovinov A., Bonnet-Bidaud J. M., Fetisova Y., Puls J., 2015, *A&A*, **577**, A130
- Farrell S. A., Sood R. K., O'Neill P. M., Dieters S., 2008, *MNRAS*, **389**, 608
- Faulkner J., 1971, *ApJ*, **170**, L99
- Filliatre P., Chaty S., 2004, *ApJ*, **616**, 469
- Foreman-Mackey D., et al., 2016, *CornerPy: CornerPy V1.0.2*, Zenodo, doi:10.5281/zenodo.45906
- Fortin F., García F., Chaty S., Chassande-Mottin E., Simaz Bunzel A., 2022, *A&A*, **665**, A31
- Fortin F., García F., Simaz-Bunzel A., Chaty S., 2023, *arXiv e-prints*, p. [arXiv:2302.02656](https://arxiv.org/abs/2302.02656)
- Fragos T., Willems B., Kalogera V., Ivanova N., Rockefeller G., Fryer C. L., Young P. A., 2009, *ApJ*, **697**, 1057
- Freire P. C. C., Tauris T. M., 2014, *MNRAS*, **438**, L86
- Fryer C. L., Kalogera V., 2001, *ApJ*, **554**, 548
- Fryer C. L., Belczynski K., Wiktorowicz G., Dominik M., Kalogera V., Holz D. E., 2012, *ApJ*, **749**, 91
- Fujita Y., Inoue S., Nakamura T., Manmoto T., Nakamura K. E., 1998, *ApJ*, **495**, L85
- Gaia Collaboration et al., 2016, *A&A*, **595**, A1
- Gaia Collaboration et al., 2022, *arXiv e-prints*, p. [arXiv:2208.00211](https://arxiv.org/abs/2208.00211)
- Galloway D. K., Cumming A., 2006, *ApJ*, **652**, 559
- Galloway D. K., Psaltis D., Chakrabarty D., Muno M. P., 2003, *ApJ*, **590**, 999
- Galloway D. K., Psaltis D., Muno M. P., Chakrabarty D., 2006, *ApJ*, **639**, 1033
- Galloway D. K., Muno M. P., Hartman J. M., Psaltis D., Chakrabarty D., 2008, *ApJS*, **179**, 360

- Gamen R., Barbà R. H., Walborn N. R., Morrell N. I., Arias J. I., Maíz Apellániz J., Sota A., Alfaro E. J., 2015, *A&A*, **583**, L4
- Gandhi P., Rao A., Johnson M. A. C., Paice J. A., Maccarone T. J., 2019, *MNRAS*, **485**, 2642
- Gandhi P., Rao A., Charles P. A., Belczynski K., Maccarone T. J., Arur K., Corral-Santana J. M., 2020, *MNRAS*, **496**, L22
- Gandhi P., et al., 2022, *MNRAS*, **510**, 3885
- Gelino D. M., 2002, in American Astronomical Society Meeting Abstracts #200. p. 08.11
- Gelino D. M., Harrison T. E., 2003, *ApJ*, **599**, 1254
- Gelino D. M., Balman Ş., Kızıloğlu Ü., Yılmaz A., Kalemci E., Tomsick J. A., 2006, *ApJ*, **642**, 438
- Gelman A., Rubin D. B., 1992, *Statistical Science*, **7**, 457
- Gessner A., Janka H.-T., 2018, *ApJ*, **865**, 61
- Gies D. R., Bolton C. T., 1986, *ApJS*, **61**, 419
- Gies D. R., et al., 2008, *ApJ*, **678**, 1237
- Gomez S., Grindlay J. E., 2021, *ApJ*, **913**, 48
- Gontcharov G. A., 2006, *Astronomy Letters*, **32**, 759
- González-Galán A., Negueruela I., Castro N., Simón-Díaz S., Lorenzo J., Vilardell F., 2014, *A&A*, **566**, A131
- González Hernández J. I., Casares J., 2010, *A&A*, **516**, A58
- González Hernández J. I., Rebolo R., Peñarrubia J., Casares J., Israelian G., 2005, *A&A*, **435**, 1185
- González Hernández J. I., Rebolo R., Israelian G., 2008a, *A&A*, **478**, 203
- González Hernández J. I., Rebolo R., Israelian G., Filippenko A. V., Chornock R., Tominaga N., Umeda H., Nomoto K., 2008b, *ApJ*, **679**, 732
- González Hernández J. I., Rebolo R., Casares J., 2014, *MNRAS*, **438**, L21
- González Hernández J. I., Suárez-Andrés L., Rebolo R., Casares J., 2017, *MNRAS*, **465**, L15
- Goodwin A. J., Galloway D. K., in't Zand J. J. M., Kuulkers E., Bilous A., Keek L., 2019, *MNRAS*, **486**, 4149
- Gould A., Salim S., 2002, *ApJ*, **572**, 944
- Green G. M., 2018, *The Journal of Open Source Software*, **3**, 695
- Green G. M., Schlafly E., Zucker C., Speagle J. S., Finkbeiner D., 2019, *ApJ*, **887**, 93
- Gregory P. C., 2002, *ApJ*, **575**, 427
- Greiner J., Dennerl K., Predehl P., 1996, *A&A*, **314**, L21
- Grindlay J. E., Petro L. D., McClintock J. E., 1984, *ApJ*, **276**, 621
- Grundstrom E. D., et al., 2007a, *ApJ*, **656**, 431
- Grundstrom E. D., et al., 2007b, *ApJ*, **660**, 1398
- Gunn J. E., Ostriker J. P., 1970, *ApJ*, **160**, 979
- Habets G. M. H. J., 1985, PhD thesis, University of Amsterdam, Netherlands
- Hakala P., Ramsay G., Muhli P., Charles P., Hannikainen D., Mukai K., Vilhu O., 2005, *MNRAS*, **356**, 1133
- Hambaryan V., et al., 2022, *MNRAS*, **511**, 4123
- Harlaftis E. T., Steeghs D., Horne K., Filippenko A. V., 1997, *AJ*, **114**, 1170
- Heida M., Jonker P. G., Torres M. A. P., Chiavassa A., 2017, *ApJ*, **846**, 132
- Heinz S., et al., 2015, *ApJ*, **806**, 265
- Henleywillis S., Cool A. M., Haggard D., Heinke C., Callanan P., Zhao Y., 2018, *MNRAS*, **479**, 2834
- Hills J. G., 1976, *MNRAS*, **175**, 1P
- Hinkle K. H., Fekel F. C., Joyce R. R., Wood P. R., Smith V. V., Lebzelter T., 2006, *ApJ*, **641**, 479
- Hinkle K. H., Fekel F. C., Joyce R. R., Mikołajewska J., Gałan C., Lebzelter T., 2019, *ApJ*, **872**, 43
- Hjellming R. M., Rupen M. P., 1995, *Nature*, **375**, 464
- Hobbs G., Lorimer D. R., Lyne A. G., Kramer M., 2005, *MNRAS*, **360**, 974
- Hoffman M. D., Gelman A., 2011, *arXiv e-prints*, p. arXiv:1111.4246
- Holland-Ashford T., Lopez L. A., Auchettl K., Temim T., Ramirez-Ruiz E., 2017, *ApJ*, **844**, 84
- Homan J., Wijnands R., Kong A., Miller J. M., Rossi S., Belloni T., Lewin W. H. G., 2006, *MNRAS*, **366**, 235
- Hutchings J. B., 1984, *PASP*, **96**, 312
- Hutchings J. B., Crampton D., Cowley A. P., Thompson I. B., 1987, *PASP*, **99**, 420
- Iaria R., et al., 2018, *MNRAS*, **473**, 3490
- Igoshev A. P., 2020, *MNRAS*, **494**, 3663
- Islam N., Paul B., 2016, *MNRAS*, **461**, 816
- Israel G. L., et al., 2000, *MNRAS*, **314**, 87
- Ivanova N., Heinke C. O., Rasio F. A., Belczynski K., Fregeau J. M., 2008, *MNRAS*, **386**, 553
- Janka H.-T., 2013, *MNRAS*, **434**, 1355
- Janka H.-T., 2017, *ApJ*, **837**, 84
- Janot-Pacheco E., Ilovaisky S. A., Chevalier C., 1981, *A&A*, **99**, 274
- Jayasinghe T., et al., 2019, *MNRAS*, **486**, 1907
- Jennings R. J., Kaplan D. L., Chatterjee S., Cordes J. M., Deller A. T., 2018, *ApJ*, **864**, 26
- Johnston S., Manchester R. N., Lyne A. G., Bailes M., Kaspi V. M., Qiao G., D'Amico N., 1992, *ApJ*, **387**, L37
- Jonker P. G., Nelemans G., 2004, *MNRAS*, **354**, 355
- Jonker P. G., van der Klis M., 2001, *ApJ*, **553**, L43
- Jonker P. G., Steeghs D., Nelemans G., van der Klis M., 2005, *MNRAS*, **356**, 621
- Jonker P. G., Kaur K., Stone N., Torres M. A. P., 2021, *ApJ*, **921**, 131
- Kalogera V., 1996, *ApJ*, **471**, 352
- Kalogera V., 1998, *ApJ*, **493**, 368
- Kaper L., van der Meer A., Najjarro F., 2006, *A&A*, **457**, 595
- Kapil V., Mandel I., Berti E., Müller B., 2023, *MNRAS*, **519**, 5893
- Kaplan D. L., Bhlerao V. B., van Kerkwijk M. H., Koester D., Kulkarni S. R., Stovall K., 2013, *ApJ*, **765**, 158
- Kaplan D. L., et al., 2016, *ApJ*, **826**, 86
- Keane E. F., et al., 2018, *MNRAS*, **473**, 116
- Kharchenko N. V., Scholz R. D., Piskunov A. E., Röser S., Schilbach E., 2007, *Astronomische Nachrichten*, **328**, 889
- Khargharia J., Froning C. S., Robinson E. L., 2010, *ApJ*, **716**, 1105
- Khargharia J., Froning C. S., Robinson E. L., Gelino D. M., 2013, *AJ*, **145**, 21
- Khokhlov S. A., et al., 2018, *ApJ*, **856**, 158
- Kimball C., et al., 2022, *arXiv e-prints*, p. arXiv:2211.02158
- Kitaura F. S., Janka H. T., Hillebrandt W., 2006, *A&A*, **450**, 345
- Knigge C., Coe M. J., Podsiadlowski P., 2011, *Nature*, **479**, 372
- Kremer K., Chatterjee S., Rodriguez C. L., Rasio F. A., 2018, *arXiv e-prints*, p. arXiv:1802.04895
- Kumar R., Carroll C., Hartikainen A., Martin O., 2019, *Journal of Open Source Software*, **4**, 1143
- Kuulkers E., van der Klis M., 2000, *A&A*, **356**, L45
- Kuulkers E., et al., 2013, *A&A*, **552**, A32
- LaSala J., Thorstensen J. R., 1985, *AJ*, **90**, 2077
- LaSala J., Charles P. A., Smith R. A. D., Balucinska-Church M., Church M. J., 1998, *MNRAS*, **301**, 285
- Lai D., 2004, in Höflich P., Kumar P., Wheeler J. C., eds, *Cosmic explosions in three dimensions*. p. 276 (arXiv:astro-ph/0312542), doi:10.48550/arXiv.astro-ph/0312542
- Lam C. Y., et al., 2022, *ApJ*, **933**, L23
- Lin J., Yu W., 2020, *ApJ*, **903**, 37
- Lin J., et al., 2023, *ApJ*, **944**, L4
- Linares M., 2018, *MNRAS*, **473**, L50
- Linares M., Shahbaz T., Casares J., 2018, *ApJ*, **859**, 54
- Lindgren L., et al., 2021, *A&A*, **649**, A4
- Ling J. C., Wheaton W. A., 2005, *ApJ*, **622**, 492
- Liu Q. Z., van Paradijs J., van den Heuvel E. P. J., 2006, *A&A*, **455**, 1165
- Liu Q. Z., van Paradijs J., van den Heuvel E. P. J., 2007, *A&A*, **469**, 807
- Lorimer D. R., et al., 2006, *MNRAS*, **372**, 777
- Lü G. L., Zhu C. H., Postnov K. A., Yungelson L. R., Kuranov A. G., Wang N., 2012, *MNRAS*, **424**, 2265
- Lutovinov A. A., Tsygankov S. S., Karasev D. I., Molkov S. V., Doroshenko V., 2019, *MNRAS*, **485**, 770
- Lyne A. G., Lorimer D. R., 1994, *Nature*, **369**, 127
- Lyne A. G., Anderson B., Salter M. J., 1982, *MNRAS*, **201**, 503
- Lyne A. G., Stappers B. W., Keith M. J., Ray P. S., Kerr M., Camilo F., Johnson T. J., 2015, *MNRAS*, **451**, 581
- Lyubimkov L. S., Rostopchin S. I., Roche P., Tarasov A. E., 1997, *MNRAS*, **286**, 549
- MacDonald R. K. D., et al., 2014, *ApJ*, **784**, 2
- Maccarone T. J., 2005, *MNRAS*, **360**, L30

- Maccarone T. J., Osler A., Miller-Jones J. C. A., Atri P., Russell D. M., Meier D. L., McHardy I. M., Longa-Peña P. A., 2020, *MNRAS*, **498**, L40
- Manchester R. N., Hobbs G. B., Teoh A., Hobbs M., 2005, *AJ*, **129**, 1993
- Marino A., Di Salvo T., Gambino A. F., Iaria R., Burderi L., Matranga M., Sanna A., Riggio A., 2017, *A&A*, **603**, A137
- Martínez-Núñez S., et al., 2017, *Space Sci. Rev.*, **212**, 59
- Masetti N., et al., 2002, *A&A*, **382**, 104
- Mason K. O., Cordova F. A., 1982, *ApJ*, **262**, 253
- Mata Sánchez D., Muñoz-Darias T., Casares J., Jiménez-Ibarra F., 2017, *MNRAS*, **464**, L41
- Mata Sánchez D., Rau A., Álvarez Hernández A., van Grunsven T. F. J., Torres M. A. P., Jonker P. G., 2021, *MNRAS*, **506**, 581
- Mazeh T., et al., 2022, *MNRAS*, **517**, 4005
- McBride V. A., et al., 2006, *A&A*, **451**, 267
- McCullough M. L., Corrales L., Dunham M. M., 2016, *ApJ*, **830**, L36
- Megier A., Strobel A., Galazutdinov G. A., Krelowski J., 2009, *A&A*, **507**, 833
- Miller-Jones J. C. A., Jonker P. G., Dhawan V., Brisken W., Rupen M. P., Nelemans G., Gallo E., 2009, *ApJ*, **706**, L230
- Miller-Jones J. C. A., et al., 2018, *MNRAS*, **479**, 4849
- Miller-Jones J. C. A., et al., 2021, *Science*, **371**, 1046
- Mirabel F., 2017, *New Astron. Rev.*, **78**, 1
- Mirabel I. F., Dhawan V., Mignani R. P., Rodrigues I., Guglielmetti F., 2001, *Nature*, **413**, 139
- Miyaji S., Nomoto K., Yokoi K., Sugimoto D., 1980, *PASJ*, **32**, 303
- Molkov S., Revnivtsev M., Lutovinov A., Sunyaev R., 2005, *A&A*, **434**, 1069
- Moritani Y., Kawano T., Chimasu S., Kawachi A., Takahashi H., Takata J., Carciofi A. C., 2018, *PASJ*, **70**, 61
- Muñoz-Darias T., Casares J., Martínez-Pais I. G., 2005, *ApJ*, **635**, 502
- Nagase F., 1989, *PASJ*, **41**, 1
- Natalucci L., Bazzano A., Cocchi M., Ubertini P., Heise J., Kuulkers E., in 't Zand J. J. M., Smith M. J. S., 2000, *ApJ*, **536**, 891
- Negueruela I., Roche P., Fabregat J., Coe M. J., 1999, *MNRAS*, **307**, 695
- Negueruela I., Smith D. M., Harrison T. E., Torrejón J. M., 2006, *ApJ*, **638**, 982
- Nelemans G., Tauris T. M., van den Heuvel E. P. J., 1999, *A&A*, **352**, L87
- Nespoli E., Fabregat J., Mennickent R. E., 2008, *A&A*, **486**, 911
- Neustroev V. V., Veledina A., Poutanen J., Zharikov S. V., Tsygankov S. S., Sjoberg G., Kajava J. J. E., 2014, *MNRAS*, **445**, 2424
- Nicastro L., Lyne A. G., Lorimer D. R., Harrison P. A., Bailes M., Skidmore B. D., 1995, *MNRAS*, **273**, L68
- Nieder L., et al., 2020, *ApJ*, **902**, L46
- Nikolaeva E. A., Bikmaev I. F., Melnikov S. S., Galeev A. I., Zhuchkov R. Y., Irtuganov E. N., 2013, *Bulletin Crimean Astrophysical Observatory*, **109**, 27
- Nomoto K., 1984, *ApJ*, **277**, 791
- O'Doherty T. N., Bahramian A., Miller-Jones J. C. A., Goodwin A. J., Mandel I., Willcox R., Atri P., Strader J., 2023, *MNRAS*,
- Oosterbroek T., et al., 1999, *A&A*, **351**, L33
- Orosz J. A., 2003, in van der Hucht K., Herrero A., Esteban C., eds, Vol. 212, *A Massive Star Odyssey: From Main Sequence to Supernova*. p. 365 ([arXiv:astro-ph/0209041](https://arxiv.org/abs/astro-ph/0209041)), doi:10.48550/arXiv.astro-ph/0209041
- Orosz J. A., Jain R. K., Bailyn C. D., McClintock J. E., Remillard R. A., 1998, *ApJ*, **499**, 375
- Orosz J. A., et al., 2001, *ApJ*, **555**, 489
- Orosz J. A., et al., 2002, *ApJ*, **568**, 845
- Orosz J. A., Steiner J. F., McClintock J. E., Torres M. A. P., Remillard R. A., Bailyn C. D., Miller J. M., 2011, *ApJ*, **730**, 75
- Paczynski B., 1976, in Eggleton P., Mitton S., Whelan J., eds, Vol. 73, *Structure and Evolution of Close Binary Systems*. p. 75
- Parkes G. E., Murrin P. G., Mason K. O., 1980, *MNRAS*, **190**, 537
- Pfahl E., Rappaport S., Podsiadlowski P., 2002a, *ApJ*, **573**, 283
- Pfahl E., Rappaport S., Podsiadlowski P., Spruit H., 2002b, *ApJ*, **574**, 364
- Picchi P., Shore S. N., Harvey E. J., Berdyugin A., 2020, *A&A*, **640**, A96
- Pike S. N., et al., 2021, *ApJ*, **918**, 9
- Pletsch H. J., Clark C. J., 2015, *ApJ*, **807**, 18
- Podsiadlowski P., Rappaport S., Pfahl E. D., 2002, *ApJ*, **565**, 1107
- Podsiadlowski P., Langer N., Poelarends A. J. T., Rappaport S., Heger A., Pfahl E., 2004, *ApJ*, **612**, 1044
- Ponti G., Bianchi S., Muñoz-Darias T., Nandra K., 2018, *MNRAS*, **481**, L94
- Premachandra S. S., Galloway D. K., Casares J., Steeghs D. T., Marsh T. R., 2016, *ApJ*, **823**, 106
- Priedhorsky W. C., Terrell J., 1983, *ApJ*, **273**, 709
- Pylyser E., Savonije G. J., 1988, *A&A*, **191**, 57
- Ransom S. M., et al., 2014, *Nature*, **505**, 520
- Rappaport S., Verbunt F., Joss P. C., 1983, *ApJ*, **275**, 713
- Ratti E. M., et al., 2012, *MNRAS*, **423**, 2656
- Ray P. S., Chakrabarty D., 2002, *ApJ*, **581**, 1293
- Ray P. S., et al., 2012, *arXiv e-prints*, p. arXiv:1205.3089
- Reardon D. J., et al., 2021, *MNRAS*, **507**, 2137
- Reid M. J., et al., 2009, *ApJ*, **700**, 137
- Reid M. J., et al., 2014a, *ApJ*, **783**, 130
- Reid M. J., McClintock J. E., Steiner J. F., Steeghs D., Remillard R. A., Dhawan V., Narayan R., 2014b, *ApJ*, **796**, 2
- Reig P., Chakrabarty D., Coe M. J., Fabregat J., Negueruela I., Prince T. A., Roche P., Steele I. A., 1996, *A&A*, **311**, 879
- Reig P., Fabregat J., Coe M. J., Roche P., Chakrabarty D., Negueruela I., Steele I., 1997, *A&A*, **322**, 183
- Reig P., Negueruela I., Fabregat J., Chato R., Coe M. J., 2005, *A&A*, **440**, 1079
- Reig P., Blay P., Blinov D., 2017, *A&A*, **598**, A16
- Remillard R. A., Orosz J. A., McClintock J. E., Bailyn C. D., 1996, *ApJ*, **459**, 226
- Reynolds A. P., Bell S. A., Hilditch R. W., 1992, *MNRAS*, **256**, 631
- Reynolds A. P., Quaintrell H., Still M. D., Roche P., Chakrabarty D., Levine S. E., 1997, *MNRAS*, **288**, 43
- Riquelme M. S., Torrejón J. M., Negueruela I., 2012, *A&A*, **539**, A114
- Romani R. W., 2012, *ApJ*, **754**, L25
- Romani R. W., Shaw M. S., 2011, *ApJ*, **743**, L26
- Romani R. W., Filippenko A. V., Silverman J. M., Cenko S. B., Greiner J., Rau A., Elliott J., Pletsch H. J., 2012, *ApJ*, **760**, L36
- Romani R. W., Filippenko A. V., Cenko S. B., 2014, *ApJ*, **793**, L20
- Russell T. D., Soria R., Motch C., Pakull M. W., Torres M. A. P., Curran P. A., Jonker P. G., Miller-Jones J. C. A., 2014, *MNRAS*, **439**, 1381
- Russell T. D., et al., 2015, *MNRAS*, **450**, 1745
- Sadakane K., Hirata R., Jugaku J., Kondo Y., Matsuoka M., Tanaka Y., Hammerschlag-Hensberge G., 1985, *ApJ*, **288**, 284
- Sahu K. C., et al., 2022, *ApJ*, **933**, 83
- Sala G., Greiner J., Ajello M., Primak N., 2008, *A&A*, **489**, 1239
- Salvatier J., Wieckiá T. V., Fonnesbeck C., 2016, PyMC3: Python probabilistic programming framework, *Astrophysics Source Code Library*, record ascl:1610.016 (ascl:1610.016)
- Sanpa-Arsa S., 2016, PhD thesis, University of Virginia
- Sarty G. E., et al., 2009, *MNRAS*, **392**, 1242
- Segreto A., La Parola V., Cusumano G., D'Ai A., Masetti N., Campana S., 2013, *A&A*, **558**, A99
- Seifina E., Titarchuk L., Shaposhnikov N., 2014, *ApJ*, **789**, 57
- Shahbaz T., 2003, *MNRAS*, **339**, 1031
- Shahbaz T., Watson C. A., Dhillion V. S., 2014, *MNRAS*, **440**, 504
- Shaw A. W., Charles P. A., Casares J., Hernández Santisteban J. V., 2016, *MNRAS*, **463**, 1314
- Smits M., Maccarone T. J., Kundu A., Zepf S. E., 2006, *A&A*, **458**, 477
- Steeghs D., Casares J., 2002, *ApJ*, **568**, 273
- Steeghs D., Jonker P. G., 2007, *ApJ*, **669**, L85
- Steeghs D., McClintock J. E., Parsons S. G., Reid M. J., Littlefair S., Dhillion V. S., 2013, *ApJ*, **768**, 185
- Steele I. A., Negueruela I., Coe M. J., Roche P., 1998, *MNRAS*, **297**, L5
- Stevens J. B., Reig P., Coe M. J., Buckley D. A. H., Fabregat J., Steele I. A., 1997, *MNRAS*, **288**, 988
- Stickland D., Lloyd C., Radziun-Woodham A., 1997, *MNRAS*, **286**, L21
- Stiele H., Muñoz-Darias T., Motta S., Belloni T. M., 2012, *MNRAS*, **422**, 679
- Storm J., Carney B. W., Gieren W. P., Fouqué P., Latham D. W., Fry A. M., 2004, *A&A*, **415**, 531
- Stovall K., et al., 2014, *ApJ*, **791**, 67

Strader J., Chomiuk L., Cheung C. C., Salinas R., Peacock M., 2015, *ApJ*, **813**, L26

Strader J., et al., 2019, *ApJ*, **872**, 42

Strohmayr T. E., Markwardt C. B., Swank J. H., in't Zand J., 2003, *ApJ*, **596**, L67

Swihart S. J., Strader J., Chomiuk L., Shishkovsky L., 2019, *ApJ*, **876**, 8

Taam R. E., Sandquist E. L., 2000, *ARA&A*, **38**, 113

Tanikawa A., Hattori K., Kawanaka N., Kinugawa T., Shikauchi M., Tsuna D., 2022, *arXiv e-prints*, p. arXiv:2209.05632

Thompson T. A., et al., 2019, *Science*, **366**, 637

Thorne K. S., Zytow A. N., 1975, *ApJ*, **199**, L19

Thorne K. S., Zytow A. N., 1977, *ApJ*, **212**, 832

Thorstensen J. R., Armstrong E., 2005, *AJ*, **130**, 759

Tomsick J. A., Heindl W. A., Chakrabarty D., Halpern J. P., Kaaret P., 2001, *ApJ*, **559**, L123

Torrejón J. M., Negueruela I., Smith D. M., Harrison T. E., 2010, *A&A*, **510**, A61

Torres M. A. P., Casares J., Jiménez-Ibarra F., Muñoz-Darias T., Armas Padilla M., Jonker P. G., Heida M., 2019, *ApJ*, **882**, L21

Torres M. A. P., Casares J., Jiménez-Ibarra F., Álvarez-Hernández A., Muñoz-Darias T., Armas Padilla M., Jonker P. G., Heida M., 2020, *ApJ*, **893**, L37

Trimble V., 1971, in Davies R. D., Graham-Smith F., eds, Vol. 46, The Crab Nebula. p. 12

Tsygankov S. S., et al., 2021, *ApJ*, **909**, 154

Tutukov A. V., Fedorova A. V., Ergma E. V., Yungelson L. R., 1985, *Soviet Astronomy Letters*, **11**, 52

Van K. X., Ivanova N., Heinke C. O., 2019, *MNRAS*, **483**, 5595

Vasiliev E., 2019, *MNRAS*, **484**, 2832

Vehtari A., Gelman A., Gabry J., 2017, *Statistics and Computing*, **27**, 1413

Verbiest J. P. W., Weisberg J. M., Chael A. A., Lee K. J., Lorimer D. R., 2012, *ApJ*, **755**, 39

Verbunt F., 1993, *ARA&A*, **31**, 93

Verbunt F., van den Heuvel E. P. J., 1995, in *X-ray Binaries*. pp 457–494

Verbunt F., Igoshev A., Cator E., 2017, *A&A*, **608**, A57

Vinciguerra S., et al., 2020, *MNRAS*, **498**, 4705

Virtanen P., et al., 2020, *scipy/scipy: SciPy 1.5.3*, Zenodo, doi:10.5281/zenodo.4100507

Waisberg I. R., Romani R. W., 2015, *ApJ*, **805**, 18

Wang L., Steeghs D., Casares J., Charles P. A., Muñoz-Darias T., Marsh T. R., Hynes R. I., O'Brien K., 2017, *MNRAS*, **466**, 2261

Waters L. B. F. M., Pols O. R., Hogeveen S. J., Cote J., van den Heuvel E. P. J., 1989, *A&A*, **220**, L1

Watts A. L., Krishnan B., Bildsten L., Schutz B. F., 2008, *MNRAS*, **389**, 839

Werner N., et al., 2004, *A&A*, **416**, 311

Williams S. J., Gies D. R., Matson R. A., Touhami Y., Grundstrom E. D., Huang W., McSwain M. V., 2010, *ApJ*, **723**, L93

Wilson C. A., Finger M. H., Coe M. J., Negueruela I., 2003, *ApJ*, **584**, 996

Wilson C. A., Weisskopf M. C., Finger M. H., Coe M. J., Greiner J., Reig P., Papamastorakis G., 2005, *ApJ*, **622**, 1024

Wu J., et al., 2015, *ApJ*, **806**, 92

Wu J., Orosz J. A., McClintock J. E., Hasan I., Bailyn C. D., Gou L., Chen Z., 2016, *ApJ*, **825**, 46

Yao J. M., Manchester R. N., Wang N., 2017, *ApJ*, **835**, 29

Yi T., et al., 2022, *Nature Astronomy*, **6**, 1203

Yuan H., et al., 2022, *ApJ*, **940**, 165

Zheng L.-L., et al., 2022, *arXiv e-prints*, p. arXiv:2210.04685

Zurita C., Durant M., Torres M. A. P., Shahbaz T., Casares J., Steeghs D., 2008, *ApJ*, **681**, 1458

de Martino D., et al., 2014, *MNRAS*, **444**, 3004

della Valle M., Mirabel I. F., Rodriguez L. F., 1994, *A&A*, **290**, 803

den Hartog P. R., Kuiper L. M., Corbet R. H. D., in't Zand J. J. M., Hermsen W., Vink J., Remillard R., van der Klis M., 2004, *The Astronomer's Telegram*, **281**, 1

in't Zand J. J. M., Kuulkers E., Verbunt F., Heise J., Cornelisse R., 2003, *A&A*, **411**, L487

in't Zand J. J. M., Cornelisse R., Méndez M., 2005, *A&A*, **440**, 287

van Leeuwen F., 2007, *A&A*, **474**, 653

van Staden A. D., Antoniadis J., 2016, *ApJ*, **833**, L12

van den Heuvel E. P. J., Heise J., 1972, *Nature Physical Science*, **239**, 67

van den Heuvel E. P. J., Portegies Zwart S. F., Bhattacharya D., Kaper L., 2000, *A&A*, **364**, 563

van der Hooft F., Heemskerk M. H. M., Alberts F., van Paradijs J., 1998, *A&A*, **329**, 538

van der Meer A., Kaper L., van Kerkwijk M. H., Heemskerk M. H. M., van den Heuvel E. P. J., 2007, *A&A*, **473**, 523

APPENDIX A: GALACTIC POSITIONS AND PROPER MOTIONS OF THE BINARIES

Galactic positions and proper motion vectors of the binaries in our compilation are shown in Figure A1 and A2.

APPENDIX B: PECULIAR VELOCITY DISTRIBUTIONS

In this section, we present distributions of potential peculiar velocity at birth ($v_{\text{pec}}^{z=0}$) for binaries in our compilation in Figure B2, B1, B3, and B4.

APPENDIX C: LITERATURE DISTANCES USED FOR MODELING THE PRIOR

Here we summarise a list of literature distances (d_{lit}) that are measured separately from *Gaia* in Table C1. These distances are used for fitting the scaling parameter (L) of the exponential prior (eq 4) and for calculating $v_{\text{pec,p}}$ when *Gaia* parallax is poorly constrained.

Table C1. Literature distances (d_{lit})

Name	d_{lit} (kpc)	Ref	Name	d_{lit} (kpc)	Ref	Name	d_{lit} (kpc)	Ref
IGR J00291+5934	4.2 ± 0.5	[1]	Aql X-1	5.2 ± 0.8	[17]	4U 0115+634	7.0 ± 0.3	[73]
4U 0919-54	4.2 ± 1.3	[2]	4U 1916-05	6.8 ± 1.0	[9]	V 0332+53	7.5 ± 1.5	[74]
2S 0921-630	8.5^*	[3]	XTE J2123-058	8.5 ± 2.5	[36]	4U 0352+309	0.7 ± 0.3	[75]
XTE J0929-314	≥ 7.4	[4]	Cyg X-2	11.0 ± 2.0	[9]	RX J0440.9+4431	3.3 ± 0.5	[76]
4U 1254-69	13.0 ± 3.0	[5]	GRO J0422+32	2.5 ± 0.3	[37]	A 0535+262	2.0 ± 0.7	[77]
Cen X-4	1.4 ± 0.3	[6]	A 0620-00	1.1 ± 0.1	[38]	XTE J0658-073	3.9 ± 0.1	[78]
Cir X-1	9.3 ± 0.9	[7]	MWC 656	2.6 ± 1.0	[39]	3A 0726-260	4.6 ± 1.3	[79]
UW CrB	≥ 5.0	[8]	GRS 1009-45	3.8 ± 0.3	[40]	RX 0812.4-3114	8.6 ± 1.8	[80]
4U 1608-52	3.2 ± 0.3	[9]	HD 96670	2.8 ± 0.8	[41]	GS 0834-430	4.0 ± 1.0	[81]
Sco X-1	2.8 ± 0.3	[10]	XTE J1118+480	1.7 ± 0.1	[42]	Vela X-1	1.9 ± 0.2	[82]
4U 1626-67	9.0 ± 4.0	[11]	GRS 1124-684	5.0 ± 0.7	[43]	GRO J1008-57	5.8 ± 0.5	[73]
4U 1636-536	6.0 ± 0.5	[12]	MAXI J1305-704	7.7 ± 1.6	[44]	1A 1118-615	5.0 ± 2.0	[83]
Her X-1	6.6 ± 0.4	[13]	MAXI J1348-630	2.1 ± 0.6	[45]	1E 1145.1-6141	8.5 ± 1.5	[84]
MXB 1659-298	9.0 ± 2.0	[9]	BW Cir	≥ 25.0	[46]	1H 1249-637	0.4 ± 0.0	[85]
4U 1700+24	0.4 ± 0.0	[14]	Swift J1357.2-0933	≥ 6.0	[47]	1H 1253-761	0.2 ± 0.0	[86]
4U 1702-429	4.2 ± 0.1	[9]	4U 1543-475	7.5 ± 0.5	[17]	1H 1255-567	0.1 ± 0.0	[86]
4U 1705-32	13.0 ± 2.0	[15]	MAXI J1543-564	≥ 8.5	[48]	GX 304-1	2.4 ± 0.5	[87]
4U 1705-44	5.8 ± 0.2	[9]	XTE J1550-564	4.5 ± 0.5	[49]	2S 1417-62	6.2 ± 4.8	[88]
SAX J1712.6-3739	5.1 ± 0.5	[16]	4U 1630-472	10.0^*	[50]	SAX J1452.8-5949	9.0 ± 3.0	[89]
1H 1715-321	6.0 ± 0.9	[17]	XTE J1650-500	2.6 ± 0.7	[51]	4U 1538-52	6.4 ± 1.0	[90]
1RXS J171824.2-402934	6.5 ± 0.5	[15]	GRO 1655-40	3.2 ± 0.2	[52]	IGR J16318-4848	3.5 ± 2.6	[91]
GRO J1719-24	2.4 ± 0.4	[18]	MAXI J1659-152	8.6 ± 3.7	[53]	IGR J16465-4507	13.7 ± 9.9	[92]
GX 1+4	4.3^*	[19]	GX 339-4	≥ 5.0	[54]	OAO 1657-415	6.4 ± 1.5	[93]
4U 1728-34	4.8 ± 0.3	[20]	H1705-250	8.6 ± 2.1	[17]	XTE J1739-302	2.4 ± 0.6	[94]
SLX 1735-269	6.0 ± 1.2	[21]	GRS 1716-249	2.4 ± 0.4	[55]	GRO J1750-27	18.0 ± 4.0	[95]
4U 1735-444	8.5 ± 1.3	[22]	XTE J1720-318	6.5 ± 3.5	[56]	IGR J17544-2619	3.0 ± 1.0	[96]
GRS 1741.9-2853	9.0 ± 0.5	[23]	GRS 1739-278	7.2 ± 1.2	[57]	SAX J1802.7-2017	12.4 ± 0.1	[97]
GX 3+1	6.1 ± 0.1	[24]	XTE J1752-223	6.0 ± 2.0	[58]	SAX J1818.6-1703	2.7 ± 0.3	[80]
SAX J1747.0-2853	7.5 ± 1.3	[25]	Swift J1753.5-0127	6.0 ± 2.0	[59]	AX J1820.5-1434	4.8 ± 1.2	[98]
IGR J17473-2721	6.4 ± 0.9	[26]	V4134 Sgr	6.5 ± 2.5	[60]	LS 5039	2.5 ± 0.1	[99]
SAX J1750.8-2900	5.2 ± 0.1	[9]	XTE J1818-245	3.5 ± 0.8	[61]	AX J1841.0-0536	3.2 ± 1.5	[100]
SAX J1808.4-3658	3.5 ± 0.1	[27]	V4641 Sgr	6.2 ± 0.7	[62]	AX J1845.0-0433	6.4 ± 0.8	[80]
SAX J1810.8-2609	4.9 ± 0.3	[28]	MAXI J1820+070	3.0 ± 0.3	[63]	IGR 18483-0311	2.8 ± 0.1	[97]
GX 13+1	7.0 ± 1.0	[29]	XTE J1859+226	16.5 ± 2.5	[64]	XTE J1858+034	10.5 ± 3.5	[101]
XMMU J181227.8-181234	14.0 ± 2.0	[30]	XTE J1908+094	6.5 ± 3.5	[65]	IGR J19140+0951	3.6 ± 0.0	[97]
GX 17+2	9.8 ± 0.4	[9]	Cyg X-1	2.2 ± 0.2	[66]	XTE 1946+274	9.5 ± 2.9	[102]
XTE J1814-338	8.0 ± 1.6	[31]	GRS 1915+105	8.8 ± 1.8	[67]	GRO J2058+42	9.0 ± 1.3	[103]
2A 1822-371	2.5 ± 0.5	[32]	4U 1957+11	9.0 ± 6.0	[68]	Cep X-4	3.8 ± 0.6	[104]
GS 1826-238	5.7 ± 0.2	[33]	GS 2000+251	2.7 ± 0.7	[17]	4U 2206+543	3.1 ± 0.1	[105]
Ser X-1	7.7 ± 0.9	[9]	Cyg X-3	7.4 ± 1.1	[69]	SAX J2239.3+6116	4.9 ± 0.8	[106]
XTE J1856+053	≥ 1.0	[34]	V404 Cyg	2.4 ± 0.1	[70]	AS 386	2.4 ± 0.3	[107]
HETE J1900.1-2455	3.6 ± 0.5	[9]	2S 0053+604	0.1 ± 0.0	[71]	J05215658	3.2 ± 0.8	[108]
4U 1905+000	8.0 ± 1.0	[35]	2S 0114+650	4.5 ± 1.5	[72]			

References: [1] De Falco et al. (2017), [2] Cornelisse et al. (2002), [3] Cowley et al. (1982), [4] Marino et al. (2017), [5] in't Zand et al. (2003), [6] González Hernández et al. (2005), [7] Heinz et al. (2015), [8] Hakala et al. (2005), [9] Galloway et al. (2008), [10] Bradshaw et al. (1999), [11] Chakrabarty (1998), [12] Galloway et al. (2006), [13] Reynolds et al. (1997), [14] Masetti et al. (2002), [15] in't Zand et al. (2005), [16] Lin & Yu (2020), [17] Jonker & Nelemans (2004), [18] Ling & Wheaton (2005), [19] Hinkle et al. (2006), [20] Galloway et al. (2003), [21] Molkov et al. (2005), [22] Watts et al. (2008), [23] Pike et al. (2021), [24] Kuulkers & van der Klis (2000), [25] Werner et al. (2004), [26] Chen et al. (2010), [27] Galloway & Cumming (2006), [28] Natalucci et al. (2000), [29] Bandyopadhyay et al. (1999), [30] Goodwin et al. (2019), [31] Strohmayer et al. (2003), [32] Mason & Cordova (1982), [33] Chenevez et al. (2016), [34] Sala et al. (2008), [35] Chevalier & Ilovaisky (1990), [36] Tomsick et al. (2001), [37] Gelino & Harrison (2003), [38] Cantrell et al. (2010), [39] Casares et al. (2012), [40] Gelino (2002), [41] Gomez & Grindlay (2021), [42] Gelino et al. (2006), [43] Wu et al. (2016), [44] Mata Sánchez et al. (2021), [45] Chauhan et al. (2021), [46] Casares et al. (2009), [47] Charles et al. (2019), [48] Stiele et al. (2012), [49] Orosz et al. (2011), [50] Seifina et al. (2014), [51] Homan et al. (2006), [52] Hjellming & Rupen (1995), [53] Kuulkers et al. (2013), [54] Heida et al. (2017), [55] della Valle et al. (1994), [56] Chaty & Bessolaz (2006), [57] Greiner et al. (1996), [58] Ratti et al. (2012), [59] Cadolle Bel et al. (2007), [60] Angelini & White (2003), [61] Cadolle Bel et al. (2009), [62] MacDonald et al. (2014), [63] Atri et al. (2020), [64] Corral-Santana et al. (2011), [65] Chaty et al. (2006), [66] Miller-Jones et al. (2021), [67] Reid et al. (2014b), [68] Maccarone et al. (2020), [69] McCollough et al. (2016), [70] Miller-Jones et al. (2009), [71] Megier et al. (2009), [72] Farrell et al. (2008), [73] Riquelme et al. (2012), [74] Negueruela et al. (1999), [75] Lyubimkov et al. (1997), [76] Reig et al. (2005), [77] Steele et al. (1998), [78] McBride et al. (2006), [79] Corbet & Mason (1984), [80] Coleiro & Chaty (2013), [81] Israel et al. (2000), [82] Sadakane et al. (1985), [83] Janot-Pacheco et al. (1981), [84] Densham & Charles (1982), [85] van Leeuwen (2007), [86] Chevalier & Ilovaisky (1998), [87] Parkes et al. (1980), [88] Grindlay et al. (1984), [89] Oosterbroek et al. (1999), [90] Reynolds et al. (1992), [91] Filliatre & Chaty (2004), [92] Clark et al. (2010), [93] Chakrabarty et al. (2002), [94] Negueruela et al. (2006), [95] Lutovinov et al. (2019), [96] Martínez-Núñez et al. (2017), [97] Torrejón et al. (2010), [98] Segreto et al. (2013), [99] Casares et al. (2005), [100] Nespoli et al. (2008), [101] Tsygankov et al. (2021), [102] Wilson et al. (2003), [103] Wilson et al. (2005), [104] Bonnet-Bidaud & Mouchet (1998), [105] Hambaryan et al. (2022), [106] Reig et al. (2017), [107] Khokhlov et al. (2018), [108] Thompson et al. (2019)

*: Distances that have no literature constraints.

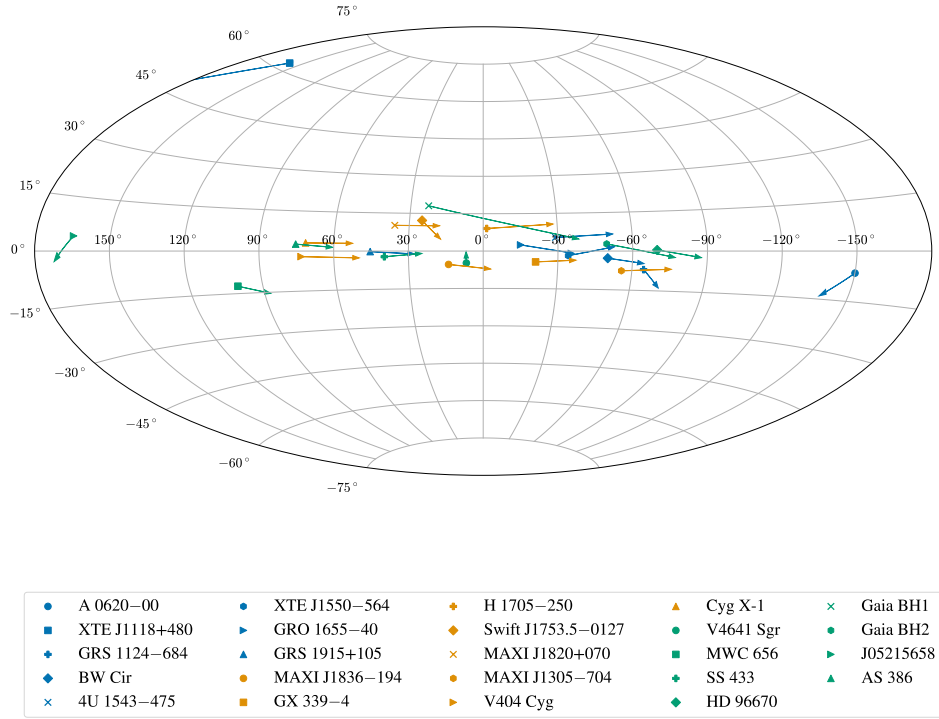


Figure A1. Galactic map of binaries that host a BH. Displacement due to proper motion is indicated by the length and direction of the arrows.

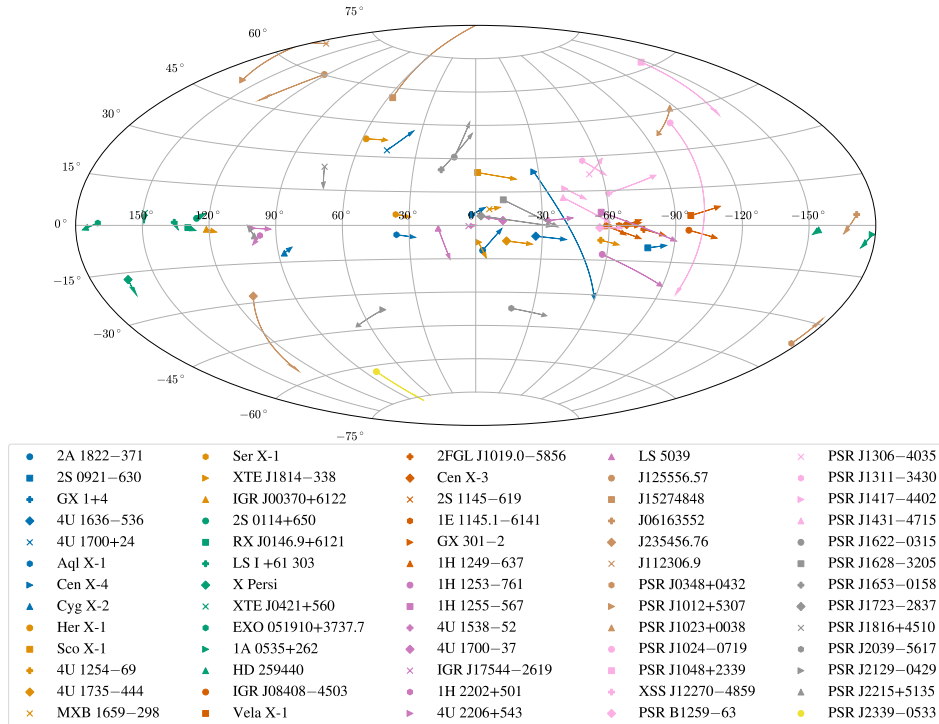


Figure A2. The same as Figure A1 but plotted for binaries hosting a NS.

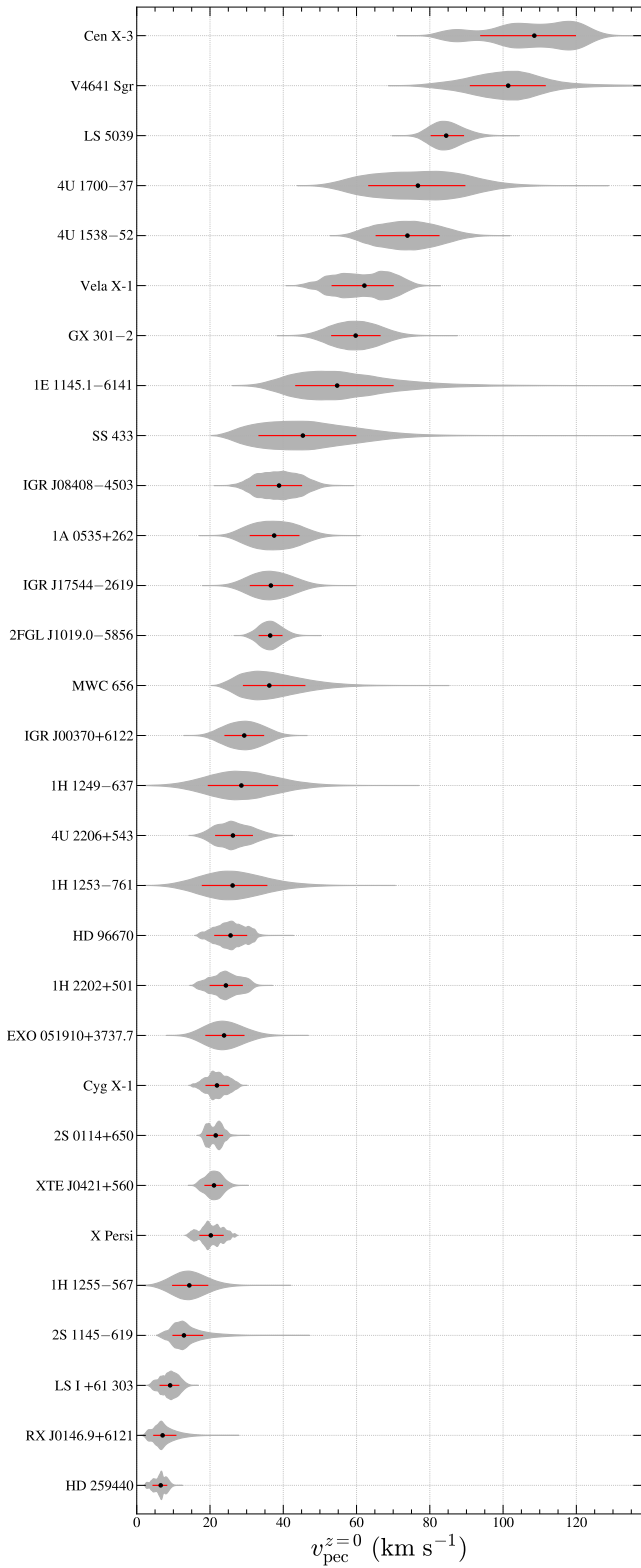


Figure B1. Probability density distribution of $v_{\text{pec}}^{z=0}$ of HMXBs, sorted by their medians. The median is marked by a filled black circle, and the range corresponding to the 16th and 84th percentiles are indicated with a red horizontal line in each distribution.

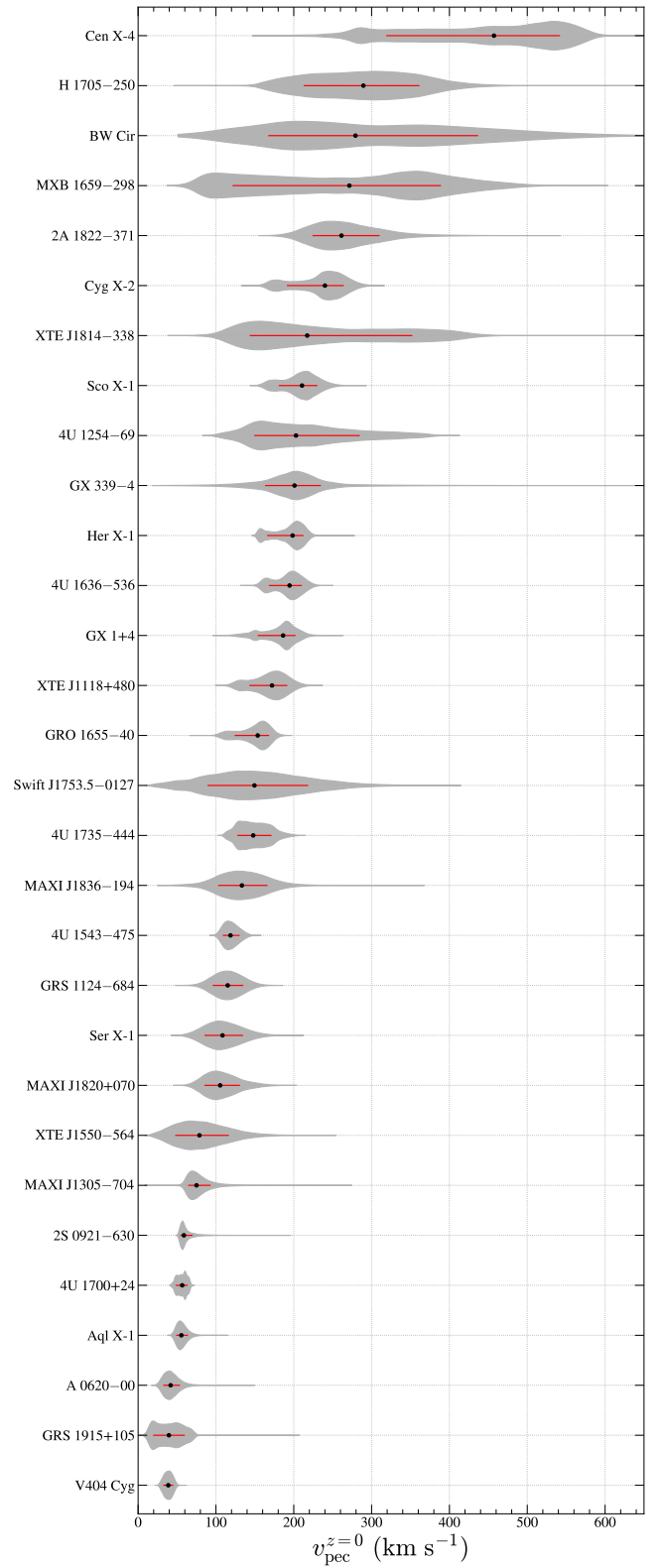


Figure B2. The same as Figure B1, but plotted for $v_{\text{pec}}^{z=0}$ of LMXBs.

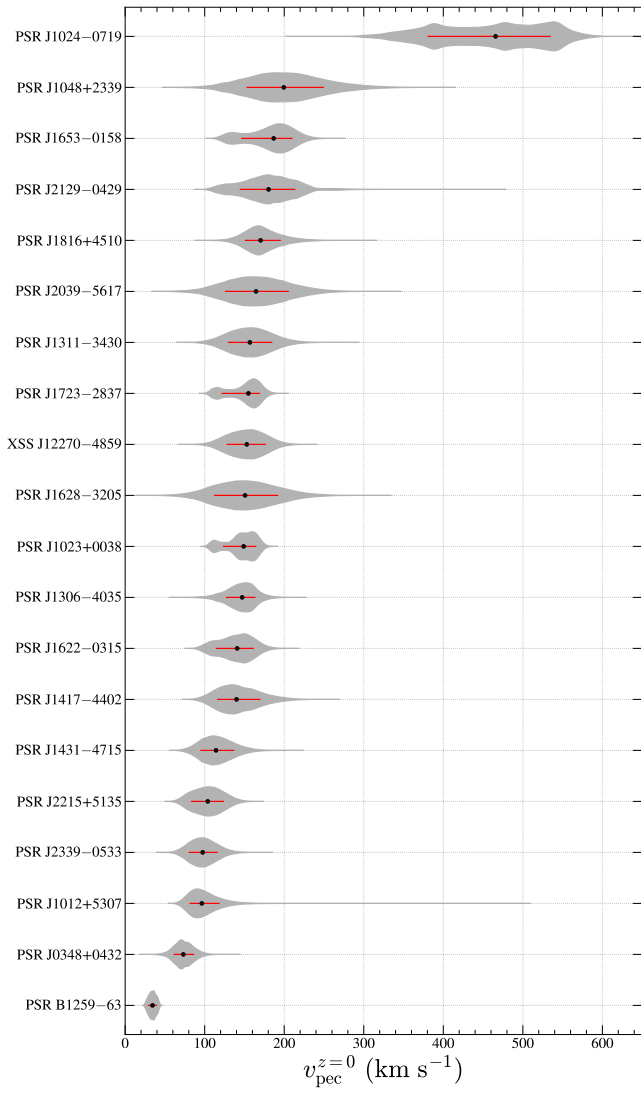


Figure B3. The same as Figure B1, but plotted for $v_{\text{pec}}^{z=0}$ of PSRs.

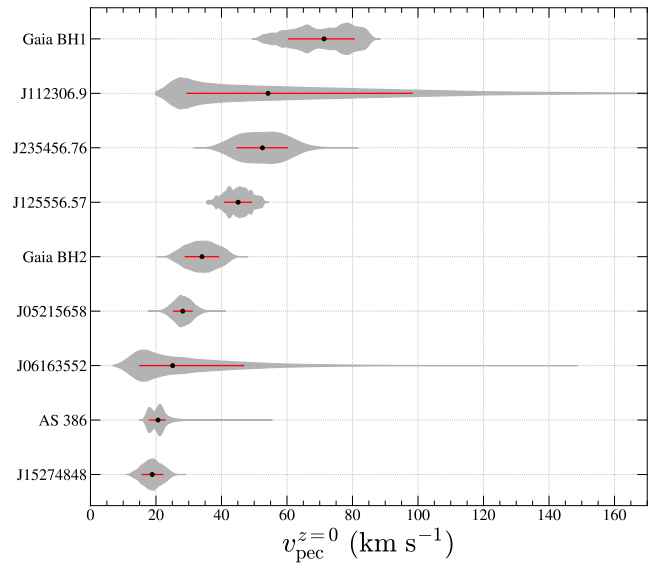


Figure B4. The same as Figure B1, but plotted for $v_{\text{pec}}^{z=0}$ of non-interacting (NI) binaries.

APPENDIX D: NOTATIONS AND TERMINOLOGY

This section lists salient notations and terminology used in this work.

Natal kick (kick): A general term used to refer to the impulsive acceleration imparted on a BH or NS.

Blaauw kick: A kick due to mass ejection.

Additional kick: Kicks that are caused by mechanisms other than mass ejection.

d_{lit} : Literature distance.

d_{ϖ} : Parallax-inferred distance.

γ : Systemic radial velocity.

M_1 : Mass of the compact object.

M_2 : Mass of the non-degenerate companion. In XRBs, this refers to the donor mass.

M_{tot} : Binary total mass. $M_{\text{tot}} = M_1 + M_2$.

ΔM : Ejecta mass. This is the amount of mass that the helium core ejected at SN.

σ_v : Scale parameter that characterises the Maxwellian distribution. For two-component Maxwellian model, $\sigma_{v,1}$ and $\sigma_{v,2}$ are used.

f_{rej} : Fraction of simulations that reject the null hypothesis of a test.

f_{err} : Fraction of additional error (see eq 8)

f_{diverge} : Fraction of chains that diverge ($|\hat{R} - 1|/R \geq 0.01$)

w_{loo} : The weight value associated with the leave-one-out cross-validation (LOO).

P_{orb} : Present-day orbital period.

$P_{\text{orb,SN}}$: Orbital period at the instant of a SN.

$P_{\text{orb, post-SN}}$: Orbital period right after a SN.

ρ_p : The Pearson correlation coefficient.

ρ_s : The Spearman's rank correlation coefficient.

\hat{R} : The Gelman-Rubin diagnostic used to test convergence of MCMC chains.

v_{pec} : Peculiar velocity in general. This is the velocity of an object relative to Galactic rotation.

$v_{\text{pec,p}}$: Present-day peculiar velocity. The v_{pec} calculated using the current astrometric parameters of the object.

$v_{\text{pec}}^{z=0}$: Potential birth peculiar velocity. This is the v_{pec} at Galactic disc ($z = 0$).

V_r : Relative orbital velocity at the instant of SN (see eq 10).

This paper has been typeset from a $\text{\TeX}/\text{\LaTeX}$ file prepared by the author.